1979

Fast neutron spectrum measurement with threshold detectors

Mohammad Moghari
Iowa State University

PLEASE NOTE:

In all cases this material has been filmed in the best possible way from the available copy. Problems encountered with this document have been identified here with a check mark ✓.

1. Glossy photographs _____
2. Colored illustrations _____
3. Photographs with dark background _____
4. Illustrations are poor copy _____
5. Print shows through as there is text on both sides of page _____
6. Indistinct, broken or small print on several pages ✓ throughout ✓
7. Tightly bound copy with print lost in spine _____
8. Computer printout pages with indistinct print _____
9. Page(s) _____ lacking when material received, and not available from school or author _____
10. Page(s) _____ seem to be missing in numbering only as text follows _____
11. Poor carbon copy _____
12. Not original copy, several pages with blurred type _____
13. Appendix pages are poor copy _____
14. Original copy with light type _____
15. Curling and wrinkled pages _____
16. Other _____

University Microfilms International

300 N. ZEEB RD., ANN ARBOR, MI 48106 (313) 761-4700

Fast neutron spectrum measurement with threshold detectors

by

Mohammad Moghari

A Dissertation Submitted to the
Graduate Faculty in Partial Fulfillment of
The Requirements for the Degree of
DOCTOR OF PHILOSOPHY

Major: Nuclear Engineering

Approved:

Signature was redacted for privacy.

In Charge of Major Work

Signature was redacted for privacy.

For the Major Department

Signature was redacted for privacy.

For the Graduate College

Iowa State University
Ames, Iowa
1979

TABLE OF CONTENTS

INTRODUCTION

The knowledge of the neutron flux and energy spectrum of a given reactor facility is essential for the evaluation of experimental results involving irradiation of materials. Furthermore, the interpretation of experiments dealing with such disciplines as radiobiology, radiochemistry, as well as the study of radiation damage produced by fast neutrons require an accurate knowledge of neutron flux and spectrum. For instance, the phenomenon of neutron-produced increases in the ductile-to-brittle transition temperature of ferritic steels has been studied extensively. The experimental studies conducted have permitted the formulation of a theory for the increase in transition temperature as a function of neutron fluence, typically reported as neutrons per square centimeter with energies greater than 0.1 MeV (or occasionally greater than 1 MeV).

The criterion or assumption has traditionally been made that only when neutrons have energies above a specified threshold will damage result and that neutron with energies above this threshold are equally effective in causing damage. In nearly all studies involving radiation damage it is assumed that neutrons of energies greater than 0.1 MeV all contribute equally to the damage process. Although this assumption has served successfully for many types of studies, there have been instances where it has failed to yield acceptable corre-

lation between fluence and neutron-induced embrittlement. This lack of agreement has been traced to the energy spectrum of the neutron radiation environment which, in most cases, is markedly different from the assumed step function.

Generally in the field of radiation effects on materials, changes in physical properties produced by transmutation reactions require an accurate knowledge of neutron spectrum before theory and experiment can be adequately correlated. Furthermore, the present incomplete understanding of the damage producing mechanism hampers attempts to correlate neutron fluence with the neutron-induced damage in the specimen. Consequently, in order to analyze and compare results obtained by irradiation studies - and especially - in different reactor facilities, it is necessary to have an accurate knowledge of the energy dependence of the neutron flux, i.e. the spectrum and the neutron fluence.

The best way of measuring reactor neutron spectra, with energies ranging typically from approximately 10^{-10} MeV to about 15 MeV, is to irradiate activation foils whose energy dependent cross sections for a particular reaction are known. The induced activities are then measured and used to find, with one of the spectrum unfolding techniques, a neutron spectrum capable of explaining the observed activities.

The objectives of this investigation were a) to select a system of activation detectors that will enable the experi-

menter to determine the neutron flux and spectrum at all energies, and b) to measure the neutron spectra in two Ames Laboratory Research Reactor (ALRR) radiation facilities.

Given the higher damaging capability of the fast neutrons, more emphasis is placed upon the determination of the spectrum at energies greater than 100 KeV. Hence, the activation foils used in this work were in most cases selected to be threshold detectors.

The neutron induced activities in the irradiated foils were analyzed and measured with the aid of a Ge(Li) detector and associated counting system. In order to determine the spectrum from the measured activities, use was made of a modified SAND-II (Spectrum Analysis by Neutron Detectors) computer code. SAND-II is based on an iterative unfolding technique which provides a best fit neutron spectrum for a given set of experimentally determined foil activites. The determination of the errors involved in this work was carried out using a Monte Carlo error analysis code. The code takes into account experimental errors in collecting the experimental data as well as errors related to the SAND-II unfolding technique.

I. LITERATURE SEARCH

Various techniques are available for the measurement of neutron spectrum; these include nuclear emulsions, proton recoil spectrometry, time-of-flight techniques, and neutron activation. However, when measurements are to be made inside the reactor and the spectrum runs from thermal to fast neutron energies, only neutron activation turns out to be practical.

Neutron activation was originally used in 1936 by von Heresy and Levi (1) to detect the presence of dysprosium and europium in rare earth mixtures by means of their measured activities. Neutron activation for the measurement of neutron spectra was considered in 1951. Cohen (2) was the first to consider the use of activation detectors for the measurement of neutron energies above the thermal energy region. He suggested the use of (n,p) and (n,2n) threshold detectors for the energy range between 1 and 25 MeV. In 1956 Hurst (3) extended the energy coverage of threshold detectors to the KeV region by introducing such fission detectors as ^{239}Pu, ^{238}U, and ^{237}Np.

Hurst used boron shielding to give the ^{239}Pu (n,fission) reaction an effective threshold energy of approximately 1 KeV. ^{238}U (n,fission) and ^{237}Np (n,fission) reactions with threshold energies of about 0.6 MeV and 1.5 MeV respectively were also used.

Details for boron shielding geometry irradiation consid-

erations, and calibrations procedures for the above reactions and for the ^{32}S (n,p) ^{32}P reaction were given.

In 1958, Reinhardt and Davis (4) presented a number of improvements in the use of fission detectors. These included techniques for sample preparation and fission reaction standardization with the sulfur threshold reaction. Following Reinhardt's paper, Hurst and Ritchie (5) described a new calibration procedure and introduced the concept of the "equivalent foil technique" for calibrating counting systems used for counting the gamma radiation from neutron activated fission detectors.

Within recent years many publications have appeared which form the basis for many of the techniques, both experimental and mathematical, currently in use for neutron spectrum measurement. Wechsler and Trice (6) described general procedures for neutron spectrum measurement in connection with radiation effects on materials. Stiller (7) used ^{31}P (n,p)^{31}Si; ^{58}Ni (n,p)^{58}Co; ^{32}S (n,p)^{32}P; ^{27}Al (n,p)^{27}Mg; ^{56}Fe (n,p)^{56}Mn; ^{24}Mg (n,p)^{24}Na; ^{27}Al (n,α)^{24}Na; ^{63}Cu (n,2n)^{62}Cu; ^{28}Si (n,p)^{28}Al; threshold reactions for the measurement of fast neutron spectra. He adopted Grundl and Usner's (8) method of effective threshold for spectrum unfolding. Levine et al. (9) presented the procedure used for neutron spectrum measurement in the Northrop Triga Reactor.

In 1965 Zijp (10, 11) presented a comprehensive review of

activation methods for the determination of neutron spectra. In addition to the basic concepts, Zijp presented details of threshold reactions of interest and reported some important methods for the determination of a neutron spectrum from the response integral of the activation detectors. McElroy et al. (12) reported a manual iterative unfolding method to obtain neutron spectra from the results of foil activation. Their analytical studies showed that integral neutron flux might be obtained from foil data with accuracies to within ±10% to ±30% at any point over the energy range from 4×10^{-7} to 18 MeV, if the activation cross section data and measured activation were accurate to ±10%.

Later, McElroy et al. (13) used a fully-automated computer code to perform spectral analysis by a substantially improved iterative method. This multiple foil activation iterative method, called SAND-II (14) has been used to experimentally determine the neutron spectra in various types of neutron environment. Comparisons with reactor physics calculations and spectrometer measurements indicated that the method should give results with accuracies between ±10% and ±30%, depending on experimental conditions.

Grundl (15) employed eight activation detectors to compare the thermal-neutron-induced fission-neutron spectra of ^{235}U, ^{233}U, and ^{239}Pu. The activation reactions were as follows: ^{235}U (n,f); ^{237}Np (n,f); ^{238}U (n,g); ^{31}P (n,p)^{31}Si; ^{27}Al (n,p)^{27}Mg;

$^{56}Fe\ (n,p)^{56}Mn$; $^{27}Al\ (n,\alpha)^{24}Na$; and $^{63}Cu\ (n,2n)^{62}Cu$. The eight detectors provided a good sampling of the spectra in wide, but distinct, energy intervals. The results were generally in good agreement with other methods of spectrum determination such as time-of-flight and nuclear emulsion. Dodds (16) utilized seven activation reactions to measure the fast neutron spectrum in the permanent beryllium reflector of the High Flux Isotope Reactor. The reactions employed were: $^{27}Al\ (n,\alpha)^{24}Na$; $^{56}Fe\ (n,p)^{56}Mn$; $^{54}Fe\ (n,p)^{54}Mn$; $^{238}U(n,f)^{140}Ba$; $^{58}Ni\ (n,p)^{58}Co$; $^{24}Mg\ (n,p)^{24}Na$; and $^{32}S\ (n,p)^{32}P$. The author presents a good description of the materials and apparatus associated with the irradiations, counting equipment, and an excellent analysis of the Relative Deviation Minimization Method (RDMM) (17), the unfolding technique employed to obtain the solution.

McElroy and Kellog (18) reported the progress made in achieving high-accuracy measurements of fission rates, fuel burnup, and neutron exposure for material property changes through a coordinated interlaboratory effort. In addition to such subjects as foil set selection, neutron self-shielding corrections, and perturbation effects, the paper reports a number of improvements that have been made in the SAND-II algorithm. The improved procedure produces a smooth realistic appearing curve by reducing the amount of artificial structure originally generated by the iterative method of solution.

Greenwood et al. (19) reported an interlaboratory compar-

ison of the reaction rates measured by five groups. Nonfissile activation foils were irradiated in the Coupled Fast Reactivity Measurements Facility and gamma counted. Each group used an independently calibrated Ge(Li) detector, and in some cases a NaI (Tl) detector as well. The reaction rate values were all in good agreement, generally consistent to within ±2% with respect to each other. Based upon this report, it was concluded that for nonfissile foils, where the nuclear data are adequate, reaction rates can be determined with an accuracy of approximately ±2%.

As foil activation techniques gained increasing use in the area of spectrum measurement, many techniques were developed to calculate differential neutron flux from foil activation data. A review of these techniques is presented in section II.

II. THEORETICAL DEVELOPMENT

A. Spectrum Unfolding Techniques

The foil activation method for measuring neutron energy spectra involves the irradiation and activation of a set of selected foils followed by the subsequent determination of their saturated activities. Let m and n respectively be the number of target atoms and the reaction product atoms at time t and m_o be the initial number of target atoms (at t=o). The specific saturated activity (or response integral) A_{sp} of a given foil is

$$A_{sp} = \frac{A}{m_o} = \int_0^\infty \sigma(E)\, \varphi(E)\, dE \qquad (1)$$

where $\sigma(E)$ is the energy dependent microscopic cross section and $\varphi(E)$ is the steady state differential flux*. If N activation foils are irradiated, there are N response integrals defined by Equation (1) which could be solved for $\varphi(E)$.

Generally the number of energy groups of interest, M, is larger than the number of reactions used, and therefore there are N equations with M>N unknowns. To reach a solution, some assumptions have to be made as to the analytical form of $\varphi(E)$. Based upon the assumptions chosen, the methods to solve Equation (1) for $\varphi(E)$ can be divided into three main groups:

---

* For more details see section IV.

1. Mathematical methods

2. Perturbation methods

3. Weighting methods

As will be seen in the following pages, the above classification does not provide a sharp distinction among the various unfolding methods. This is because there are cases which feature an overlap of methods.

1. Mathematical methods

The assumptions concerning the analytical form of $\varphi(E)$ are purely mathematical. The methods which fall into this category include a) Flux Integral b) Step Function Approximation c) Polygonal d) Simple Polynonials e) Expansion in Orthonormal Combinations of Cross Section Curves f) Expansion in Orthonormal Combinations of Simple Polynomials and g) Successive Exponentials.

a) Flux integral method In this method, as discussed by Hughes (20), the cross sections for the threshold reactions used are assumed to be step functions. The step functions are characterized by their σ_{eff} and E_{eff} values. Therefore, the response integral of a detector can be expressed as

$$A_{sp} = \int_0^\infty \sigma(E)\,\varphi(E)\,dE = \sigma_{eff} \int_{E_{eff}}^\infty \varphi(E)\,dE$$

Values of E_{eff} for each threshold reaction employed are obtained by using an assumed fission spectrum for calibration as explained below.

The following is an example of how an unknown spectrum is obtained using this method. Suppose there are two different reactions characterized by σ_{eff_1}, E_{eff_1} and σ_{eff_2}, E_{eff_2}. The experimentally determined response integrals are given by

$$A_{sp1} = \underbrace{\int_0^\infty \varphi(E)\,\sigma_1(E)\,dE}_{A} = \sigma_{eff_1} \underbrace{\int_{E_{eff_1}}^{E_{max}} \varphi(E)\,dE}_{B} = \sigma_{eff_1} \Phi_1 \quad (1\text{-A})$$

$$A_{sp2} = \int_0^\infty \varphi(E)\,\sigma_2(E)\,dE = \sigma_{eff_2} \int_{E_{eff_2}}^{E_{max}} \varphi(E)\,dE = \sigma_{eff_2} \Phi_2 \quad (1\text{-B})$$

In Equations (1-A) and (1-B), σ_{eff_1} and σ_{eff_2} represent an average value of the cross sections $\sigma_1(E)$ and $\sigma_2(E)$. If A_{sp1} and A_{sp2} are measured and values of σ_{eff} and E_{eff} are selected, then the neutron flux in the energy interval $E_{eff_2} - E_{eff_1}$ can be calculated

$$\Phi_{12} = \Phi_1 - \Phi_2 = \int_{E_{eff_1}}^{E_{eff_2}} \varphi(E)\,dE = \frac{A_{sp1}}{\sigma_{eff_1}} - \frac{A_{sp2}}{\sigma_{eff_2}}$$

Extending the above procedure to a system of N reactions, the flux integrals could be evaluated for N-1 intervals. Values for σ_{eff_i} and E_{eff_i} are selected as follows:

- σ_{eff_i} is selected as the best average value of $\sigma i(E)$ over the energy interval of interest ($E_{eff_i} - E_{max}$), and equal to zero elsewhere.

- Once the value of σ_{eff_i} is chosen, a fission spectrum

(e.g. Cranberg or Watt) is selected to replace $\varphi(E)$ in Equation (1-A) part A. This part of Equation (1-A) can now be integrated to yield a value for Eeffi and finally the flux can be evaluated.

This is the simplest method; however, it provides no information for energies below the lowest threshold energy. Furthermore, its use is limited to cases where the actual spectrum is a close approximation to the fission spectrum.

b) Step function approximation In this method as outlined by Delattre, the total energy range of the fast neutrons is divided into N energy intervals; N being the number of threshold reactions used. The flux is assumed constant in each energy region. The energy range starts with E_1 as the lowest energy threshold and ends with E_{N+1} as the highest energy threshold (21, 22).

For the ith reaction the response integral is expressed as

$$A_{spi} = \int_{E_1}^{E_{N+1}} \sigma i(E)\,\varphi(E)\,dE = \varphi_1 \frac{\int_{E_1}^{E_2} \sigma i(E)\,dE}{E_2 - E_1} + \varphi_2 \frac{\int_{E_2}^{E_3} \sigma i(E)\,dE}{E_3 - E_2} + \cdots + \varphi_{N+1} \frac{\int_{E_N}^{E_{N+1}} \sigma i(E)\,dE}{E_{N+1} - E_N} \qquad (2)$$

Since $\sigma i(E)$ are considered to be known, φ_1, φ_2, ..., φ_{N+1} can be solved by solving N linear equations with N unknowns as defined by Equation (2). The solution provides a step function approximation to the actual spectrum. The set of Equations (2) can be written in a matrix notation:

$$[A] = [b][\varphi] \qquad (2\text{-}A)$$

where

$$[A] = \begin{vmatrix} A_1 \\ A_2 \\ \vdots \\ A_N \end{vmatrix} \qquad A_i = A_{spi}$$

$$[\varphi] = \begin{vmatrix} \varphi_1 \\ \varphi_2 \\ \vdots \\ \varphi_N \end{vmatrix}$$

and b_{ij} = general term of $[b]$

$$b_{ij} = \frac{1}{E_{j+1}-E_j} \int_{E_j}^{E_{j+1}} \sigma i(E)\, dE \qquad \text{with} \quad \begin{matrix} i = 1,N \\ j = 1,N \end{matrix}$$

Upon inverting Equation (2-A), values of φi can be calculated

$$[\varphi] = [b]^{-1}[A]$$

Although this is a simple method to use, a problem arise in selecting the energies E_2, E_3, ..., E_N. In fact, the main disadvantage of this method is that there are no logical methods for choosing E_1, ..., E_N. If it were to be used, the best scheme according to Ringle* is to choose a variety of energy arrays, to calculate the absolute value of $\left(\det\,[b]\right)$ for each array, and then to use the array which yields the largest value of $\left|\det\,[b]\right|$.

c) Polygonal method $\varphi(E)$ is represented by straight lines (23). The method assumes that the actual spectrum can be represented by a set of N values for the flux corresponding to points E_1, E_2, ..., E_N. N is the number of reactions used. It is further assumed that within each energy interval the flux varies linearly.

As in the Step Function Approximation, the number of flux constants and energy points must equal N. The energy point E_1 is chosen as the lowest energy at which activation can occur for any reaction, with E_N being the energy above which either $\varphi(E)$ or $\sigma(E)$ is zero.

The flux $\varphi(E)$ between E_1 and E_2 is

$$\varphi(E) = \varphi_1 + \left(\frac{\varphi_2 - \varphi_1}{E_2 - E_1}\right)(E - E_1) =$$

$$= \varphi_2 \left(\frac{E - E_1}{E_2 - E_1}\right) + \varphi_1 \left(\frac{E_2 - E}{E_2 - E_1}\right) \qquad (3)$$

---

* See page 28.

and

$$\varphi(E) = \varphi_N \left(\frac{E - E_{N-1}}{E_N - E_{N-1}} \right) + \varphi_{N-1} \left(\frac{E_N - E}{E_N - E_{N-1}} \right) \qquad (3\text{-A})$$

with $E_{N-1} \leqslant E \leqslant E_N$ and $i = 1, N$

Inserting Equations (3) and (3-A) in Equation (1), the following expression is obtained:

$$A_{spi} = \int_{E_1}^{E_2} \left[\varphi_2 \left(\frac{E - E_1}{E_2 - E_1} \right) + \varphi_1 \left(\frac{E_2 - E}{E_2 - E_1} \right) \right] \sigma i(E)\, dE +$$

$$+ \int_{E_2}^{E_3} \left[\varphi_3 \left(\frac{E - E_2}{E_3 - E_2} \right) + \varphi_2 \left(\frac{E_3 - E}{E_3 - E_2} \right) \right] \sigma i(E)\, dE + \ldots +$$

$$+ \int_{E_{N-1}}^{E_N} \left[\varphi_N \left(\frac{E - E_{N-1}}{E_N - E_{N-1}} \right) + \varphi_{N-1} \left(\frac{E_N - E}{E_N - E_{N-1}} \right) \right] \sigma i(E)\, dE \qquad (3\text{-B})$$

The set of Equations (3-B) can be written in matrix notation, thus

$$\left[A \right] = \left[b \right] \left[\varphi \right]$$

In this case the terms of matrix $\left[b \right]$ are given by

$$b_{ij} = \frac{1}{E_j - E_{j-1}} \int_{E_{j-1}}^{E_j} E\,\sigma i(E)\,dE - \frac{E_{j-1}}{E_j - E_{j-1}} \int_{E_{j-1}}^{E_j} \sigma i(E)\,dE +$$

$$+ \frac{E_{j+1}}{E_{j+1} - E_j} \int_{E_j}^{E_{j+1}} \sigma i(E)\,dE - \frac{1}{E_{j+1} - E_j} \int_{E_j}^{E_{j+1}} E\,\sigma i(E)\,dE$$

$$\text{for} \quad \begin{matrix} i = 1,N \\ j = 2,N-1 \end{matrix}$$

These coefficients can be calculated by selecting the energy intervals $E_1, \ldots, E_N$ and using the cross section data for each reaction. Once the elements of $\left[b \right]$ are determined, $\left[\varphi \right]$ can be obtained by solving the matrix equation.

$$\left[\Phi \right] = \left[b \right]^{-1} \left[A \right]$$

A comparison of experimental results using this method with the results of a 20 group calculation indicated that for neutron energies below 350 KeV, the polygonal method provides good agreement. However, for energies above 350 KeV the results are not satisfactory (22). This method suffers from the same disadvantages as the Step Function Approximation method.

d) Simple polynomial method In this method $\varphi(E)$ is represented by a polynomial in E (23)

$$\varphi(E) = a_0 + a_1 E + \dots + a_{N-1} E^{N-1}$$

Using N reactions, the coefficients a_0, a_1, ..., a_{N-1} can be determined in a polynomial of degree N-1.

Substituting the above expression in Equation (1), A_{spi} becomes

$$A_{spi} = a_0 \int_{Emin}^{Emax} \sigma i(E)\, dE = a_1 \int_{Emin}^{Emax} E\sigma i(E)\, dE + \dots +$$

$$+ a_{N-1} \int_{Emin}^{Emax} E^{N-1} \sigma i(E)\, dE$$

or, using matrix notation

$$\left[A\right] = \left[b\right] \left[a\right]$$

with the solution

$$\left[a\right] = \left[b\right]^{-1} \left[A\right]$$

where

$$b_{ij} = \int_{Emin}^{Emax} E^{j-1} \sigma i(E)\, dE$$

Reports on the use of this method are rare. Other polynomial methods, yet to be discussed, have been employed more frequently.

e) Expansion in orthonormal combinations of cross sections The spectral distribution $\varphi(E)$ is represented by a series of orthonormal energy dependent functions $\Psi_i(E)$ (24, 25). Thus

$$\varphi(E) = a_1 \Psi_1(E) + a_2 \Psi_2(E) + \ldots + a_N \Psi_N(E) = \sum_{i=1}^{N} a_i \Psi_i(E) \tag{5}$$

where N is the number of detector reactions used, and $\Psi_i(E)$ are linear combinations of the cross sections $\sigma_i(E)$

$$\Psi_1(E) = b_{11} \sigma_1(E) \tag{6-A}$$

$$\Psi_2(E) = b_{21} \sigma_1(E) + b_{22} \sigma_2(E) \tag{6-B}$$

$$\vdots$$

$$\Psi_N(E) = n_{N1} \sigma_1(E) + \ldots + b_{NN} \sigma_N(E) \tag{6-C}$$

or

$$\left[\Psi\right] = \left[b\right]\left[\sigma\right] \tag{7}$$

This leads to $\frac{N(N+1)}{2}$ constant coefficients b_{jk} and $\frac{N(N+1)}{2}$ non duplicated orthonormal condition equations with which b_{jk} are to be evaluated.

The coefficients b_{jk} can be calculated from an orthonormality condition

$$\int_0^\infty \psi_j(E)\,\psi_k(E)\,dE = \delta_{jk}$$

In fact, multiply Equation (6-A) by $\psi_1(E)$ and integrate

$$\int_0^\infty \psi_1^2(E)\,dE = \int_0^\infty b_{11}\,\sigma_1(E)\,\psi_1(E)\,dE = b_{11}^2 \int_0^\infty \sigma_1^2(E)\,dE = 1$$

Since the cross sections are known b_{11} can be calculated.

Multiplying Equation (6-B) by $\psi_1(E)$ and $\psi_2(E)$ and integrating, the following expressions are obtained:

$$\int_0^\infty \psi_1(E)\,\psi_2(E)\,dE = b_{11}\,b_{21}\int_0^\infty \sigma_1^2(E)\,dE + b_{11}\,b_{21}\int_0^\infty \left(\sigma_1^2(E) + \sigma_2^2(E)\right)dE = 0$$

$$\int_0^\infty \psi_2^2(E)\,dE = b_{21}^2 \int_0^\infty \sigma_1^2(E)\,dE + 2b_{21}b_{22}\int_0^\infty \sigma_1(E)\,\sigma_2(E)\,dE + b_{22}^2 \int_0^\infty \sigma_2^2(E)\,dE = 1$$

From these two equations b_{21} and b_{22} are determined.

In general, writing the equations in a matrix notation, the following equations are obtained:

$$[\varphi] = [a][\psi] \qquad \text{and} \qquad [\psi] = [b][\sigma] \tag{8}$$

where

$$[\varphi] = \varphi(E)$$

$$\left[a\right] = \left[\, a_1,\ a_2,\ \cdots,\ a_N \,\right]$$

$$\left[\Psi\right] = \begin{vmatrix} \Psi_1(E) \\ \Psi_2(E) \\ \vdots \\ \Psi_N(E) \end{vmatrix}$$

$$\left[\sigma\right] = \begin{vmatrix} \sigma_1(E) \\ \sigma_2(E) \\ \vdots \\ \sigma_N(E) \end{vmatrix}$$

$$\left[b\right] = \begin{vmatrix} b_{11} & 0 & 0 & \cdots & 0 \\ b_{21} & b_{22} & 0 & \cdots & 0 \\ b_{31} & b_{32} & b_{33} & \cdots & 0 \\ b_{N1} & b_{N2} & b_{N3} & \cdots & b_{NN} \end{vmatrix}$$

The inverse of Equation (8) is

$$\left[\sigma\right] = \left[b\right]^{-1}\left[\Psi\right] = \left[c\right]\left[\Psi\right] \qquad (8\text{-A})$$

with $\left[c\right] = \left[b\right]^{-1}$

The nth equation of the expression (8-A) can be written as

$$\sigma_n(E) = \sum_{l=1}^{n} c_{nl}\,\Psi_l(E)$$

Substituting this and Equation (5) in Equation (1), the specific activation becomes:

$$A_{spn} = \int_0^\infty \sum_{i=1}^{N} a_i \psi_i(E) \sum_{l=1}^{n} c_{nl} \psi_l(E) dE$$

or

$$A_{spn} = \sum_{i=1}^{N} a_i \sum_{l=1}^{n} c_{nl} \int_0^\infty \psi_k(E) \psi_l(E) \, dE$$

$$= \sum_{i=1}^{N} a_i \sum_{l=1}^{n} c_{nl} \delta_{il} = \sum_{l=1}^{n} c_{nl} \, a_l$$

or in matrix notation

$$\left[A\right] = \left[c\right] \left[a\right]$$

Upon inverting the above equation

$$\left[c\right]^{-1} \left[A\right] = \left[a\right]$$

and knowing that $\left[c\right]^{-1} = \left[b\right]$, $\left[b\right]$ becomes

$$\left[b\right] = \left[a\right] \left[A\right] \quad \text{and} \quad \left[a\right] = \left[b\right]\left[A\right]^{-1}$$

The flux spectrum is then found from

$$\Phi(E) = \sum_{i=1}^{N} a_i \psi_i(E) = \sum_{i=1}^{N} a_i \sum_{j=1}^{i} b_{ij} E^j$$

Comparing the Orthonormal Combinations of Cross Sections method with other unfolding methods, Ringle (26) states that this method provides accurate neutron flux spectrum determination and concludes that its use should be seriously considered.

g) Successive exponentials method In this method, the neutron energy is divided into suitable intervals. The flux $\varphi(E)$ in each interval is assumed to have the form (11)

$$\varphi(E) = A \exp(-kE)$$

The values of $\sigma_i(E)$ within each interval are the values reported in the literature except for the energy interval where $\sigma_i(E)$ starts to become different from zero. In this case $\sigma_i(E)$ is assumed to be a straight line

$$\sigma_i(E) = a_i + b_i E \qquad (9)$$

Bresesti (27) states that the use of linearized cross sections, as represented by Equation (9), is a source of error for this method. This is particularly true for detectors such as ^{238}U which do not have an energy dependent cross section that can be represented by a straight line.

2. Perturbation methods

These methods assume that $\varphi(E)$ differs only slightly from a fission spectrum. Thus, the main objective of the Perturbation methods is to determine parameters which characterize the deviation of $\varphi(E)$ from a fission spectrum. The representation of the actual flux may also include a weighting function (as is the case with weighting methods) to improve the representation

of the spectrum. Four examples of Perturbation methods are described in the following paragraphs. These are: a) Semi-Empirical Deviation b) Polynomial Deviation Function c) Orthonormal Deviation Function d) Spectral Indices.

a) Semi-empirical deviation method The spectral distribution $\varphi(E)$ is expressed as the product of a fission spectrum and a function f(B,E) which corrects for the deviation of the actual spectrum from a fission spectrum represented by S(E). B is a constant discussed below.

$$\varphi(E) = S(E)f(B,E)$$

In case of an infinite medium with uniformly distributed neutron sources

$$\varphi(E) = \frac{S(E)}{\Sigma(E)}$$

where S(E) is the source density and $\Sigma(E)$ denotes a macroscopic removal cross section. $\Sigma(E)$ is taken to be the sum of a constant term Σ_c, which represents inelastic scattering and absorption of neutrons in all materials except hydrogen, and $\Sigma_H(E)$ which takes into account the elastic scattering by hydrogen

$$\Sigma(E) = \Sigma_c + \Sigma_H(E)$$

Within the energy range from 2 to 12 MeV, $\sigma_H(E)$ can be represented by the following empirical relation (11)

$$\sigma_H(E) = 5.13\ E^{-0.725}$$

where E is expressed in MeV and $\sigma_H(E)$ in barns. Thus

$$\varphi(E) = \frac{S(E)}{\Sigma_c + \Sigma_H(E)} = \frac{S(E)}{\Sigma_c(1+BE^{-0.725})}$$

where $S(E)/\Sigma_c$ is a fission flux distribution divided by a constant, and $1/1+BE^{-0.725}$ is the energy dependent perturbation parameter.

The procedure for evaluating B, proposed by Dietrich in (11), is to calculate the response integrals of several threshold detectors for different values of B, to determine the corresponding experimental values of these response integrals, and finally to select the value of B which gives the best agreement.

This method is simple, but its application is limited to homogeneous reactor cores or to their immediate surroundings.

b) Polynomial deviation function In this method the deviation of the spectrum from a fission spectrum is represented by a polynomial

$$\varphi(E) = \varphi_{fis}(E)\,(a_o + a_1E + \ldots + a_NE^N)$$

The number of the threshold detectors used is equal to N+1 so as to provide N+1 equations with which to evaluate the N+1 unknowns. The calculation procedure is similar to the one described for the simple polynomial method.

c) Orthonormal deviation function The spectral distribution is represented by a fission spectrum times an orthonor-

nal combination of simple polynomials (28)

$$\varphi(E) = \varphi_{fis}(E) \sum_{i=1}^{M} a_i \psi_i(E)$$

For $\varphi_{fis}(E) = 1$ this method collapses to the method of Expansion in Orthonormal Combinations of Simple Polynomials (11).

d) Spectral indices In this method $\varphi(E)$ is represented as

$$\varphi(E) = CE^{\frac{1}{2}} \exp(-\theta E)$$

where E is in MeV and θ in MeV^{-1}. θ is to be adjusted from the fission distribution value of 0.775 to one which is more representative of the response integral values. The distribution has its maximum at

$$Emax = \frac{1}{2\theta}$$

The spectral index, S_{ij}, as defined by Grundl and Usner (8) is

$$S_{ij} = \frac{A_i(E)}{A_j(E)} = \frac{\int_0^\infty \sigma_i(E)\varphi(E)dE}{\int_0^\infty \sigma_j(E)\varphi(E)\,E} = \frac{\bar{\sigma}_i}{\bar{\sigma}_j}$$

where i and j refer to different reactions. The procedure for the determination of θ is similar to the one described for the Semi-Empirical Deviation method. Both experimental and calculational values of S_{ij} are determined for several values of θ. The value of θ which gives the best agreement between

the experimental and calculational values is the one to be used as the deformation parameter.

3. Weighting methods

The spectral distribution is represented by a mathematical expression such as polynomials, exponentials, etc. However, because an improved representation of the spectrum can be obtained by employing a weighting function, one is included. The Relative Deviation Minimization Method (RDMM) provides a good example of spectrum representation using weighting methods.

RDMM, as proposed by Di Cola (17), assumes the following expression for the unknown spectrum:

$$\varphi(E) = W(E) \sum_{i=1}^{N} a_i \Psi_i(E)$$

where W(E) is a weghting function which can be 1, the fission spectrum, e^{-aE}, or other functions. $\Psi_i(E)$ are a series of linearly independent functions.

The best approximation to $\varphi(E)$ is a function, $\bar{\varphi}_m(E)$ which minimizes the following quadratic form:

$$Q(m, a_1, \ldots, a_N) = \sum_{j=1}^{N} \left[\frac{A_{spj} - \int_0^\infty \sigma_j(E)\, \bar{\varphi}_m(E)\, dE}{A_{spj}} \right]^2$$

where $\bar{\varphi}_m$ is given by

$$\bar{\varphi}_m(E) = W(E) \sum_{i=1}^{m} a_i \Psi_i(E)$$

with $m \leqslant N$ and N being the number of reactions used.

Minimizing $Q(m, a_1, a_2, \ldots, a_N)$, for a given m, involves differentiation of $Q(m, a_1, a_2, \ldots, a_N)$ with respect to a_k as follows

$$\frac{\partial Q}{\partial a_k} = 0 \qquad k = 1, \ldots, m$$

The result is a set of m linear equations with m unknowns. In matrix form

$$\left[S\right]^T \left[S\right] \left[a\right] = \left[S\right]^T \left[1\right]$$

where S_{ij} and $S^T{}_{ij}$ are

$$S_{ij} = \frac{1}{A_{spi}} \int_0^\infty \sigma_i(E)\, W(E)\, \Psi_j \, dE \qquad \begin{matrix} i = 1, \ldots, N \\ j = 1, \ldots, m \end{matrix}$$

$$S^T{}_{ij} = \frac{1}{A_{spj}} \int_0^\infty \sigma_j(E)\, W(E)\, \Psi_i \, dE \qquad \begin{matrix} i = 1, \ldots, m \\ j = 1, \ldots, N \end{matrix}$$

For each value of $m \leqslant N$, there is a solution. Among these solutions, the one that minimizes Q is the best approximation to the spectral distribution $\varphi(E)$.

In order to establish the dependence of RDMM on the particular choice of $\Psi_i(E)$, Di Cola and Rota in (27) tested this method with experimental and theoretical data. They used exp (-E) as the weighting function and selected the following types of polynomials for $\Psi_i(E)$:

- Simple polynomials
- Orthonormal polynomials
- Laguerre polynomials
- Chebyshev polynomials

Theoretical data consisted of computer calculations of theoretically constructed "test data", while experimental data involved the following eight detectors: ^{237}Np, ^{238}U, ^{232}Th, ^{32}S, ^{58}Ni, ^{56}Fe, ^{27}Al (n,p), and ^{27}Al (n, α).

Significant differences were observed for high energy values of the experimental data. However, these differences did not appear when "test data" were used. This indicated that the results of RDMM can be considered as independent of the type of Ψ_i (E) functions used. Furthermore, RDMM data with experimental results indicated that for m = 5, 6, 7, the values of Q were not appreciably different from each other. This would indicate that a greater number of Ψ_i(E) functions would not improve the final results.

4. Comparison of methods

Within the energy range of about 2 to 30 MeV, Ringle (26) compared the following methods:

- Flux Integral method
- Step Curve method
- Polygonal method
- Expansion in Orthonormal Combination of Cross Sections
- Legendre Polynomial Expansion method

- Fourier Expansion method

The last three methods are examples of the Orthogonal Polynomial Expansion. In order to compare the above methods, ten different "trial spectra" were selected. These spectra included:

$\varphi_1(E) = 0.7$

$\varphi_2(E) = 1 - 0.05714E$

$\varphi_3(E) = \exp(-0.115E)$

and other spectra such as step curves and oscillating curves. For each method, the cross sections of the following reactions were used:

$^{58}Ni\ (n,p)\ ^{58}Co$

$^{31}P\ (n,p)\ ^{31}Si$

$^{56}Fe\ (n,p)\ ^{56}Mn$

$^{24}Mg\ (n,p)\ ^{24}Na$

$^{203}Tl\ (n,2n)\ ^{202}Tl$

$^{63}Cu\ (n,2n)\ ^{62}Cu$

Using the above spectra and cross sections, the activities were calculated and used as inputs for each method under investigation. The calculated spectra were then compared with the trial spectra. Based on these comparisons, Ringle made the following observations:

a) Flux Integral method, being sensitive to the choice of Eeff is too subjective and should not be considered for application.

b) Step Curve and Polygonal methods provide results which are dependent upon the choice of energy intervals. They are the only methods which represent the spectra by straight line segments. The best polygonal results were clearly better than the best results obtained by means of the Step Function method.

c) Cross Sections Expansion provided results which agreed well with experiment for all trial spectra.

d) The Legendre Expansion method provided good agreement with all trial spectra except for the step function fluxes.

e) The Fourier Expansion method provided generally poor agreement with the trial spectra.

In view of these results, Ringle (26) concluded that "Three methods give good results: the Cross Section Expansion method, which is good for both step function and continuous fluxes; the Legendre method, which is good for continuous fluxes and poor for step function fluxes; and the Polygonal method, which is reasonably good for both types of fluxes. Of these three, the Cross Section Expansion method is the best."

Other intercomparisons were accomplished by several investigators. Bresesti (27) noted that if the actual shape of $\varphi(E)$ is significantly different from the proposed trial spectrum, Step Function Approximation and Polygonal methods provide poor results. The method of Successive Exponentials provided unacceptable results in the first energy interval. This was

due to the fact that a linearized cross section shape does not adequately represent the energy variation of the cross section of the ^{238}U detector. The method of Spectral Indices, with one parameter, provided satisfactory results only at energies greater than 2 MeV (28).

III. COMPUTER CODES FOR SPECTRUM UNFOLDING

Within recent years, several computer codes have been developed to unfold neutron spectra from the measured activities of a set of activation foils (29, 30, 31). The measured specific activity A_{spi} (or response integral) of activation reaction i is related to the spectrum by Equation (10)

$$A_{spi} = \int_0^\infty \sigma_i(E)\varphi(E)\,dE \qquad i = 1, 2, \ldots N \qquad (10)$$

Generally, the unfolding technique incorporated into the computer code is produced by the following procedures:

1. The energy domain of $\varphi(E)$ is divided into M energy intervals; M being generally much greater than N, the number of detector reactions to be activated.
2. Equations of type (10) are approximated by a series of linear equations

$$A_{spi} \cong \sum_{j=1}^{M} \sigma_{ij}\,\varphi_j$$

with each energy interval represented by a particular value of j.
3. A trial spectrum, based upon some a priori knowledge of $\varphi(E)$, is used as the initial or trial value for $\varphi(E)$. Detector foil activations are calculated, based on the trial spectrum. These

calculations are compared with the experimentally determined activities produced by the actual neutron flux.

4. The computer codes modify the trial spectrum so that, within experimental errors, measured activities equal calculated activities.

As mentioned earlier, the number of energy intervals M is generally greater then N, the number of reaction used. This means that the solution spectrum is not unique, and that portions of it will depend entirely on such input data as the trial spectrum, cross sections, etc.

Several spectrum unfolding codes are available; the more widely used codes are SPECTRA (developed in 1966), SAND-II (1967), and CRYSTALL BALL (1974). A brief description of SPECTRA and CRYSTALL BALL as well as a more detailed description of the SAND-II code are given below.

A. SPECTRA

This method, developed by Greer and Walker (32), Greer et al. (33), is based upon a Perturbation method in which an initial trial spectrum is assumed and then modified with successive iterations so that it will agree with the activation data. The flux evaluated with the SPECTRA code represents the flux which minimizes the least squares error between the measured and calculated activities.

Let $\varphi_1, \varphi_2, \ldots, \varphi_M$ correspond to energy values $E_1, E_2, \ldots, E_M$, respectively. Then $\varphi(E)$, in the interval E_k to E_{k+1},

is given by

$$\varphi(E) = \varphi_{k+1}\left(\frac{E - E_k}{E_{k+1} - E_k}\right) + \varphi_k\left(\frac{E_{k+1} - E}{E_{k+1} - E_k}\right) \qquad (11)$$

It is assumed that there is no flux below E_1 and that the flux at E_M is zero, i.e, $\varphi_M = 0$. Substitution of Equation (11) into Equation (10) yields

$$A_{spi} = \int_{E_1}^{E_2} \left[\varphi_2\left(\frac{E - E_1}{E_2 - E_1}\right) + \varphi_1\left(\frac{E_2 - E}{E_2 - E_1}\right)\right]\sigma_i(E)\, dE +$$

$$+ \int_{E_2}^{E_3} \left[\varphi_3\left(\frac{E - E_2}{E_3 - E_2}\right) + \varphi_2\left(\frac{E_3 - E}{E_3 - E_2}\right)\right]\sigma_i(E)\, dE + \ldots +$$

$$+ \int_{E_{M-1}}^{E_M} \left[\varphi_M\left(\frac{E - E_{M-1}}{E_M - E_{M-1}}\right) + \varphi_{N-1}\left(\frac{E_M - E}{E_M - E_{M-1}}\right)\right] \sigma_i(E)\, dE \qquad (12)$$

In Equation (12) i = 1, 2, ..., N, where N is the number of activation reactions used and $N \leqslant M$. This set of equations can be written as a matrix equation

$$[A] = [C][\varphi]$$

where

$$[A] = \begin{vmatrix} A_1 \\ A_2 \\ \vdots \\ A_M \end{vmatrix} \qquad [\varphi] = \begin{vmatrix} \varphi_1 \\ \varphi_2 \\ \vdots \\ \varphi_N \end{vmatrix}$$

and $[C]$ is an M x N matrix whose entries are defined by the following expression:

$$C_{ji} = \int_{E_{i-1}}^{E_i} \frac{E - E_{i-1}}{E_i - E_{i-1}} \sigma_j(E)\, dE + \int_{E_i}^{E_{i+1}} \frac{E_{i+1} - E}{E_{i+1} - E_i} \sigma_j(E)\, dE$$

For C_{j1} the value E_o is defined to be E_1 and for C_{jN}, E_{N+1} is defined to be E_N.

In order to solve Equation (11), it is assumed that the rank of $[C]$ is M and the first M x N submatrix of $[C]$ is nonsingular. Denoting the calculated activities by A_C, then the least squares error E between the measured activity A and the calculated activity A_C is

$$[E] = ([A_C] - [A])^T([A_C] - [A])$$

E is minimum with respect to φ when

$$\frac{\partial E}{\partial \varphi} = 0$$

$$\frac{\partial^2 E}{\partial \varphi^2} > 0$$

Thus,

$$\frac{\partial E}{\partial \varphi} = 2\,[C]^T\left([A_C]-[A]\right) = 2\left([C]^T[C][\varphi]-[C]^T[A]\right) = 0$$

If $[C]^T[C]$ is nonsingular,

$$[\varphi] = \left([C]^T[C]\right)/2[C]^T[A]$$

this is a valid solution only when the number of energy intervals is equal to the number of reactions used. However, when N is greater then M, the matrix $[C]^T[C]$ is singular so no solution can be obtained directly. In this case a best guess spectrum, denoted by $[\varphi_o]$, is selected to represent the initial values of $[\varphi]$ and a new error function is defined as follows:

$$[E_1] = \left([A_C] - [A]\right)^T\left([A_C] - [A]\right) + \left([\varphi]-[\varphi_o]\right)^T\left([\varphi] - [\varphi_o]\right)$$

The new error function $[E_1]$ is the sum of the least squares error between $[A]$ and $[A_C]$ plus the least squares error between a solution and the initial guess solution. The new function $[E_1]$ is minimal with respect to φ when the first and second partial derivatives of $[E_1]$ respect to φ are 0 and > 0, respectively.

$$\frac{\partial E_1}{\partial \varphi} = 2 C^T \left([A_C] - [A] \right) + 2[I]^T \left([\varphi] - [\varphi_o] \right) = 0 \qquad (13)$$

$$\frac{\partial^2 E_1}{\partial \varphi^2} = [C]^T [C] + [I]$$

If $[C]^T[C]+[I]$ is positive definite, then a unique solution to Equation (13) exists and φ can be determined.

The above technique is incorporated in the SPECTRA code, which is capable of computing differential flux up to a maximum of 50 energy points. The code contains a cross section library of 28 reactions, taken from the compilation of McElroy (14).

B. CRYSTALL BALL

The code, developed by Kam and Stallman (34), is based on a direct approximation of integral equations by linear combination of integral operators. In this method the measured specific saturation activities A_{spi} are related to the unknown spectrum $\varphi(E)$ through the integral

$$A_{spi} = \int_0^\infty \varphi(E)\, \sigma_i(E)\, dE + \breve{E}_i \qquad i = 1, 2, \ldots, N, \qquad (14)$$

where $\breve{E}_i$ are measuring errors which have an estimated variance ν_i defined as

$$\overline{\nu^2_i} = \left(\frac{\overline{E_i}}{A_{spi}}\right)^2$$

The method assumes that the general shape of $\varphi(E)$ is close to an a priori estimate of the actual spectrum. Denoting with $\Psi(E)$ this trial spectrum, the solution spectrum has to minimize S^2

$$S^2 = \int_0^\infty \left[\frac{d}{dE}\ \frac{\varphi(E)}{\Psi(E)}\right]^2 W(E)\, dE \qquad (15)$$

where $W(E) = \frac{k}{E}$ and k is a constant. Furthermore, the solution is subject to the condition that the weighted mean square error remains below a given tolerance limit f

$$\sum_{i=1}^{N} \left(\frac{\overline{E_i}}{\nu_i}\right)^2 < f$$

The trial spectrum in Equation (15) can be written as

$$\Psi(E) = \varphi(E) + F(E)$$

where F(E), the spectrum deviation term, is the difference between the actual and the trial spectrum. The method assumes that the trial spectrum, being a close approximation to the true spectrum, can be expressed as a linear combination of the measured activities A_{spi} as follows:

$$\Psi(E) = \varphi(E) + F(E) = \sum_{i=1}^{N} C_i \, A_{spi}$$

Therefore,

$$F(E) = \sum_{i=1}^{N} C_i \left[\int_0^{\infty} \varphi(E) \, \sigma_i(E) \quad E + \breve{E}_i \right] - \varphi(E)$$

or using Dirac's δ-function F(E) can be written as

$$F(E) = \int_0^{\infty} \left[\sum_{i=1}^{N} C_i \, \sigma_i(E) - \delta(E - E') \right] \varphi(\acute{E}) \, d\acute{E} + \sum_{i=1}^{N} C_i \, E_i$$

The problem of solving the activation equation with respect to $\varphi(E)$ becomes the problem of minimizing F(E).

Skipping the mathematical elaborations (35), the true spectrum $\varphi(E)$ at a given energy E_j is calculated to be

$$\tilde{\varphi}(E_j) = \Psi(E_j) \sum_{i=1}^{N} C_{ij} \, R_i$$

where R_i is the ratio of measured to calculated activity. Kam and Stallman arrive at an expression for the difference between $\varphi(E)$ and $\tilde{\varphi}(E)$ which is a linear functional in terms of $\frac{d}{dE} \frac{\varphi(E)}{\Psi(E)}$

and the error terms $\tilde{E}_i$. Minimizing the norm of this functional is equivalent to minimizing D, defined as

$$D = S^2 + g^2 f$$

where g determines how far the tollerance limit f is to be reduced within the approximation.

The algorithm consists of an iterative procedure in which an output spectrum for a given g is used as input spectrum in the next step. Numerical experience obtained by the authors has shown that the output spectrum is relatively insensitive to the choice of the initial estimate of the spectrum. However, this does not apply to the energy intervals which are poorly covered by the detector response. In energy regions not covered by the detectors, the unfolded spectrum is solely determined by the input spectrum. This does not necessarily mean that the solution will be equal to the trial spectrum. The solution spectrum in these energy regions may be a multiple of the trial spectrum, or changed in such a way as to provide a smooth transition from the input spectrum to the solution spectrum. The latter applies to such other codes as SPECTRA and SAND-II as well.

C. SAND-II

This code developed by McElroy and collaborators (14), provides a best fit spectrum for a given input set of "infinitely dilute" foil activities. The term "infinitely dilute"

means that the density of target nuclei is small enough to preclude such effects as self-absorption and self-shielding. The measured input activities are corrected to specific activities and expressed in disintegrations per second per target nucleus. The energy range of the solution spectrum is from 10^{-10} MeV to 18 MeV, divided in 620. There are 45 intervals per decade up to 1 MeV, and 170 intervals between 1 and 18 MeV*. The problem is essentially to solve for 621 unknown differential flux values in a system of N linear activity equations; N being the number of reactions used.

The calculational procedure consists of selecting a "best guess" for the initial input spectrum and then iterating to find a final spectrum consistent with the input data. Since the number of reactions used is much smaller than the number of energy intervals, the solution is not unique. Therefore, the appropriateness of the solution depends upon a suitable choice of the initial spectrum (e.g. fission or Maxwellian). The SAND-II iterative procedure involves the following steps:

1. Activities are calculated for each reaction employed. The calculation is based on the current iterative spectrum and an evaluated cross section library, which is part of the SAND-II

---

* The code used in this work is modified so that the energy intervals are reduced from 620 (original SAND-II) to 100. See section VI.

code.

2. The calculated and measured activities for each foil are compared and a correction factor associated with the flux in the appropiate energy range for each foil is found. This factor, $R_i^{(k)}$ is used for the determination of an "activity-weighted correction term" for the flux in each iteration.

3. A weighting function, $W_{ij}^{(k)}$, is obtained for each foil. This energy dependent function is proportional to the sensitivity function (the product of differential flux and differential cross section) of the foil calculated using the flux determined in the current iteration.

4. Since a number of different foils will have non-zero cross sections in a given energy interval, the weighting functions are combined to obtain an average correction factor at each energy. The procedure is based on the comparison of measured to calculated activity for each foil and on the relative contribution of the flux, at the given energy, to the activity of a given foil.

5. The average correction factors are then applied to the current iterative flux value at each energy to obtain the next iterative flux spectrum.

6. The criterion incorporated in SAND-II for recognizing an acceptable solution is based on a comparison of successive differential flux iterations. A solution is considered to have been achieved when the percent difference between two successive

values is smaller than a specified number, entered as an input to the program.

For a mathematical representation of the procedures, the following symbols are used.

A_{spi} = measured activity for ith foil reaction (specific saturation activity corrected for self-shielding, self-absorption, etc.);

$A_i^{(k)}$ = calculated activity for the ith reaction, based on the kth iterative spectrum;

$\varphi^{(k)}(E)$ = kth iterative differential flux;

E_j = energy of the ith energy point;

$I_j^{(k)}$ = integral flux in the jth energy interval, between E_j and E_{j+1} for the kth iteration;

$\sigma_i(E)$ = ith foil reaction cross section for a specific neutron interaction;

$A_{i,j}^{(k)}$ = the portion of $A_i^{(k)}$ contributed by neutrons in the jth energy interval between E_j and E_{j+1};

$\sigma_{Cd}(E)$ = removal cross section for cadmium covering the foils;

N_{Cd} = nuclei density for cadmium covers;

X_{Cd} = thickness of cadmium covers;

j = 1, 2, ..., M, where M is energy interval index (M=620 for original SAND-II and M=100 for the code used in

this work;

i = 1, 2, ..., N foil index;

k = 1, 2, ..., iteration index.

Starting from a set of activation equations defined by the Equation (10), the portion of activity contributed by neutrons with energy between E_j and E_{j+1} (and calculated for ith cadmium covered foil) is

$$A_{ij}^{(k)} = \int_{Ej}^{E_{j+1}} \sigma_i(E)\ \varphi^{(k)}(E)\ \exp\left(-N_{Cd}\ X_{Cd}\ \bar{\sigma}_{Cd,j}\right) dE \qquad (16)$$

In Equation (16) $\bar{\sigma}_{Cd,j}$ is cadmium removal cross section averaged over the energy interval $E_{j+1} - E_j$:

$$\bar{\sigma}_{Cd,j} = \frac{\int_{E_j}^{E_{j+1}} \sigma_{Cd}(E)\ \varphi^{(k)}(E)\ dE}{\int_{E_j}^{E_{j+1}} \varphi(E)\ dE} \cong$$

$$\cong \frac{\int_{E_j}^{E_{j+1}} \sigma_{Cd}(E)\, dE}{\int_{E_j}^{E_{j+1}} dE} \qquad (17)$$

The approximation in Equation (17) assumes that the $\bar{\sigma}_{Cd,j}$ is independent of the kth iterative flux. Errors introduced by the above assumption are negligible when compared to the errors introduced by neglecting the complicated dependence of the neutron scattering effect on the geometry of each specific case. These errors are in turn negligible because of the relative magnitudes of the cadmium attenuation effects.

The values of $\sigma_i(E)$ in Equation (16) can be substituted by the interval averaged cross section $\bar{\sigma}_{ij}^{(k)}$

$$\bar{\sigma}_{ij}^{(k)} = \frac{\int_{E_j}^{E_{j+1}} \sigma_i(E)\, \varphi^{(k)}(E)\, dE}{\int_{E_j}^{E_{j+1}} \varphi^{(k)}(E)\, dE} \qquad (18)$$

In view of the fine structure of $\sigma_i(E)$ for many activation reactions used, the numerical calculation of Equation (18) for

these reactions would require a much finer subdivision of energy interval. For the purpose of calculation, however, it is assumed that the kth iterative differential flux does not vary with energy over the $E_{j+1} - E_j$ interval, that is

$$\varphi^{(k)}(E) = \varphi_j^{(k)} \qquad \text{for} \quad E_j \leqslant E \leqslant E_{j+1}$$

thus Equation (18) reduces to

$$\bar{\sigma}_{ij}^{(k)} \cong \bar{\sigma}_{ij} = \frac{\int_{E_j}^{E_{j+1}} \sigma_i(E)\, dE}{\int_{E_j}^{E_{j+1}} dE} \tag{19}$$

The calculation of $\sigma_i(E)$, with the assumption expressed in Equation (19), becomes independent of k and Equation (16) becomes

$$A_{ij}^{(k)} = \bar{\sigma}_{ij} \int_{E_j}^{E_{j+1}} \varphi^{(k)}(E) \exp\left(- N_{Cd}\, X_{Cd}\, \bar{\sigma}_{Cd,j} \right) dE$$

or

$$A_{ij}^{(k)} = \bar{\sigma}_{ij} \Phi_j^{(k)} \exp\left(-N_{Cd} X_{Cd} \bar{\sigma}_{Cd,j}\right) \tag{20}$$

where $\Phi_j^{(k)}$, the integral flux in the jth energy interval is defined as

$$\Phi_j^{(k)} = \int_{E_j}^{E_{j+1}} \varphi^{(k)}(E) dE$$

Equation (20) is the calculated activity of the jth energy interval which summed over the M energy interval, yields the iterative calculated activity of the ith reaction over the entire energy range

$$A_i^{(k)} = \sum_{j=1}^{M} A_{ij}^{(k)}$$

For instance, at iteration 0 $\varphi^{(0)}(E)$ is unperturbed and is equal to the input spectrum) the calculated activity $A_i^{(0)}$ is given by

$$A_i^{(0)} = \sum_{j=1}^{M} \bar{\sigma}_{ij} \Phi_j^{(0)} \exp\left(-N_1 X_1 \bar{\sigma}_{1,j}\right)$$

$A_i^{(0)}$ should be iterated k times so that $A_i^{(k)}$ becomes equal to the measured activity A_{spi}, within the specified experimental error.

The mathematical procedure for the flux iteration is based on two parameters: the activity weighting function $W_{ij}^{(k)}$, and the ratio of measured to calculated activity $R_i^{(k)}$, which are defined as follows:

$$W_{i1}^{(k)} = A_{i1}^{(k)} \Big/ A_{spi}^{(k)} \qquad \text{(for } j = 1\text{)} \qquad \text{(21-A)}$$

$$W_{iM+1}^{(k)} = A_{iM}^{(k)} \Big/ A_{spi}^{(k)} \qquad \text{(for } j = M\text{)} \qquad \text{(21-B)}$$

$$W_{ij}^{(k)} = \frac{1}{2}\left(A_{ij}^{(k)} + A_{ij-1}^{(k)}\right) \Big/ A_{spi}^{(k)} \qquad \text{(for } j = 2, \ldots, M\text{)} \qquad \text{(21-C)}$$

and

$$R_i^{(k)} = A_{spi} \Big/ A_i^{(k)} \qquad \text{(22)}$$

These parameters, defined by Equations (21) and (22), are combined to give $C_j^{(k)}$, the "activity-weighted correction term."

$$C_j^{(k)} = \sum_{i=1}^{N} W_{ij}^{(k)} \ln R_i^{(k)} \Big/ \sum_{i=1}^{N} W_{ij}^{(k)}$$

Iteration are successively performed according to Equation (23)

$$\varphi_j^{(k+1)} = \varphi_j^{(k)} \exp\left[C_i^{(k)}\right] \tag{23}$$

If for a given j : $\sum_{i=1}^{N^{(k)}} W_{ij}^{(k)} = 0$, log-log interpolation is used to obtain the next (k+1) value of differential flux. The interpolation is performed between the nearest lower j and the nearest higher j for which

$$\sum_{i=1}^{N^{(k)}} W_{ij} \neq 0$$

However, if such j cannot be found, an extrapolation is performed based on one of several alternate forms such as 1/E, fission, etc., which is selected as an input option.

If the solution is obtained on the qth iteration, then the relation between $\phi_j^{(q)}$ (final solution) and $\varphi_j^{(0)}$ (initial input) is given by

$$\varphi_j^{(q)} = \varphi_j^{(0)} \exp\left[\sum_{p=0}^{q-1} C_j^{(p)}\right] \tag{24}$$

Differential flux solutions given by Equation (24) are then integrated to provide the integral flux solution defined by

$$\Phi\left(E_j,\ E_{M+1}\right) = \sum_{s=j}^{M} \Phi_s^{(1)} = \int_{E_j}^{E_{M+1}} \varphi^{(q)}(E)\, dE$$

Given the differential solutions $\varphi_j^{(q)}$, the energy limits of sensitivity E_i and E_i' can be evaluated. These limits are defined such that 95% of the activation of the ith foil is produced by $E>E_i$, and the same portion is produced by neutrons of $E<E_i'$. Equations (25) indicate the mathematical definition of E_i and E_i'

$$\int_{E_i}^{E_{M+1}} \varphi^{(q)}(E)\, \sigma_i(E)\, \exp -\left[N_{Cd}\, X_{Cd}\, \sigma_{Cd}(E)\right] dE = \int_{E_i}^{E_{M+1}} \hat{A}(E)\, dE$$

$$= \int_{E_i}^{E_i'} \hat{A}(E)\, dE = 0.95 \int_{E_i}^{E_{M+1}} \hat{A}(E)\, dE \qquad (25)$$

D. Intercomparison of the Unfolding Codes

In a mathematical intercomparison of SAND-II, SPECTRA, RDMM, and two other codes (PARAMETER and MESCO), Dierckx (36) reported the following general conclusions:

a) The codes recommended for use were either SAND-II or SPECTRA.

b) Equivalent results are obtained from both codes.

c) SAND-II is slightly superior because it is less sensitive to the choice of input spectrum and its computing speed is faster.

In another intercomparison by Dierckx, the performance characteristics of the above codes and CRYSTALL BALL were determined by using each code to analyze the same experimentally obtained activation data (37). The general results of the intercomparison are given in Table 1. In addition, the following conclusions were reported:

a) CRYSTALL BALL and SAND-II are able to calculate the desired spectra fairly well, even with unreasonable input spectra. In such cases, starting with 1% accuracy in the activation data, solution spectra with errors of $\pm$20% are obtained.

b) Only SPECTRA, SAND-II, and CRYSTALL BALL are able to give moderate spectral details.

c) The unfolding codes recommended for use are SAND-II, SPECTRA, and CRYSTALL BALL.

In order to intercompare the unfolding codes, the IAEA (International Atomic Energy Agency) provided various laboratories with experimental activation data (38). These data were obtained using different fast neutron spectra such as those from Godiva core and a fast breeder mock-up.

Table 1. Intercomparison of the spectrum unfolding codes

	PARAMETERS	RDMM	MESCO	SPECTRA	CRYSTALL BALL	SAND-II
energy range	thermal to fast (14 MeV)					
solution model	simple	matrix equations				simple no matrix equations
solution	physical bound to mathematical expressions	not always physically acceptable	sometimes no solution is found	lowest Q* avoiding oscillations and negative fluxes		
Q attainable	moderate bound to solution imposed			as low as one likes to have it		
sensitivity to trial spectrum	not	great	greatest	small	smallest	
spectral details	few, bound to solution imposed			moderate bound to broad resolution of detectors		
error in the differential spectrum**	bound to solution imposed			±5% in each point		

*Q is the least squares difference between the measured and calculated activities
** in the energy range covered by the detectors and for detector activity errors of about ±2% (intercalibrated in a standard spectra)

Since the activation data were not accompanied by either cross section information or input spectra, the intercomparison of the solutions provided by the various codes was very difficult. This is because the general shape of the solution spectrum depends in great measure on the input spectrum. The intercomparison of the results were in part a comparison of input spectra and cross sections and in part a comparison of the characteristics of the codes. In fact, the solution spectra, obtained using different cross section libraries and different "guess spectra," varied greatly. However, it was concluded that the SAND-II and SPECTRA codes were suitable for spectrum unfolding while CRYSTALL BALL needed further investigation.

Using published experimental activity data, Zijp (39) intercompared four neutron spectrum unfolding codes: CRYSTALL BALL, RFSP-JUL (a slightly modified version of SPECTRA), SAND-II, and SANDPET (mainly a SAND-II code incorporating also a Monte Carlo error analysis code). The codes were intercompared using identical activity data, input spectra, and cross sections values. The latter consisted of the ENDF/B-IV dosimetry file and an updated SAND-II library. The results can be summarized as follows:

1. Different unfolding codes do not give the same solution for the same input data. The solutions found were significantly different from each other.

2. There were no energy regions for which all the unfolding codes gave insignificant differences.

3. CRYSTALL BALL introduced the largest modification to the input spectrum, and SAND-II the smallest. The modifications seemed to be a smooth function of energy in the case of CRYSTALL BALL, while SAND-II sometimes introduced sharp oscillations reminiscent of the resonance region for certain cross sections. It should be noted that, unlike the other codes, SAND-II runs were performed without using a curve smoothing procedure.

4. Variations of the input activities in accordance with their reported experimental errors give rather small variations in the output spectrum. However, large variations in the solution are observed if cross sections variations are also considered.

IV. NEUTRON ACTIVATION EQUATIONS

A. General Equations

The neutron activation equation, in its general form, involves the flux as a function of energy and time: $\varphi = \varphi(E,t)$. To derive the equations, the symbols used in section III, including those redefined below for convenience, will be used:

n = number of activation product atom in a given target material at time t;

m = number of target atoms at time t;

m_o = number of target atoms at time $t_o=0$

$\bar{\sigma}_{mn}(t)$ = spectrum-averaged cross section for reaction transmuting the "m" atoms into the "n" atoms;

$\bar{\sigma}_n(t)$ = total spectrum-averaged cross section for reactions which remove any of the "n" atoms;

$\bar{\Phi}(t)$ = time dependent flux = $\int \varphi(E,t)\, dE$

λ_n = decay constant of the "n" atoms;

The net time-rate of production of the "n" atoms is

$$\frac{dn}{dt} = m\, \bar{\sigma}_{mn}(t)\, \bar{\Phi}(t) - n(\, \bar{\sigma}_n(t)\, \bar{\Phi}(t) + \lambda_n) \qquad (26)$$

where $\bar{\sigma}_{mn}(t)$ and $\bar{\sigma}_n(t)$ are defined as follows:

$$\bar{\sigma}_x(t) = \frac{\int_o^\infty \sigma_x(E)\, \varphi(E,t)\, dE}{\int_o^\infty \varphi(E,t)\, dE} \qquad x = n,\ mn,\ \ldots, \qquad (27)$$

The "burn-up" rate of target atoms is

$$\frac{dm}{dt} = -m\,\bar{\sigma}_m(t)\,\bar{\Phi}(t)$$

with solution

$$m = m_o \exp\left[-\int_o^t \bar{\sigma}_m(t')\,\bar{\Phi}(t')\,dt'\right] \tag{28}$$

Substituting Equation (28) in Equation (27) yields

$$\frac{dn}{dt} = \bar{\sigma}_{mn}(t)\,\bar{\Phi}(t)\,m_o \exp\left[-\int_o^t \bar{\sigma}_m(t')\,\bar{\Phi}(t')\,dt'\right]$$

$$- n\,(\bar{\sigma}_n(t)\,\bar{\Phi}(t) + \lambda_n)$$

which has the following solution:

$$n(t) = m_o \exp\left[-\lambda_n t - \int_o^t \bar{\sigma}_n(t')\,\bar{\Phi}(t')\,dt'\right] \int_o^t \bar{\sigma}_{mn}(t')\,\bar{\Phi}(t')$$

$$\exp\left[\lambda t' + \int_o^t \bar{\sigma}_n(t'')\;\bar{\Phi}\;(t'') - \bar{\sigma}_m(t'')\,dt''\right]dt' \tag{29}$$

If it is assumed that the burn-up of the "m" and the "n" atoms is negligible*, that is

---

* The burn-up case will be considered separately in this section.

$$\bar{\sigma}_m(t)\,\Phi(t) \ll \lambda_n \qquad \text{and} \quad \bar{\sigma}_n(t)\,\Phi(t) \ll \lambda_n$$

then, Equation (29) reduces to

$$n(t) = m_o \exp(-\lambda_n t) \int_o^t \bar{\sigma}_{mn}(t')\,\Phi(t')\,\exp(\lambda_n t')\,dt' \qquad (30)$$

In the steady-state case, where the flux and cross sections are constant with time, Equation (30) becomes

$$n(t) = m_o \exp(-\lambda_n t)\,(\bar{\sigma}_{mn}\Phi) \int_o^t \exp(\lambda_n t')\,dt'$$

which has the following solution:

$$n(t) = \frac{m_o}{\lambda_n}\,\bar{\sigma}_{mn}\Phi\left[1-\exp(-\lambda_n t)\right]$$

The activity of the "n" atoms is

$$a(t) = n(t)\lambda_n$$

and the corresponding saturated activity is:

$$A'(t) = \frac{a(t)}{\left[1-\exp(-\lambda_n t)\right]} = m_o\,\bar{\sigma}_{mn}\,\Phi$$

By substituting the expression for $\bar{\sigma}_{mn}$, defined by Equation (27) and recalling the definition of Φ, the following general equation is obtained:

$$A' = m_o \int_0^\infty \sigma_{mn}(E)\, \varphi(E)\, dE \qquad (31)$$

Theoretically, A'/m_o, defined by Equation (31), should be equal to the Corrected Reaction Rate (CRR) obtained from the activity measured of the irradiated foils.

B. Determination of Reaction Rates

Generally, the irradiation of activation detectors involves the exposure of a set of foils for an irradiation period t_i in the neutron environment of interest. Following a waiting period of t_w, each foil is analyzed for specific Gamma-ray photo peaks and counted for a counting period of t_c. The net area under the photopeaks of interest is computer-calculated.

The result will be CPA, the Corrected Peak Area, and is related to CRR, the Corrected Reaction Rate, through the following equations:

$$CRR = A'/m_o = \lambda \frac{CPA}{\epsilon b} \times \frac{1}{m' pf} \times \frac{\exp(\lambda t_w)}{1-\exp(-\lambda t_i)} \times$$

$$\frac{C_1\, C_2\, C_3\, C_4\, C_5}{1-\exp(-\lambda t_c)} \qquad (32)$$

where

ϵ = detector efficiency

b = Gamma-ray branching ratio

p = purity of the foil

f = fraction of the isotope of interest ($m_o = m' pf$)

C_0 = isomeric reaction correction factor

C_1 = reaction product burn up correction factor

C_2 = power correction factor

C_3 = self-shielding

C_4 = flux gradients

C_5 = other correction factors

1. Isomeric reaction correction

For such reactions as $^{58}Ni(n,p)^{58}Co$, the activation product isotope, in this case ^{58}Co, is the result of two different reactions, as shown in the following scheme:

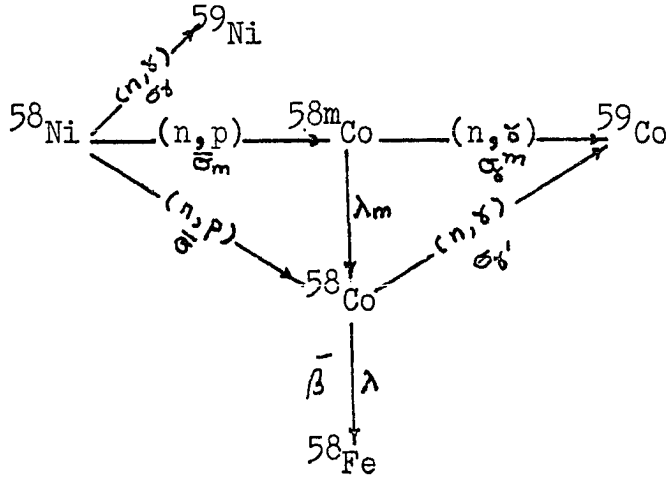

The notations used are:

σ_γ = ^{58}Ni thermal absorption cross section

$\bar{\sigma}_m$ = ^{58}Ni average fast neutron cross section for the formation of ^{58m}Co

$\bar{\sigma}$ = ^{58}Ni average fast neutron cross section for the formation of ^{58}Co

$(\bar{\sigma} + \bar{\sigma}_m)$ = ^{58}Ni total average fast neutron cross section for the formation of ^{58m}Co

σ_γ^m = ^{58m}Co thermal absorption cross section

$\sigma_{\gamma'}$ = ^{58}Co thermal absorption cross section

$n(x)$ = number of atoms of nuclide x at time t

$n_o(x)$ = number of atoms of nuclide x at time t_o

$n_{tw}(x)$ = number of atoms of nuclide x after a waiting time tw.

During irradiation, the time rate of change of the target atoms ^{58}Ni, ^{58m}Co, and ^{58}Co are as follows;

$$\frac{dn(^{58}Ni)}{dt} = -n(^{58}Ni)\left[\sigma_\gamma \int_o^{E_{thrs}} \varphi(E)\,dE + (\bar{\sigma} + \bar{\sigma}_m)\int_{E_{thrs}}^{\infty} \varphi(E)\,dE\right] \tag{33}$$

$$\frac{dn(^{58m}Co)}{dt} = n(^{58}Ni)\,\bar{\sigma}_m \int_{E_{thrs}}^{\infty} \varphi(E)\,dE - n(^{58}Co^m)\left[\lambda_m + \bar{\sigma}_m \int_o^{E_{thrs}} \varphi(E)\,dE\right] \tag{34}$$

$$\frac{dn(^{58}Co)}{dt} = n(^{58}Ni)\,\bar{\sigma}\int_{E_{thrs}}^{\infty}\varphi(E)\,dE + n(^{58m}Co)\,\lambda_m$$

$$- n(^{58}Co)\left[\lambda + \sigma_{\gamma'}\int_{0}^{E_{th}}\varphi(E)\,dE\right] \qquad (35)$$

Introducing the following abbreviations:

$$\Phi_{th} = \int_{0}^{E_{thrs}}\varphi(E)\,dE$$

$$\Phi_f = \int_{E_{thrs}}^{\infty}\varphi(E)\,dE$$

$$E_1 = \sigma_\gamma\,\Phi_{th} + (\bar{\sigma} + \bar{\sigma}_m)\,\Phi_f \qquad (36)$$

$$E_2 = \lambda_m + \sigma_\gamma^m\,\Phi_{th} \qquad (37)$$

$$E_3 = \lambda + \sigma_{\gamma'}\Phi_{th} \qquad (38)$$

Equations (33), (34), and (35) reduce to

$$\frac{dn(^{58}Ni)}{dt} = - E_1\, n(^{58}Ni)$$

$$\frac{dn(^{58m}Co)}{dt} = n(^{58}Ni)\ \bar{\sigma}_m\ \Phi_f - E_2\ n(^{58m}Co)$$

$$\frac{dn(^{58}Co)}{dt} = n(^{58}Ni)\ \Phi_f\ \bar{\sigma} + \lambda_m\ n(^{58m}Co) - E_3\ m(^{58}Co)$$

with the following solutions:

$$n(^{58}Ni) = n_o(^{58}Ni)\ \exp(-E_1\ t_i) \tag{39}$$

$$n(^{58m}Co) = n_o(^{58m}Co)\ \exp(-E_2 t_i) + n_o(^{58}Ni)\ \Phi_f$$

$$\frac{\bar{\sigma}_m}{E_2 - E_1} = \exp(-E_1 t_i) - \exp(-E_2 t_i) \tag{40}$$

$$n(^{58}Co) = n_o(^{58}Co)\ \exp(-E_3 t_i) + \lambda_m\ n_o(^{58m}Co) \times$$

$$\left[\frac{\exp(-E_3 t_i) - \exp(-E_2 t_i)}{E_2 - E_3}\right] + n_o(^{58}Ni) \times$$

$$\Phi_f\left\{\left[\bar{\sigma} + \frac{\lambda_m\ \bar{\sigma}_m}{E_2 - E_1}\right]\left[\frac{\exp(-E_1 t_i) - \exp(-E_3 t_i)}{E_3 - E_1}\right]\right.$$

$$\left. - \left[\lambda_m\ \bar{\sigma}_m / (E_2 - E_1)\right]\left[\frac{\exp(-E_3 t_i) - \exp(-E_2 t_i)}{E_2 - E_3}\right]\right\} \tag{41}$$

During the waiting time, the time rate of change of ^{58m}Co and ^{58}Co is

$$\frac{dn(^{58m}Co)}{dt} = - n(^{58m}Co)\,\lambda_m \qquad (42)$$

$$\frac{dn(^{58}Co)}{dt} = n(^{58m}Co)\,\lambda_m - \lambda\, n(^{58}Co) \qquad (43)$$

with the following solutions:

$$n_{t_w}(^{58m}Co) = n_o(^{58m}CO)\,\exp(-E_2 t_i)\,\exp(-\lambda_m t_w) + n_o(^{58}Ni)\,\Phi_f\,\bar{\sigma}_m\left[\frac{\exp(-E_1 t_i) - \exp(-E_2 t_i)\,\exp(-\lambda_m t_w)}{E_2 - E_1}\right] \qquad (43)$$

Substituting Equation (43) in Equation (42), $n(^{58}Co)$, the number of ^{58}Co atoms after a waiting time of t_w following an irradiation period of t_i is given by

$$n_{t_w}(^{58}Co) = n(^{58}Co)\,\exp(-\lambda t_w) + n(^{58m}Co)\,\lambda_m \times \left[\frac{\exp(-\lambda t_w) - \exp(-\lambda_m t_w)}{\lambda_m - \lambda}\right] =$$

$$= n_o(^{58}Co)\,\exp(-E_3 t_i) + \lambda_m\, n_o(^{58m}Co) \times \left[\frac{\exp(-E_3 t_i) - \exp(-E_2 t_i)}{E_2 - E_3}\right] + n_o(^{58}Ni)\,\Phi_f \left\{\bar{\sigma} +\right.$$

$$+\frac{\lambda_m \bar{\sigma}_m}{E_2 - E_3}\left[\frac{\exp(-E_1 t_i) - \exp(-E_3 t_i)}{E_3 - E_1}\right] -$$

$$-\frac{\lambda_m \bar{\sigma}_m}{E_2 - E_1}\left[\frac{\exp(-E_3 t_i) - \exp(-E_2 t_i)}{E_2 - E_3}\right]\Bigg\}\exp(-\lambda t_w)$$

$$+\lambda_m\Bigg\{n_o(^{58m}Co)\exp(-E_2 t_i) + \bar{\sigma}_m \Phi_f\, n_o(^{58}Ni)\times$$

$$\left[\frac{\exp(-E_1 t_i) - \exp(-E_2 t_i)}{E_2 - E_1}\right]\Bigg\}\left[\frac{\exp(-\lambda t_w) - \exp(-\lambda_m t_w)}{\lambda_m - \lambda}\right] \qquad (44)$$

Equation (44) can be simplified by considering the following nuclear data:

$t/2(^{58}Co)$ = 71.23 d

$t/2(^{58m}Co)$ = 9.0 hr

σ_γ = 4.4 barn

$\bar{\sigma}$ = 74 mbarn

$\bar{\sigma}_m$ = 28 mbarn

σ_γ' = 2.5×10^3 barn

σ_γ^m = 1.4×10^5 barn

If Φ_{th} and Φ_f are assumed to be:

$\Phi_{th} = \Phi_f = 10^{14}$ n/cm^2 sec

and $t_i < 100$ hr, then

$E_1 = 4.50 \times 10^{-10}$ sec^{-1}

$\lambda = 1.13 \times 10^{-7}$ sec^{-1}

$\lambda_m = 2.14 \times 10^{-5}$ sec^{-1}

$\exp(-E_1 t_i) \cong 1$

Furthermore, if:

$n_o(^{58}Co) = n_o(^{58m}Co) = 0$, and $t_w > 2$ d

Equation (44) reduces to

$$n_{t_w}(^{58}Co) = n_o(^{58}Ni)\,\Phi_f \exp(-\lambda t_w)\left\{\bar{\sigma} + \frac{\sigma_m \lambda_m}{E_2}\right.$$

$$\left[1 - \exp(-E_3 t_i)\right]/E_3 + \bar{\sigma}_m \frac{\Phi_{th}\,\sigma_\gamma^m}{E_2}$$

$$\left.\left[\frac{1 - \exp(-E_2 t_i)}{E_2}\right]\right\} \qquad (45)$$

2. Reaction product burn-up

This correction factor applies to such reactions as $^{58}Ni(n,p)^{58}Co$ where the reaction product isotope has a high capture cross section. In this case, the reaction product, ^{58}Co, has a capture cross section of 2.5×10^3 barn, while ^{58m}Co has a capture cross section of 1.4×10^5 barn. This means that during the irradiation time t_i, part of ^{58}Co atoms are subject to "burn-up" by thermal neutrons. If C_1 denotes

the burn-up correction factor and $n'_{t_w}(^{58}Co)$ the number of ^{58}Co atoms with no burn-up, is given by Equation (45). Substituting Equations (47) and (45) in Equation (46) the burn-up correction becomes:

$$C_1 = (\bar{\sigma}+\bar{\sigma}_m)\left[1 - \exp(-\lambda t)\right]/\lambda \left\{\left(\bar{\sigma} + \frac{\bar{\sigma}_m \lambda_m}{E_2}\right)\left[1 - \exp(-\lambda)\right]/\lambda + (\bar{\sigma}_m \sigma_\gamma^m \Phi_{th} / E_2)\left[1 - \exp(-E_2 t)\right] / E_2\right\}^{-1}$$

3. Power correction

This factor is used to determine any possible reactor power fluctuation during the irradiation time. For this purpose, each set of activation foils intended for a given irradiation included an Au-Al wire. After the irradiation, the wire activity, A_x, is measured and compared with the "reference" activity, A_{ref}. The latter is the activity of an identical Au-Al wire irradiated in a constant flux corresponding to 5 MW. Both A_x and A_{ref} are expressed in terms of the net area under the 0.412 MeV photopeak of ^{198}Au, corrected for t_i and t_w. The power correction factor C_2 is defined by

$$C_2 = \frac{A_{ref}}{A_x}$$

As the calibration wires used with each foil set had the same

weight and dimension of the "reference" wire and were counted under identical conditions, no efficiency correction was needed.

4. Detector efficiency

Detector efficiency as a function of energy was determined for the Ge(Li) detector by comparing known emission rates with the measured counting rates for gamma radiations of various energies provided by absolute standards. The principal standards used in this experiment were ^{133}Ba, ^{22}Na, ^{137}Cs, and ^{60}Co, of very similar geometry. Each standard consisted of the actual radiation source with a diameter of approximately 1/8" thick deposited at the center of 1" disks.

The activity of the standards was calculated on the basis of the following gamma peaks:

^{133}Ba: 0.276, 0.302, 0.356, and 0.382 MeV
^{27}Na: 0.511, and 1.275 MeV
^{137}Cs: 0.622 MeV
^{60}Co: 1.173, and 1.332 MeV

covering an energy range of 0.28 MeV to 1.33 MeV. The detection efficiency vs. gamma energy, plotted on a log-log basis, was found to be a straight line, consequently, the gamma efficiencies at energies greater than 1.33 MeV could be obtained by extrapolation. In order to verify the validity of the extrapolation, used primarily to obtain the 1.596 MeV gamma detec-

tion efficiency of ^{140}La, a ^{207}Bi standard was used. As this standard had a slightly different geometry, it was intercalibrated with the other four standards. ^{207}Bi with its gamma energies of 0.570, 1.063, and 1.771 MeV extended the range of measured detection efficiency to 1.771 MeV.

Efficiency measurements were carried out for several assembly shelves. In each case the natural logarithm of the detection efficiency vs. the natural logarithm of the photopeak energies was plotted. The results for each shelf yielded straight lines with identical slopes.

5. Other corrections

Equations (40) show other possible correction factors that may need to be determined for specific foils and/or particular counting condition

$$C_5 = \frac{\Lambda_1}{\Lambda_2 \Lambda_3}$$

where

Λ_1 = correction factor for variations in foil diameter

Λ_2 = correction for gamma self-shielding

Λ_3 = foil weight normalization factor

Λ_1 had to be accounted for in a limited number of cases where the foil diameters were appreciably different than the diameter of the absolute standards. This factor was defined as

$$\Lambda_1 = \frac{A(d = 1/8")}{A(d \neq 1/8")}$$

where A($d = 1/8"$) is the net area under the photopeak of a foil with the standard size, and A($d \neq 1/8"$) indicates the net photopeak area of a foil with a different diameter.

To determine Λ_1 experimentally, two foils of identical properties but different diameters (one with $d = 1/8"$) were irradiated together for a specific t_i. The net area under the principal photopeak of each foil was corrected for the foil mass, t_w and t_c.

Λ_2, negligible for nearly all foils (except In), is defined by the following approximation (40):

$$\Lambda_2 = 1 - \exp(-\mu x) \; / \mu x \qquad (47)$$

where μ is the mass absorption coefficient of the foil (cm^{-1}) and x is the thickness of the foil. For In and Au foils Equation (47) was substituted for by Bothe's approximation (41) defined as

$$\Lambda_2 = 1 - \Sigma_a x \; (\; 1 - \log \Sigma_a x)$$

Λ_3 was used for the foils which were weighed at the ALRR. Since the majority of the foils were obtained and weighed with high precision at ANL, the weight of foils weighed at ALRR was normalized to ANL values. This was accomplished by weighing several foils at both ANL and ALRR. The ratios of ALRR weight to ANL weight, W_i(ALRR) / W_i(ANL), were plotted vs. the ALRR weights W_i(ALRR) and a best fit straight line drawn. The value of Λ_3 for each foil weighed at ALRR was selected to

be the ratio $W_i(\text{ALRR}) / W_i(\text{ANL})$ corresponding to $W_i(\text{ALRR})$.

For the special case of ^{238}U foils an additional correction factor was considered. This correction factor, Ω, was to take into account the presence of 0.04% ^{235}U in the ^{238}U samples. Ω, defined as the ratio of the fission rate of pure ^{238}U to the fission rate of the ^{238}U sample, is given by

$$\Omega = \left[1 + 4 \times 10^{-4} \left(\bar{\sigma}^f_{25} / \bar{\sigma}^f_{28}\right) \left(\bar{\Phi}_{Cd} / \bar{\Phi}_f\right) \right]^{-1}$$

where $\bar{\Phi}_{Cd}$ and $\bar{\Phi}_f$ indicate neutron flux above the cadmium cut-off, and the flux above the $^{238}U(n,f)$ reaction threshold, respectively. Using several conservative estimates of $\bar{\Phi}_{Cd}/\bar{\Phi}_f$, it was determined that the value of Ω was very close to 1 and thus, no correction was needed.

V. EXPERIMENT

The purpose of the experiment was to measure the energy distribution of neutrons in certain ALRR experimental facilities.

Neutron induced reactions with various nuclides were studied and a number were selected which satisfied the dual requirement of having adequate detector response in the energy range of $0.1\ \text{MeV} \leqslant E \leqslant 10\ \text{MeV}$ and leading to detectable photon emission.

Packets of activation foils were assembled, observing necessary precaution to prevent cross-contamination, high exposure to thermal neutrons, and physical damage. Packets were inserted into the irradiation region of interest and exposed to the neutron flux for an appropriate period of time.

The activated foils were taken from the reactor, the packets were disassembled, and each foil was allowed to decay for an appropriate time until a decay rate was reached which permitted accurate measurement. Each foil activity was measured using conventional detector and multichannel analyzer procedures.

The experiment was analyzed for departure from ideal or theoretical conditions, appropriate correction factors were devised, and necessary numerical corrections determined. The apparatus was calibrated, and routine checks were conducted to ascertain that consistent performance was maintained.

A. Irradiation Facilities

All irradiations were conducted in the Ames Laboratory Research Reactor (ALRR)*. The ALRR was a heterogenous, heavy water reactor with an operating power level of 5 MW. The fully enriched core was moderated, cooled, and reflected by heavy water.

The core contained 24 fuel elements of the parallel plate type. Each element was 3" x 3" in cross section and 52½" long overall with the fueled region being 24 5/8" long.

A total of 35 experimental facilities penetrated the shielding to permit access to core radiation. The facilities selected for this work were the R-3 (a rabbit facility) and the V-1 (vertical thimble). The locations and dimensions of these facilities are illustrated in Appendix A.

B. Counting Equipment

The photon emissions from irradiated foils were analyzed according to their energies using an ORTEC WIN series coaxial Ge(Li) detector with the following peripheral equipment:

- ORTEC model 120-4 preamplifier
- Canberra model 1417B amplifier
- Canberra model 1400 Nim Bin

---

* This reactor was decommissioned in January, 1978

- Nuclear Data 50/50 analyzer system - 4096 channels PDP-8/L minicomputer
- Peripheral Equipment 9-track tape drive
- 16" x 16" x 20" inside dimensions lead cave with 2" thick lead and an inner lining of cadmium and copper
- Radiation Instrument Development Laboratory pulser model 47-2
- Berkley Nucleonics tail pulse generator model RP-1.

Foils were placed in the lead cave in an aluminum holder which fixed the distance between the foils and the Ge(Li) detector at a value between 10 and 30 cm. The system's live time was checked by the pulser. The area under each photoelectric peak of interest was determined with the aid of the ICPEAX computer program*. ICPEAX fits an experimentally determined photoelectric peak with a gaussian curve, determines the background-corrected area under the gaussian peak, and finds the energy to be associated with the peak (42).

C. Choice of Detectors

The criteria for the selection of specific nuclides to be employed as threshold detector were based upon such requirements as target material characteristics (availability, puri-

---

* This program was developed at ALRR.

ty, etc.); reaction data (type, magnitude and knowledge of cross section, etc.); and the product isotope nuclear data (decay scheme, half life, etc.). The above criteria are listed as follows:

- The available material purity should be high enough that interferring impurity reactions can be neglected.
- The material should be chemically stable and capable of being formed into thin (few mils) foils.
- The reaction should have a reasonably well known cross section.
- The reaction should have adequate "sensitivity" and a high enough yield to provide good counting statistics.
- The product isotope must be capable of being gamma counted, it should have an adequate half life (more than 10 minutes), and a well established decay scheme.

Based upon the above considerations, an optimum set of threshold detectors was selected to yield the reactions listed in Table 2. In addition to the relatively high energy detector reactions listed in Table 2, the (n, γ) reactions listed in Table 3 were used to measure lower energy neutrons. The uncertainty associated with $\sigma(E)$ of the above reactions are listed in Table 6 (43, 44).

Table 2. Threshold reaction data

Reaction	Reaction product half life	Gamma energy (KeV)	Gamma yield %	Target purity %
$^{24}Mg(n,p)^{24}Na$	15.00 hr	1368.60	99.993	99.8
$^{27}Al(n,\alpha)^{24}Na$	15.00 hr	1368.60	99.993	99.99
$^{27}Al(n,p)^{27}Mg$	9.46 min	E_1=843.73 E_2=1014.44	y_1=71.4 y_2=28.6	99.99
$^{46}Ti(n,p)^{46}Sc$	83.85 d	E_1=889.258 E_2=1120.516	y_1=99.984 y_2=99.987	99
$^{47}Ti(n,p)^{47}Sc$	3.39 d	159.39	69.0	99
$^{48}Ti(n,p)^{48}Sc$	43.8 hr	E_1=983.4 E_2=1037.4 E_3= 1311.8	y_1=99.987 y_2=97.5 y_3=99.992	99
$^{54}Fe(n,p)^{54}Mn$	312.6 d	834.827	99.97	99.9
$^{56}Fe(n,p)^{56}Mn$	2.576 hr	846.9	99	99.9
$^{58}Ni(n,p)^{58}Co$	71.23 d	810.757	99.44	99.99
$^{63}Cu(n,\alpha)^{60}Co$	5.268 y	E_1=1173.208 E_2=1332.464	y_1=99.86 y_2=99.986	99.9
$^{90}Zr(n,2n)^{89}Zr$	78.4 hr	910	99	99.942
$^{115}In(n,n^1)^{115}In^m$	4.50 hr	336.2	47	99.99
$^{232}Th(n,f)^{140}La$	40.26 hr	1596.18	95.33	99.8
$^{238}U(n,f)^{140}La$	40.26 hr	1596.18	95.33	99.96

Table 3. Activation reactions data

Reaction	Reaction product half-life	Gamma energy (KeV)	Gamma yield (%)	Target purity (%)
$^{58}Fe(n,\gamma)^{59}Fe$	44.6 d	E_1=1099.224 E_2=1291.564	y_1=55.5 y_2=44.1	99.9
$^{59}Co(n,\gamma)^{60}Co$*	5.268 d	E_1=1173.208 E_2=1332.464	y_1=99.86 y_2=99.986	99.9
$^{63}Cu(n,\gamma)^{64}Cu$	12.701 hr	511.002	36.8	99.9
$^{197}Au(n,\gamma)^{198}Cu$**	2.698 d	411.794	95.48	99.999

* 0.1% Co-Al Al: 99.999%; Co: 99.9%

** 0.135% Au-Al Au: 99.999%; Al: 99.999%

D. Irradiation of Detectors

High purity activation detectors, provided by ALRR and Argonne National Laboratory, were prepared in the form of 1/8" diameter and 0.5 to 5 mils thick foils. Each set of foils, to be irradiated simultaneously, was packed, cadmium covered, and contained in an aluminum or polyethylene rabbit, the choice depending on the duration of irradiation.

Aluminum spacers, approximately 10 mils thick, were used to separate the foils. ^{238}U and ^{232}Th foils were individually wrapped in 5 mils thick aluminum to contain possible recoil fission fragments and to prevent cross-contamination between foils.

Comparison of experimental results involving the irradiation of single foils (1 foil with no aluminum spacer) and sets of activation foils indicated that, within experimental errors, the perturbation effects on the fast neutron flux are negligible due to the presence of multiple foil in a set. Furthermore, irradiation of foils with diameters as large as 1.5" indicated that the neutron flux at the center of the rabbit tube (where the cadmium-covered foil set is mounted) is uniform over the region occupied by the foils. Therefore, no corrections for flux perturbation due to the presence of multiple foil set or for the lack of uniformity were necessary.

The duration of an irradiation was dictated by the following:

- The activity of the isotope of interest should be high enough to provide good counting statistics.
- The isotope activity should not be great enough to cause a dead time problem with the counting equipment.
- The irradiation time should be less than the effective in-reactor half life of the foil, T 1/2(eff), defined below, to prevent saturation activity problems.

In order to determine T 1/2(eff), the production rate of an isotope can be written as

$$\frac{dn}{dt} = N_0 \sigma(E) \varphi(E)$$

The concentration will be diminished by radioactive decay and the transmutation of the product radionuclide

$$-\frac{dn}{dt} = n\left[\lambda + \varphi(E)\, \sigma'(E)\right] = n\, \lambda_{eff}$$

where $\sigma'(E)$ is the microscopic cross section of the resultant nuclide for transmutation to still another nuclide. Saturation activity occurs when the rate of production equals the rate of loss:

$$N_0\, \sigma(E)\, \varphi(E) = n_{equil}\, \lambda_{eff}$$

and the time constant that determines the approach to saturated activity is

$$T\ 1/2(eff) = \ln 2/\lambda_{eff} = \ln 2/\left[\lambda + \varphi(E)\, \sigma'(E)\right]$$

By using conservative estimates of $\varphi(E)$ and $\sigma'(E)$, approximate values of T 1/2(eff) were determined. The irradiation time t_i of each set of foils was selected to be less than the lowest T 1/2(eff) of each set.

Based upon these considerations, the foil sets were irradiated as indicated below:

- Short irradiations, with $t_i < 30$ minutes, were used for foil sets containing ^{27}Al, ^{115}In, ^{197}Au, ^{56}Fe, ^{238}U, ^{59}Co, and ^{63}Cu isotopes.
- Long irradiations, with $t_i \leqslant 15$ hours, were used for foil sets containing ^{63}Cu (for n, α reaction), ^{90}Zr, and ^{54}Fe.
- Intermediate irradiations, with $t_i \leqslant 5$ hours, were used for foil sets containing the other foils.

Each foil set contained at least two reference monitors, Au-Al wire and Ni foil, for the purpose of run-to-run power level normalization.

E. Counting

The half life of the isotope of interest, the half lives of interferring isotopes, and the activity levels of the various nuclides at the end of the irradiation dictated the waiting time t_w. At the time when the activities were measured, the counting rates had to be within the limits imposed by good counting statistics and the dead time of the counting equipment.

To establish the geometry to be used when the Ge(Li) count-

ing efficiency was determined, each foil was placed at the center of a "dummy source." The "dummy source" consisted of a plastic disk having the same dimensions and material properties of the absolute standards used for the detector efficiency determinations. The "dummy source" containing the sample was placed on the same aluminum planchet used for the absolute standards and counted.

Each sample was counted at least three times within a time period of 3-4 half lives after the end of the irradiation. If the three counts, corrected for waiting and counting time, did not agree to within ±4%, additional counts were taken. Furthermore, in cases with possible interferring activities, the source of the counts was checked by determining the actual half life of the activity being measured and comparing this value with the published half life of the nuclide of interest.

The principal gamma ray of each radionuclide was counted for a sufficiently long period of time to provide counting statistics uncertainty of less than 2%. The source-to-detector distance was adjusted to provide maximum count rate without exceeding 15% analyzer dead time. The typical source-to-detector distance was 20 cm.

VI. RESULTS AND DISCUSSIONS

Preliminary analysis of the experimental data indicated a high degree of inconsistency between $^{27}Al(n,p)^{27}Mg$ reaction rates and the reaction rates determined for other foils used in this work. Such inconsistencies were attributed to the experimental limitations associated with the relatively short half life (9.46 minutes) of ^{27}Mg. Since the ^{27}Mg activity had to be measured soon after the end of irradiation, the exposure of aluminium foils were kept at a minimal level. A short irradiation time, resulting in low induced activity, made the safe handling of the samples possible with no needed recourse to the use of the hot cell facility.

Generally, handling the irradiated foils consisted of opening the rabbit, removing the cadmium cover, identifying the foils, and finally preparing the foils for analysis. This process required a cooling period ranging from a few hours to several days, depending on the exposure, type, and number of foils. In order to reduce the ^{27}Mg cooling period to a few minutes, several measurements involving foils with irradiation times ranging from 0.5 to 4 minutes were taken. To further reduce the total activity of the foil set, the diameters of some selected foils were reduced to half the standard size.

The reaction rates obtained from these irradiation were inconsistent with each other and with the results obtained from the other foil sets involving longer irradiation times. The

deviation from the mean $(\bar{x} - x_i)$* ranged from $|(18.89 - 12.1)| =$ $= 6.79$ cpm for $t_i = 2$ min, $t_w = 75$ min, and d = 1/16"; to $|(18.89 - 28.9)| = 10.01$ cpm for $t_i = 0.5$ min, $t_w = 25$ min, and d = 1/8". The standard deviation was

$$\sigma_{\bar{x}} = \left[\frac{1}{7} \sum_{i=1}^{8} (\bar{x} - x_i)^2\right]^{1/2} = 6.29 \text{ cpm}$$

In order to make a qualitative determination of the experimental errors, it was assumed that the major sources of errors were: $\Delta t_i = \pm 5$ seconds in t_i and $\Delta A = A^{1/2}$ in the measured activity A. For $t_i = 0.5$ minute, $t_w = 20$ minutes, and A = 152 counts; $\frac{\sigma A_o}{A_o}$ was found to be

$$A_o/A_o = \sqrt{\left\{\exp(\lambda tw)\ (\Delta A/A_o) \Big/ \left[1 - \exp(-\lambda ti)\right]\right\}^2 + \left\{\lambda \Delta ti \exp(-\lambda ti) \Big/ \left[1 - \exp(-\lambda ti)\right]\right\}^2} =$$

$$= 18.3\ \%$$

---

* x_i is the reaction rate, in counts per minute, corrected for t_i, t_w, t_c, m(Al), and C_2 (the power correction factor).

For t_i = 1 minute, t_w = 35 minutes, and A = 123 counts/10 minutes; the result was

σ_{A_o}/A_o = 12 %

Based on the above considerations, it was concluded that:

- the errors introduced by Δt_i ($\pm$5 sec) and $\pm \Delta A$ were substantial, but could not account for the inconsistencies observed in the reaction rates;
- Δt_i could vary from irradiation to irradiation, and its value could be higher than the assumed $\pm$5 seconds (in fact, the power correction factors showed a fluctuation of 0.89 to 1.07);
- at higher t_i (where the relative contribution of Δt_i was expected to be less) the reduction in the foil diameter could have introduced errors in the value of detector efficiency.

Because the inconsistencies in the uncertainties related to the $^{27}Al(n,p)^{27}Mg$ reaction could not be understood, all the experimental data obtained for this reaction were discarded. The deletion of $^{27}Al(n,p)^{27}Mg$ reaction would not alter the final unfolding solution appreciably. This is so because the $^{27}Al(n,p)^{27}Mg$ response function, covering an energy range from about 3 to 13 MeV, is replaced by the response function of the $^{46}Ti(n,p)^{46}Sc$ reaction which covers approximately the same energy range. However, within this energy range the cross section uncertainty of the $^{46}Ti(n,p)^{46}Sc$ reaction is higher than that for the aluminum reaction (see Table 6).

A. SAND-II Runs

As mentioned in section IV, the original SAND-II code uses an energy range between 10^{-10} and 18 MeV which is divided into 620 intervals. Thus, with a given input spectrum, the original code solves N (number of foils used) linear activity equations for 621 unknowns. However, given the limited number of appropriate activation reactions and the smooth behavior of $\sigma(E)$ for most threshold reactions of interest, the number of energy intervals can be reduced. Many laboratories (e.g. ANL, RCN-Netherlands, KFA-Germany, etc.) use modified SAND-II codes with the energy range divided into a much smaller number of energy intervals. For instance, SAND-50 (Euroatom-Ispra, Italy) has only 50 energy subdivisions.

The code used in this work covers an energy range between 10^{-10} and 20 MeV, divided into 100 intervals. The first 10 intervals cover the range 10^{-10} to 5.5×10^{-7} MeV, the next 60 intervals cover 5.5×10^{-7} to 1.0 MeV, and the last 30 intervals cover the range from 1.0 to 20 MeV.

For an adequate choice of input spectrum several spectra were tested (45). Included were:

$$\varphi_o = 1/E, \text{ and}$$

$$\varphi_o = k\, E^{\alpha} \exp(-3E/2\beta) + K \frac{1}{E^{\beta}}$$

which were used with several values of k, α, β, and K (46). The spectra shown in Figures 1 and 2 were selected as the R-3

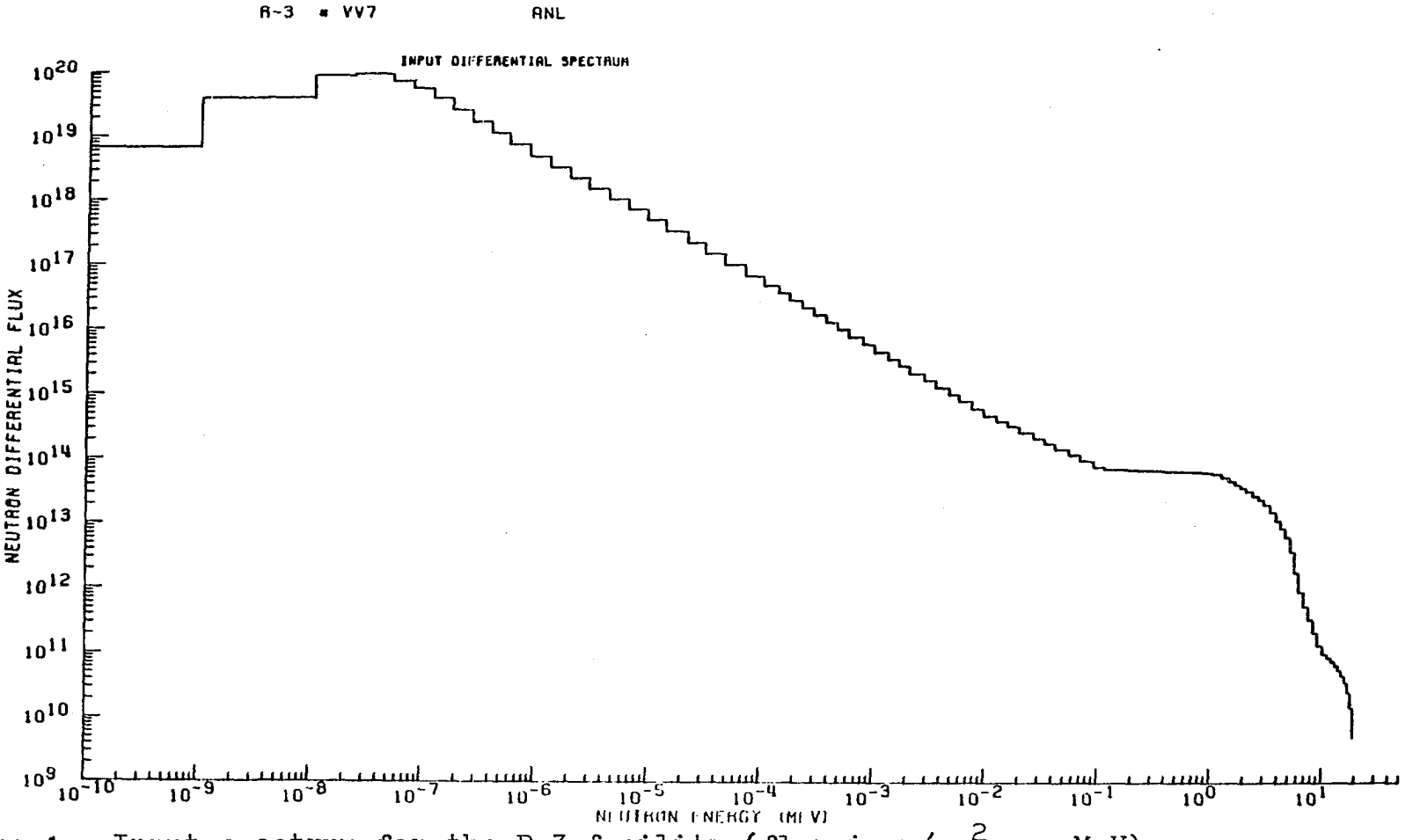

Figure 1. Input spectrum for the R-3 facility (flux in n/cm^2 sec MeV)

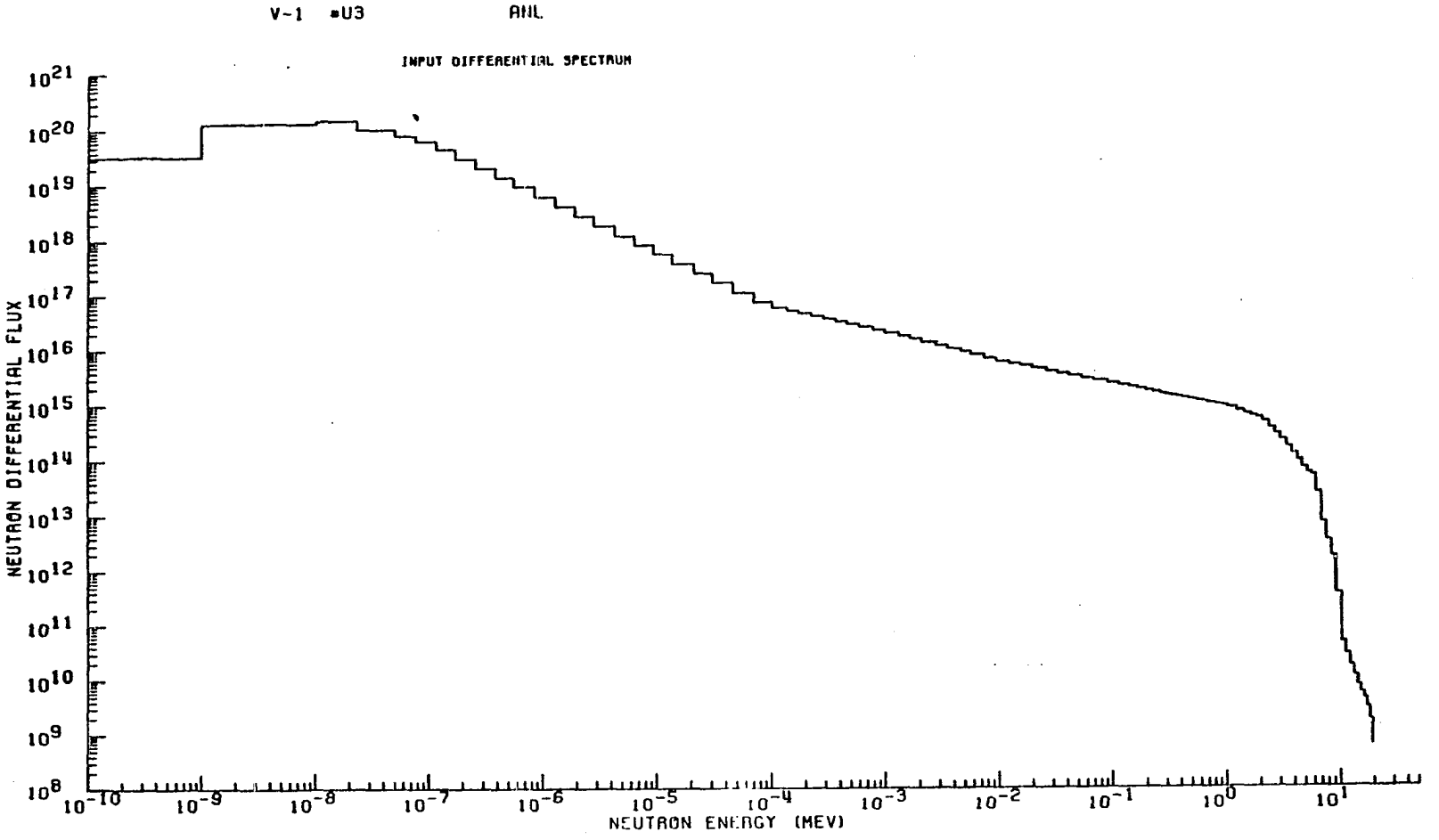

Figure 2. Input spectrum for the V-1 facility (flux in n/cm^2 sec MeV)

and V-1 ALRR facilities input spectra for the SAND-II code. These spectra, φ_o(R-3) and φ_o(V-1), provided the final solution with the least number of iterations.

B. Solution Spectrum for the R-3 Facility

The solution spectrum for R-3 involved the use of φ_o(R-3) as the input spectrum and the 17 foil reaction data, presented in Table 4. The final unfolding solution was reached after a total of 4 iterations (2 iterations prior to the deletion of ^{48}Ti, and 2 iterations after) with = ±3.36% as the deviation of measured from calculated activities (see Appendix B). In reaching the final solution, SAND-II discarded the ^{48}Ti(n,p)^{48}Sc reaction. In fact, following the first two iterations, the "percent deviation" of this reaction, defined as: [100 (measured activity/calculated activity - 1)] was the highest.

Figures 3 and 4 illustrate the initial solution (before the rejection of the ^{48}Ti(n,p)^{48}Sc) and the final solution (after the rejection of the ^{48}Ti(n,p)^{48}Sc reaction) over the entire energy range: 10^{-10} to 20 MeV. The SAND-II integral flux results indicated that the flux of fast neutron with E$\geqslant$1 MeV in R-3 was 1.12 x 10^{13} n/cm^{2}sec. This figure is in good agreement with the ALRR measured value of 10^{13} ±25%*.

---

* Based on ^{58}Ni(n,p)^{58}Co reaction (private communication from Bruce Link of ALRR).

Table 4. R-3 saturated measured activities and reactions response boundaries

Reaction	measured activity (dps/nucleus)	reaction response boundaries (MeV)	
		lower	upper
$^{27}Al(n,\alpha)^{24}Na$	1.6×10^{-14}	6.7	1.7×10^{1}
$^{197}Au(n,\gamma)^{198}Au$	3.6×10^{-8}	4.2×10^{-6}	4.5×10^{-5}
$^{59}Co(n,\gamma)^{60}Co$	1.8×10^{-9}	8.4×10^{-7}	1.7×10^{-4}
$^{63}Cu(n,\gamma)^{64}Cu$	1.3×10^{-10}	5.5×10^{-7}	1.9×10^{-2}
$^{58}Fe(n,\gamma)^{59}Fe$	4.2×10^{-11}	8.4×10^{-7}	3.6×10^{-4}
$^{54}Fe(n,p)^{54}Mn$	1.1×10^{-12}	2.3	9.0
$^{115}In(n,n)^{115}In^{m}$	3.0×10^{-12}	6.6×10^{-1}	5.5
$^{58}Ni(n,p)^{58}Co$	1.4×10^{-12}	2.0	8.2
$^{90}Zr(n,2n)^{89}Zr$	4.2×10^{-14}	1.3×10^{1}	1.9×10^{1}
$^{46}Ti(n,p)^{46}Sc$	1.4×10^{-13}	3.7	1.4×10^{1}
$^{47}Ti(n,p)^{47}Sc$	3.0×10^{-13}	1.8	8.2
$^{232}Th(n,f)^{140}La$	1.1×10^{-12}	1.4	8.2
$^{238}U(n,f)^{140}La$	4.5×10^{-12}	1.4	6.7
$^{63}Cu(n,\alpha)^{60}Co$	6.7×10^{-15}	6.0	1.6×10^{1}
$^{56}Fe(n,p)^{56}Mn$	1.8×10^{-14}	5.5	1.6×10^{1}
$^{24}Mg(n,p)^{24}Na$	3.0×10^{-14}	6.7	1.7×10^{1}
$^{48}Ti(n,p)^{48}Sc$	7.6×10^{-15}	6.7	1.7×10^{1}

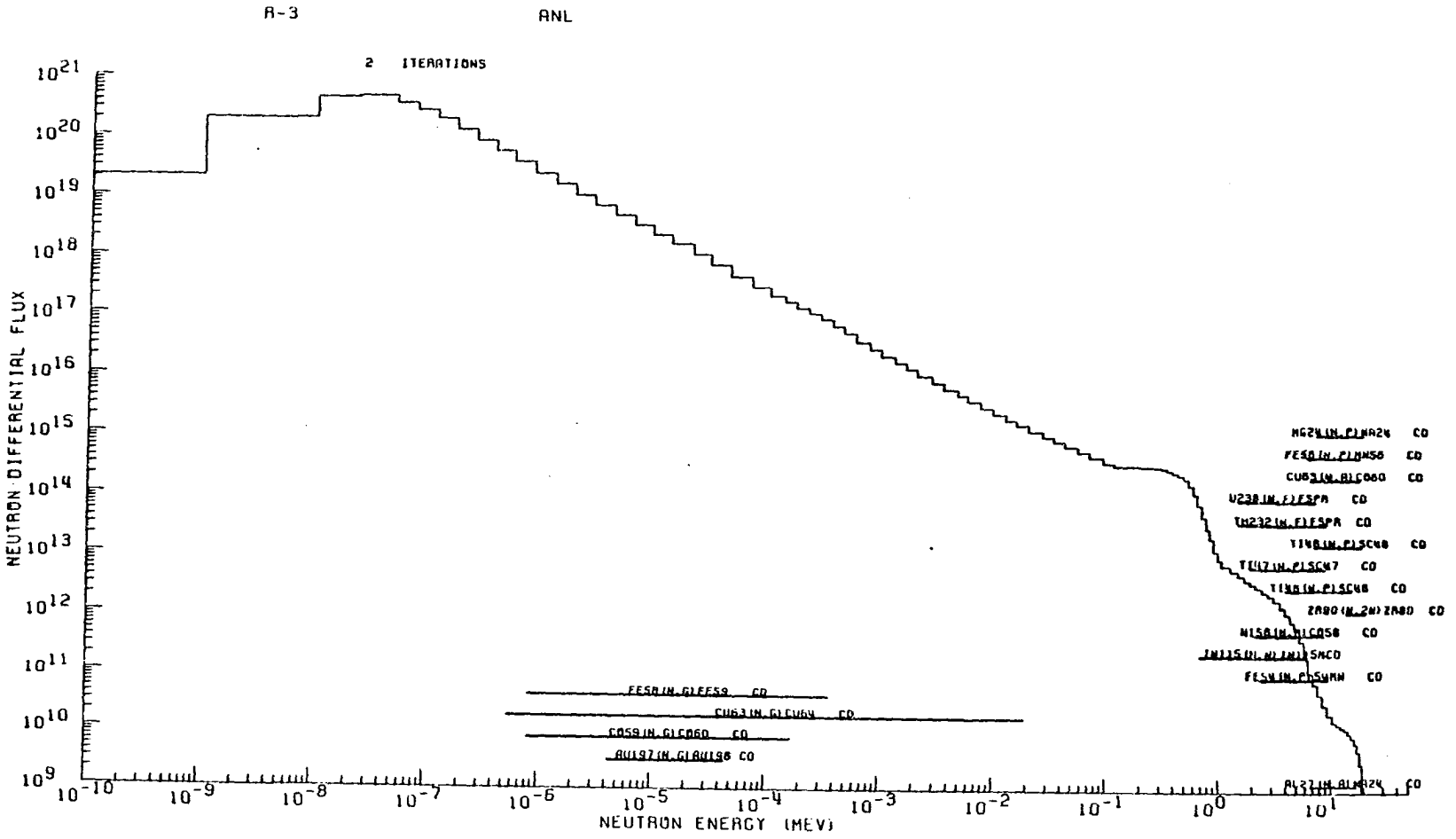

Figure 3. R-3 initial solution (flux in n/cm^2 sec MeV)

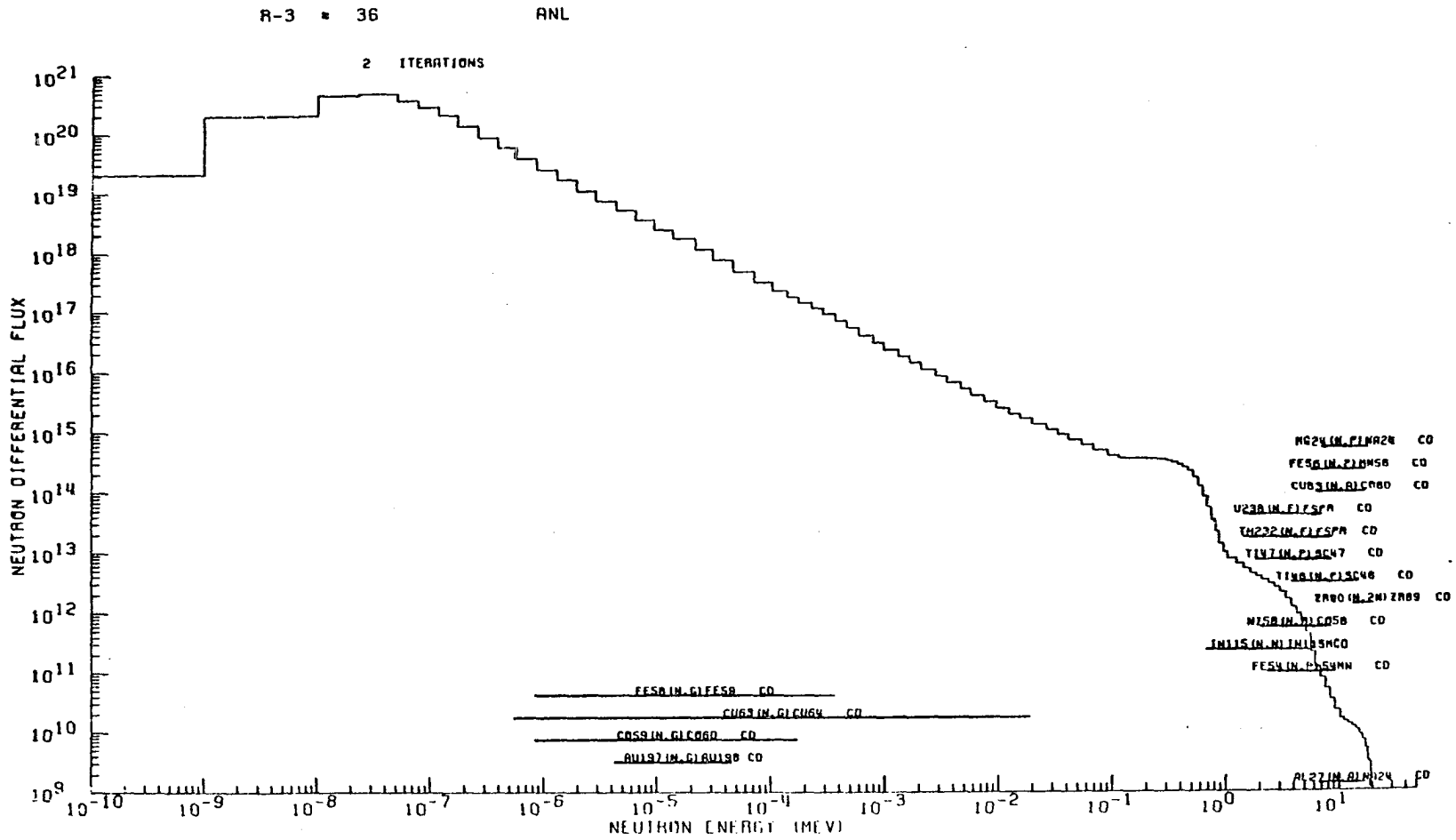

Figure 4. R-3 final solution (flux in n/cm^2 sec MeV)

C. Solution Spectrum for V-1 Facility

Foil reaction data used as the input for V-1 solution are presented in Table 5. The first solution spectrum, obtained after 16 iterations, had a standard deviation of $\sigma = \pm 27\%$. At the 16th iteration the $^{48}Ti(n,p)^{48}Sc$ had a percent deviation of + 36.53, the highest of all reactions used. Following the rejection of ^{48}Ti activity, the code reached the final solution in 9 iterations (see Appendix C).

The V-1 initial solution spectrum (prior to the rejection of $^{48}Ti(n,p)^{48}Sc$) and final spectrum (after the rejection of the $^{48}Ti(n,p)^{48}Sc$ reaction) are presented in Figures 5 and 6, respectively. The SAND-II integral flux values indicated that the flux of fast neutrons with $E \geqslant 0.11$ MeV was 6.74×10^{14} $n/cm^2 sec$. This is 4.3 times greater than the fast flux (with $E \geqslant 0.11$ MeV) for the R-3 facility. However, the integral flux of neutrons with $E \geqslant 1$ MeV was 1.18×10^{13} $n/cm^2 sec$. This value, comparable to the integral flux of the R-3 facility, is in fair agreement with the ALRR measured value of $2 \times 10^{13} \pm 25\%$ n/cm^2 sec*.

D. Error Analysis

Errors affecting the final solution spectrum can be divided into two groups. The first group consists of errors in the

---

* From M. S. Wechsler's internal report: Radioactivity of thorium in ALRR, dated 7-22-1976, page 1 (flux determined by flux integral method).

Table 5. V-1 saturated measured activities and reactions response boundaries

Reaction	measured activity (dps/nucleus)	reaction response boundaries (MeV)	
		lower	upper
$^{27}Al(n,\alpha)^{24}Na$	2.1×10^{-14}	6.0	1.6×10^{1}
$^{197}Au(n,\gamma)^{198}Au$	5.7×10^{-8}	4.2×10^{-6}	6.3×10^{-6}
$^{59}Co(n,\gamma)^{60}Co$	2.7×10^{-9}	1.9×10^{-6}	1.7×10^{-4}
$^{63}Cu(n,\gamma)^{64}Cu$	1.4×10^{-10}	8.4×10^{-7}	2.6×10^{-1}
$^{58}Fe(n,\gamma)^{59}Fe$	5.2×10^{-11}	1.3×10^{-6}	6.6×10^{-2}
$^{54}Fe(n,p)^{54}Mn$	1.1×10^{-12}	2.3	8.2
$^{115}In(n,n)^{115}In^{m}$	3.2×10^{-12}	5.5×10^{-12}	6.0
$^{58}Ni(n,p)^{58}Co$	1.6×10^{-12}	2.0	8.2
$^{90}Zr(n,2n)^{89}Zr$	3.7×10^{-14}	1.3×10^{1}	1.9×10^{1}
$^{46}Ti(n,p)^{46}Sc$	1.9×10^{-13}	4.1	1.3×10^{1}
$^{47}Ti(n,p)^{47}Sc$	3.4×10^{-13}	1.8	8.2
$^{232}Th(n,f)^{140}La$	1.2×10^{-12}	1.4	8.2
$^{238}U(n,f)^{140}La$	5.0×10^{-12}	1.2	7.4
$^{63}Cu(n,\alpha)^{60}Co$	9.2×10^{-15}	6.0	1.5×10^{1}
$^{56}Fe(n,p)^{56}Mn$	2.8×10^{-14}	5.5	1.5×10^{1}
$^{24}Mg(n,p)^{24}Na$	4.1×10^{-14}	6.0	1.6×10^{1}
$^{48}Ti(n,p)^{48}Sc$	1.3×10^{-14}	6.0	1.7×10^{1}

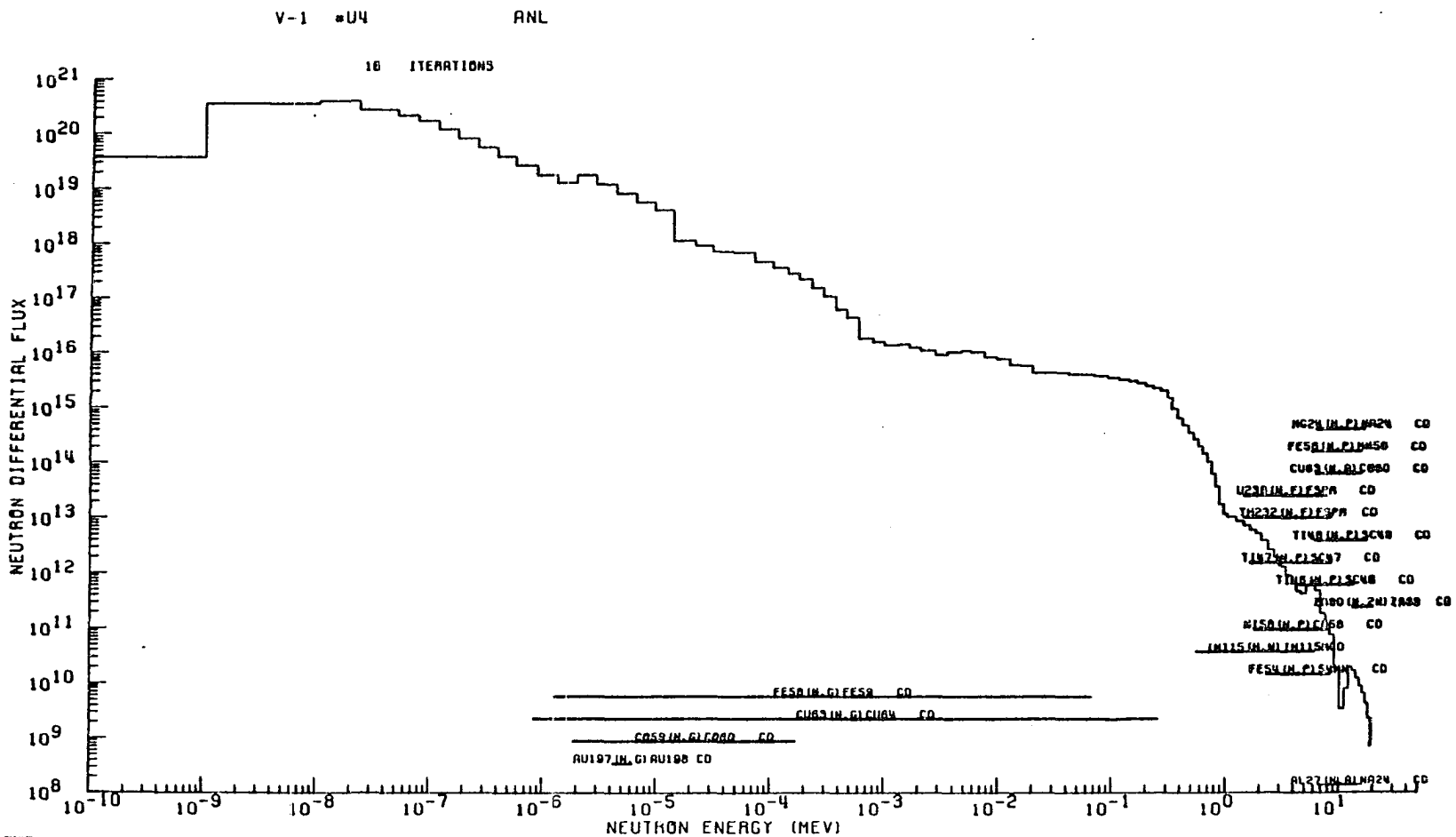

Figure 5. V-1 initial solution (flux in n/cm^2 sec MeV)

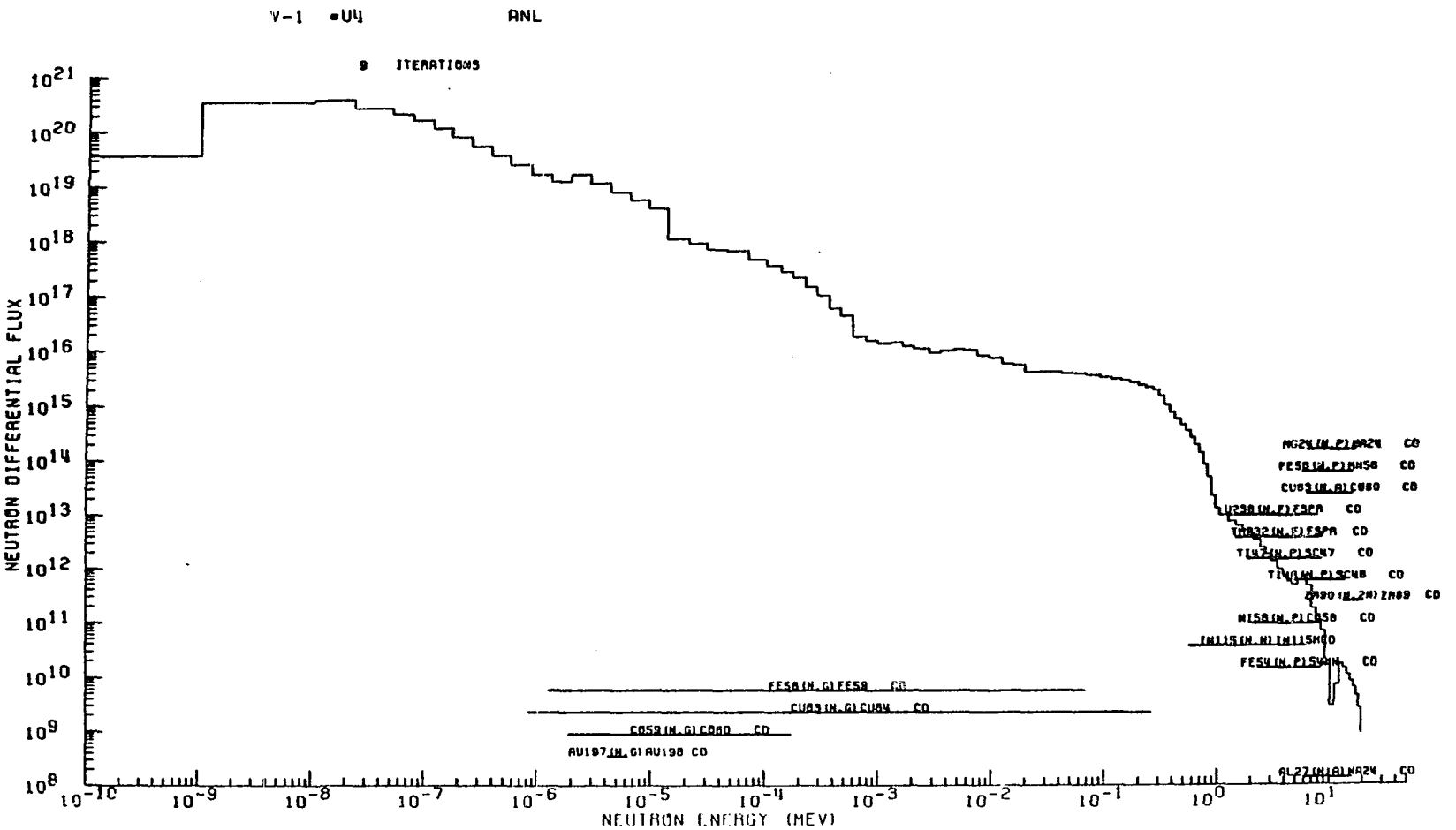

Figure 6. V-1 final solution (flux in n/cm^2 sec MeV)

input data, and the second consists of errors due to the fact that the mathematical model cannot yield a unique solution.

To quantify the errors in the final solution spectra obtained for R-3 and V-1 facilities, a SAND-II Monte Carlo error analysis code was run. The code combines uncertainties in the cross sections and input activities to provide estimates of uncertainty for the solution spectrum (43, 47). For a given reaction the exact value of the cross section uncertainty as a function of energy, $\pm \Delta\sigma_i(E)$, is not known. To provide an estimate for the uncertainties in the cross sections, the energy range E is divided into 15 intervals and within each of these intervals, an average error is assumed to apply uniformly to each value of the cross section within the energy range (43). The Monte Carlo code selects values of input activities and cross sections with assigned errors (see Table 6) for a preselected number of SAND-II runs. The values of input activities and cross sections, corresponding to the various runs, are used to generate sets of solution spectra, which, by virtue of their differences, provide the error estimates.

Results of the estimated errors for the R-3 and V-1 solution spectra are presented in Figures 7 and 8 (see also Appendix D). In both cases, the error band is widest at energy intervals not well covered by the reactions. This is particularly noticeable at energies below the cadmium cut-off and the KeV region. Within the energy range of 1 to 10 MeV, the magnitude

Table 6. SAND-II evaluated cross section error assignment

Reaction	uncertainty (%)						
Energy bounds (MeV)	$1^{-10}/4^{-7}$	$4^{-7}/1^{-5}$	$1^{-5}/1^{-2}$	$1^{-2}/1^{-1}$	$1^{-1}/6^{-1}$	$6^{-1}/1.4$	1.4/2.2
$^{24}Mg(n,p)^{24}Na$	-	-	-	-	-	-	-
$^{27}Al(n,\alpha)^{24}Na$	-	-	-	-	-	-	-
$^{46}Ti(n,p)^{46}Sc$	-	-	-	-	-	-	50
$^{47}Ti(n,p)^{47}Sc$	-	-	-	-	50	50	50
$^{48}Ti(n,p)^{48}Sc$	-	-	-	-	-	-	-
$^{54}Fe(n,p)^{54}Mn$	-	-	-	-	30	30	30
$^{56}Fe(n,p)^{56}Mn$	-	-	-	-	-	-	-
$^{58}Fe(n,\gamma)^{59}Fe$	8	8	28	15	15	15	15
$^{58}Ni(n,p)^{58}Co$	-	-	-	-	-	20	10
$^{59}Co(n,\gamma)^{60}Co$	4	5	10	10	10	10	10
$^{63}Cu(n,\alpha)^{60}Co$	-	-	-	-	-	-	-
$^{63}Cu(n,\gamma)^{64}Cu$	5	5	10	10	10	10	10
$^{90}Zr(n,2n)^{89}Zr$	-	-	-	-	-	-	-
$^{115}In(n,n)^{115}In^{m}$	-	-	-	-	30	20	10
$^{197}Au(n,\gamma)^{198}Au$	0.5	4	5	6	6	7	7
$^{232}Th(n,f)FP$	-	-	-	-	-	30	25
$^{238}U(n,f)FP$	-	-	-	-	30	30	4

* $1^{-10}/4^{-7}$ = from 1×10^{-10} to 4×10^{-7} MeV

Table 6. (continued)

Reaction	uncertainty (%)							
Energy bounds MeV)	2.2/3.0	3.0/4.0	4.0/5.0	5.0/6.0	6.0/8.0	8.0/11.0	11.0/13.0	13.0/20
$^{24}Mg(n,p)^{24}Na$	-	-	50	50	10	10	10	10
$^{27}Al(n,\alpha)^{24}Na$	-	-	30	20	6	6	10	10
$^{46}Ti(n,p)^{46}Sc$	50	25	20	20	10	10	20	20
$^{47}Ti(n,p)^{47}Sc$	50	15	15	15	15	15	15	15
$^{48}Ti(n,p)^{48}Sc$	-	50	50	25	15	15	15	15
$^{54}Fe(n,p)^{54}Mn$	10	10	8	8	7	7	10	10
$^{56}Fe(n,p)^{56}Mn$	-	8	8	8	6	6	15	15
$^{58}Fe(n,\ )^{59}Fe$	15	15	15	15	15	15	15	15
$^{58}Ni(n,p)^{58}Co$	5	5	5	6	6	6	10	10
$^{59}Co(n,\gamma)^{60}Co$	10	10	10	10	10	10	10	10
$^{63}Cu(n,\alpha)^{60}Co$	-	-	50	25	10	10	10	10
$^{63}Cu(n,\gamma)^{64}Cu$	10	10	10	10	10	10	10	10
$^{90}Zr(n,2n)^{89}Zr$	-	-	-	-	-	-	10	10
$^{115}In(n,n)^{115}In^{m}$	10	10	8	8	8	8	10	10
$^{197}Au(n,\gamma)^{198}Au$	7	7	7	7	7	7	7	7
$^{232}Th(n,f)FP$	20	10	10	10	10	10	10	10
$^{238}U(n,f)FP$	3	3	3	4	6	6	10	10

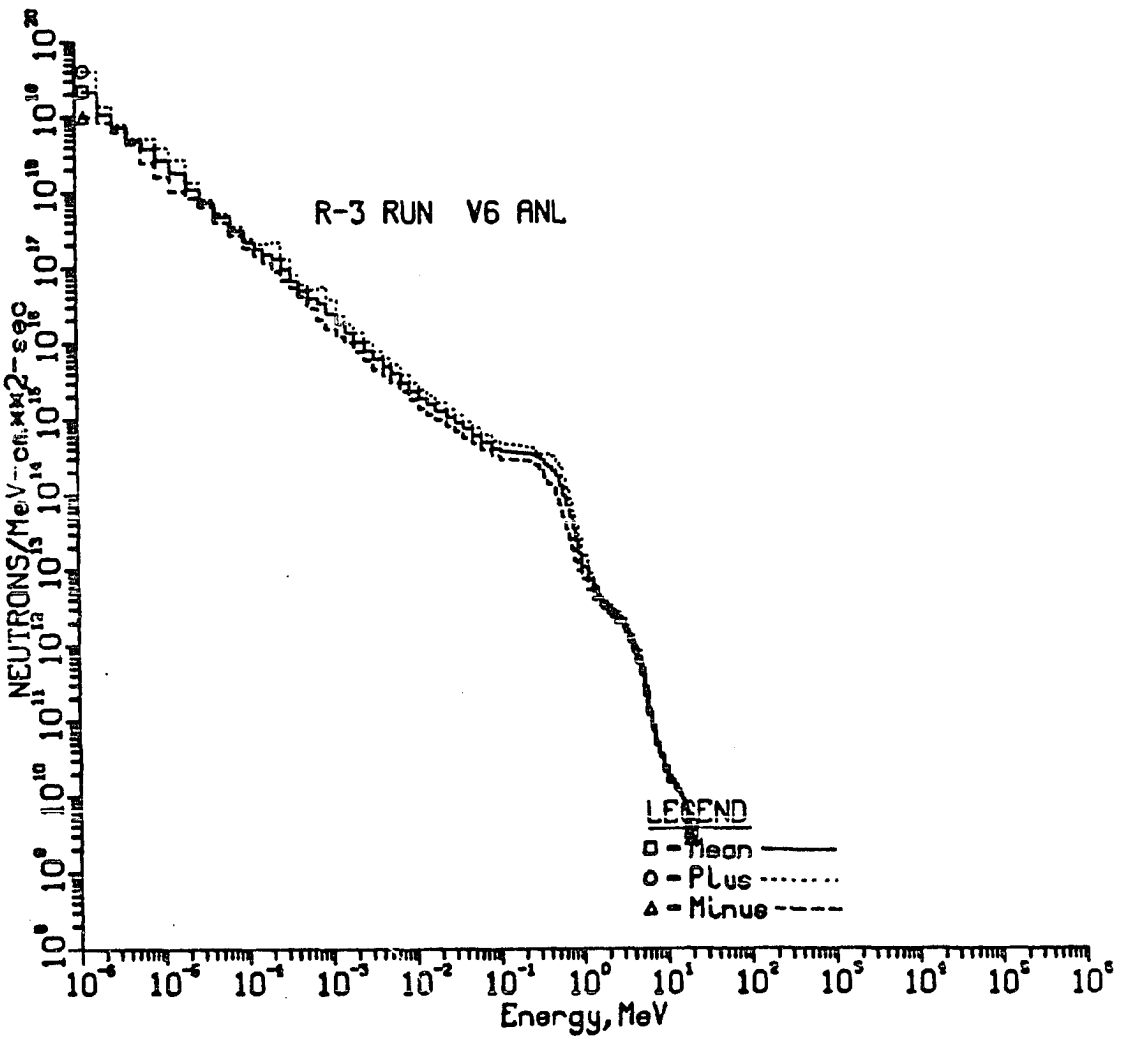

Figure 7. R-3 solution spectrum error analysis

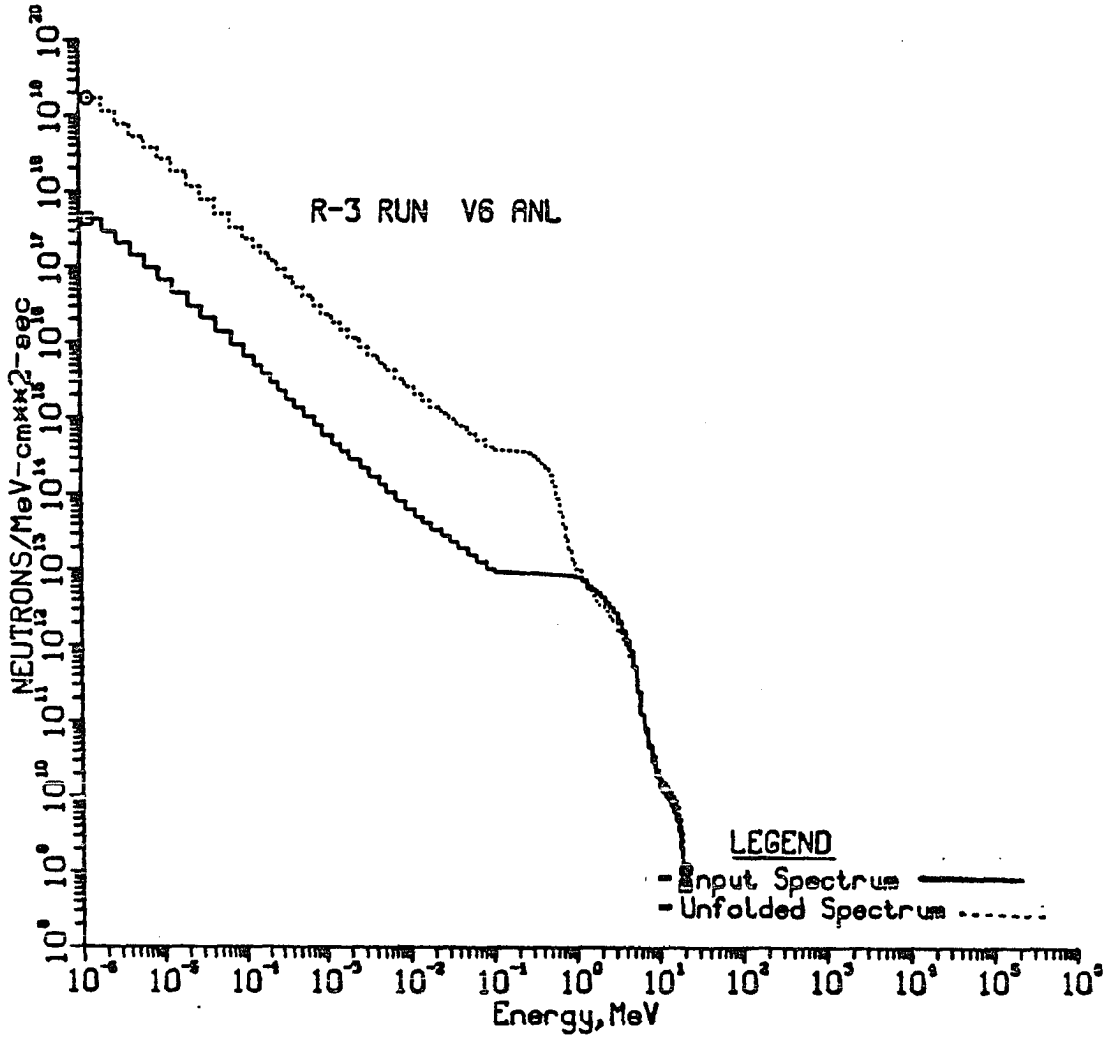

Figure 7-A. R-3 input and solution spectra

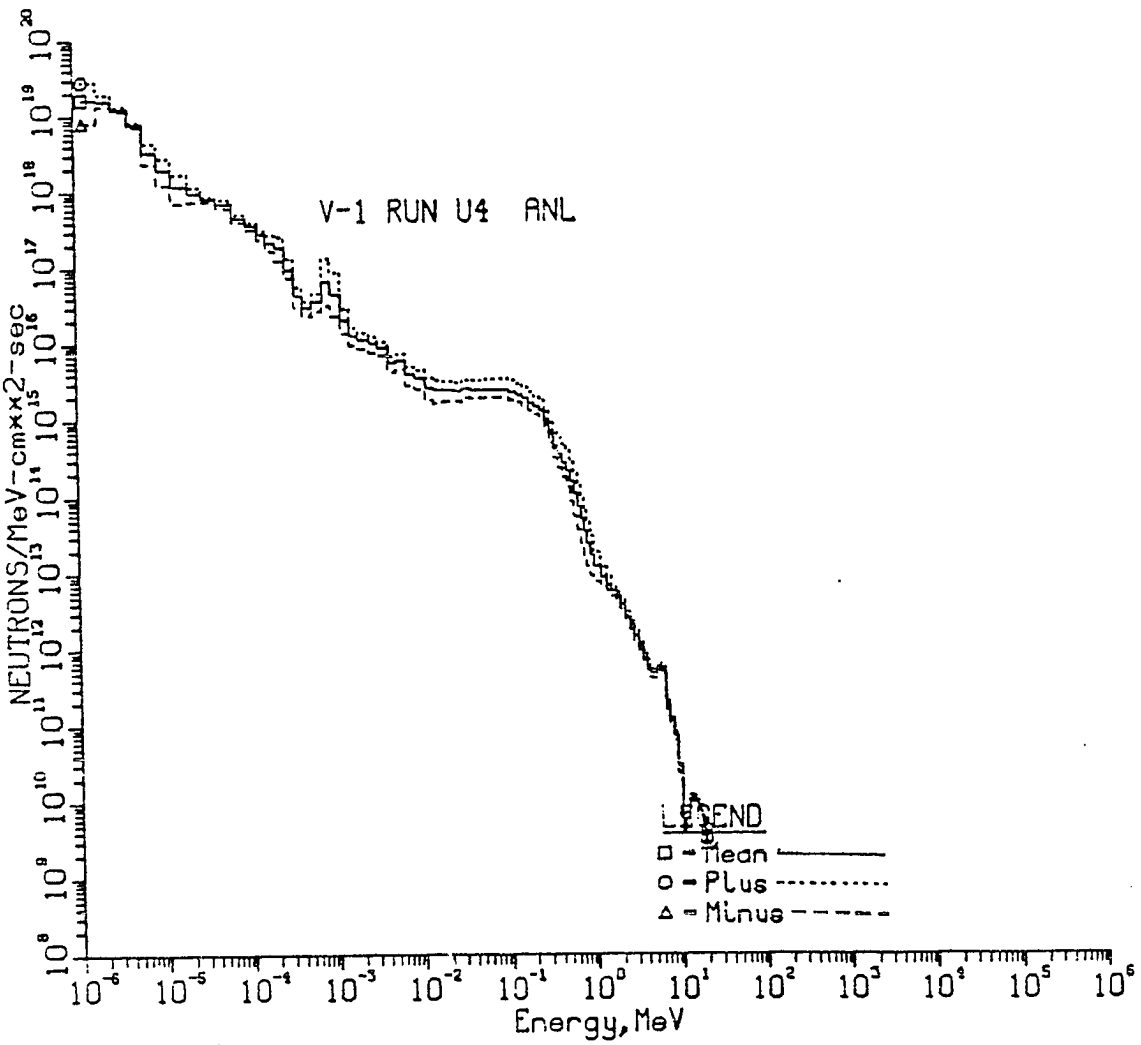

Figure 8. V-1 solution spectrum error analysis

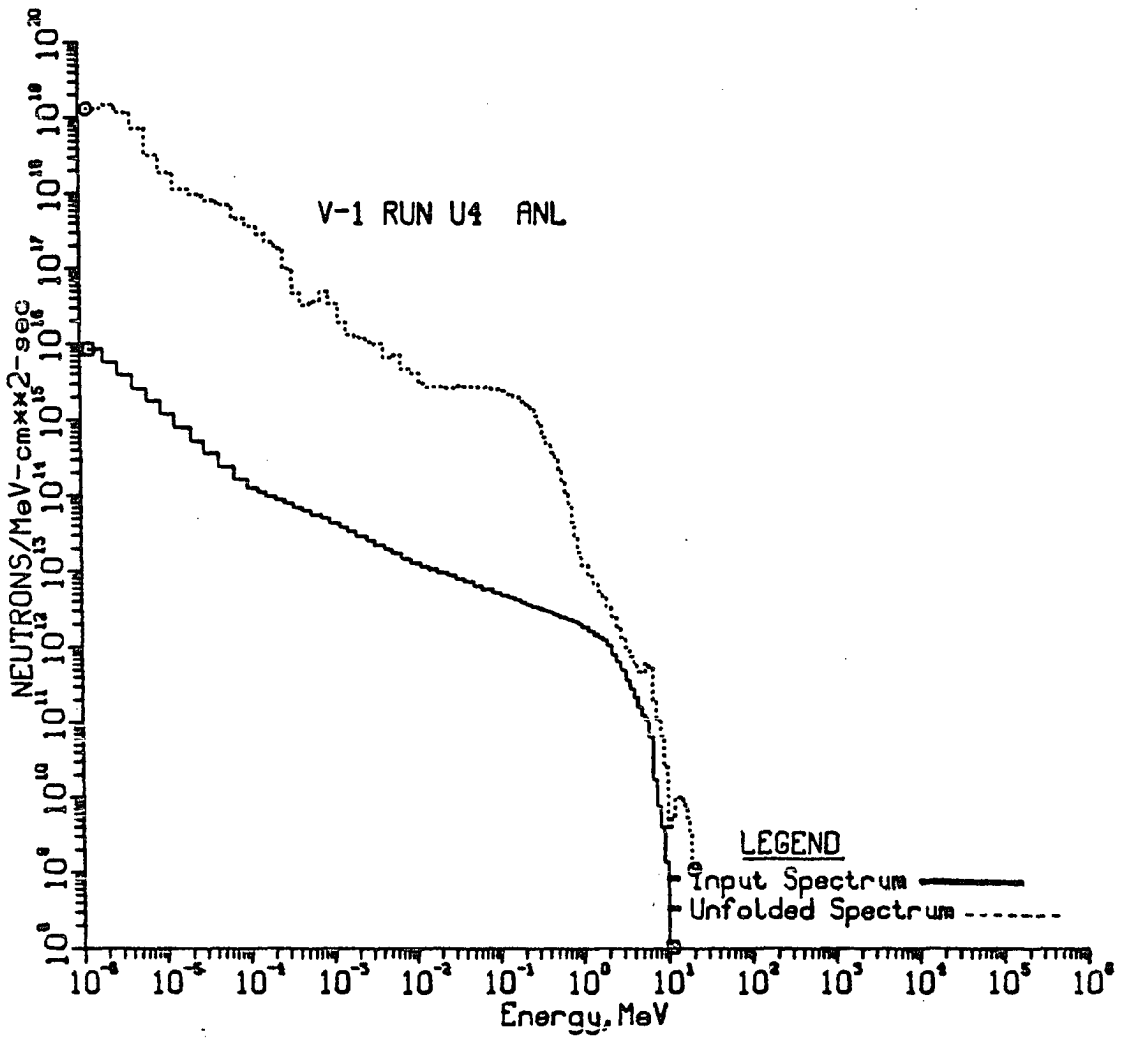

Figure 8-A. V-1 input and solution spectra

of the final solution is generally within ±10%. But at energies greater than 10 MeV, the error band widens. This is due to greater uncertainties associated with the values of $\sigma_i(E)$ at higher energies. Another contributing factor is the lesser coverage of these high energy regions by the reactions available to be used.

The results of several SAND-II runs involving different sets of experimentally measured activities showed that generally after a number of iterations the $^{48}Ti(n,p)^{48}Sc$ reaction was rejected. The percent deviation of the ^{48}Sc activity was positive for all runs and had a value ranging from 9% to 38%. Since the input spectra and the cross section values were not changed from run to run, it was concluded that the values of the $^{48}Ti(n,p)^{48}Sc$ reaction cross section with uncertainties up to ±50% (see Table 6) were the main cause of the rejection. The rejection of the $^{48}Ti(n,p)^{48}Sc$ reaction data and such other reaction data as $^{90}Zr(n,2n)^{89}Zr$ and $^{63}Cu(n,\alpha)^{60}Co$ has been reported by other investigators*. In these cases a higher level of uncertainty in the value of cross sections was found to be the main cause of the rejection. In fact, as may be noted from Table 6, the uncertainty of the above reactions is

---

* Private communication from Larry Greenwood of Argonne National Laboratory.

generally higher than the corresponding uncertainty for the other reactions used.

The values of the R-3 facility differential neutron flux, although reasonable up to E ≃10 MeV, seemed to be rather high for energies greater than 10 MeV. To study the spectral shape of the R-3 flux at higher energies, the SAND-II solution was compared with a fission spectrum $\varphi^*_{R-3}(E)$, obtained from the following Equation:

$$\varphi^*_{R-3}(E) = \Phi_{R-3} \times 0.770\ E^{1/2} \exp(-0.776E)$$

where $\Phi_{R-3} = 1.547 \times 10^{14}$ n/cm^{2}sec is the integral flux of the neutrons with E≥0.11 MeV and E is the neutron energy in MeV.

As shown in Figure 9, at energies greater than approximately 13 MeV, the actual R-3 flux, $\varphi_{R-3}(E)$, becomes increasingly greater than the fission flux $\varphi^*_{R-3}(E)$. As indicated in the preceding pages, part of this error is due to the greater cross section uncertainties and to the lack of sufficient foil coverage at higher energies. Another contributing factor to the discrepancy is the shape of the input spectrum used for the R-3 facility (Figure 10).

Starting from the input spectrum, the SAND-II code reached a reasonable final solution in a small number of iterations. To reach the solution, however, the input spectrum was extensively reduced at the low energy portion of the spectrum, as is

Figure 9. High energy portion of the R-3 solution spectrum compared with a fission spectrum

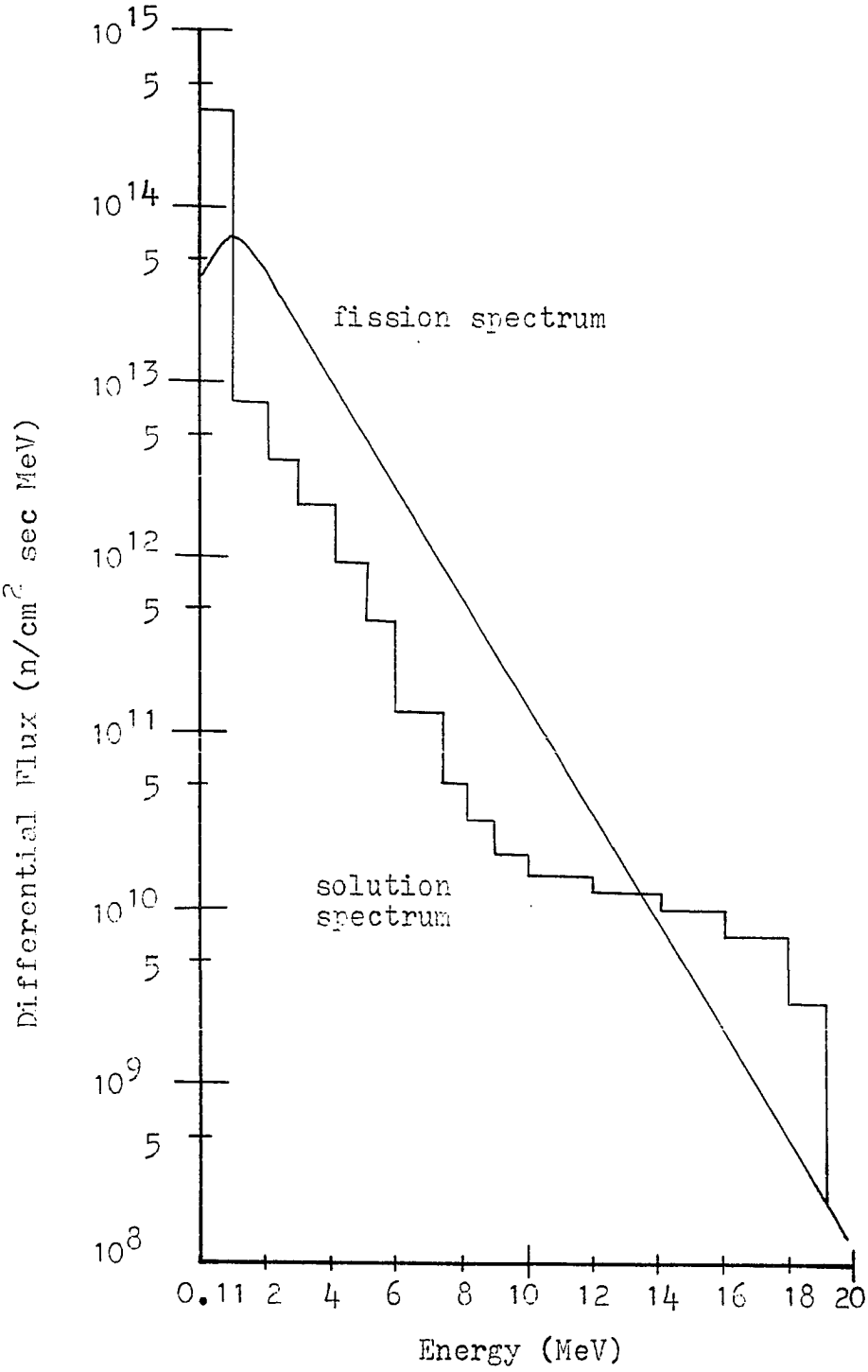
Differential Flux (n/cm² sec MeV)
10^15
5
10^14
5
10^13
5
10^12
5
10^11
5
10^10
5
10^9
5
10^8
fission spectrum
solution spectrum
0.1 1 2 4 6 8 10 12 14 16 18 20
Energy (MeV)

Figure 10. High energy portion of the R-3 input spectrum

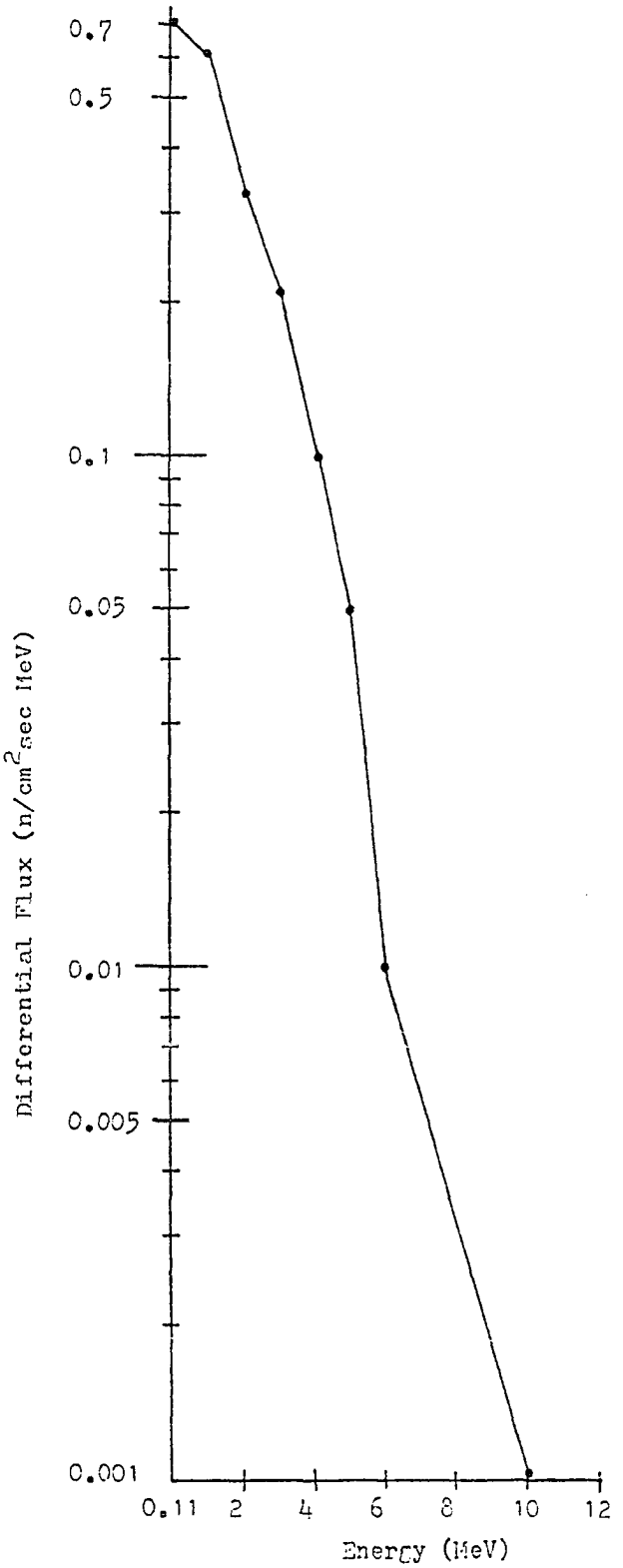
0.7
0.5
0.1
0.05
0.01
0.005
0.001
Differential Flux (n/cm^{2}sec MeV)
0.1
1
2
4
6
8
10
12
Energy (MeV)

shown in Figure 7-A. This resulted in what may be termed a "spectrum distortion": a reduction in magnitude at the low energy portion and an increase in magnitude for $E > 10$ MeV.

A similar trend, although to a lesser extent, was observed for the V-1 solution spectrum. At energies greater than 10 MeV, the actual spectrum approached the values of $\varphi^*_{V-1}(E)$ defined by

$$\varphi^*_{V-1}(E) = \Phi_{V-1} \times 0.770E^{1/2} \exp(-0.776E)$$

with $\Phi_{V-1} = 6.745 \times 10^{14}$ n/cm^{2}sec being the integral flux of the V-1 neutrons with $E \geq 0.11$ Mev. The values of $\varphi_{V-1}(E)$ and $\varphi^*_{V-1}(E)$ are plotted in Figure 11. The high energy portion of the V-1 input spectrum is illustrated in Figure 12.

Figure 11. High energy portion of the V-1 solution spectrum compared with a fission spectrum

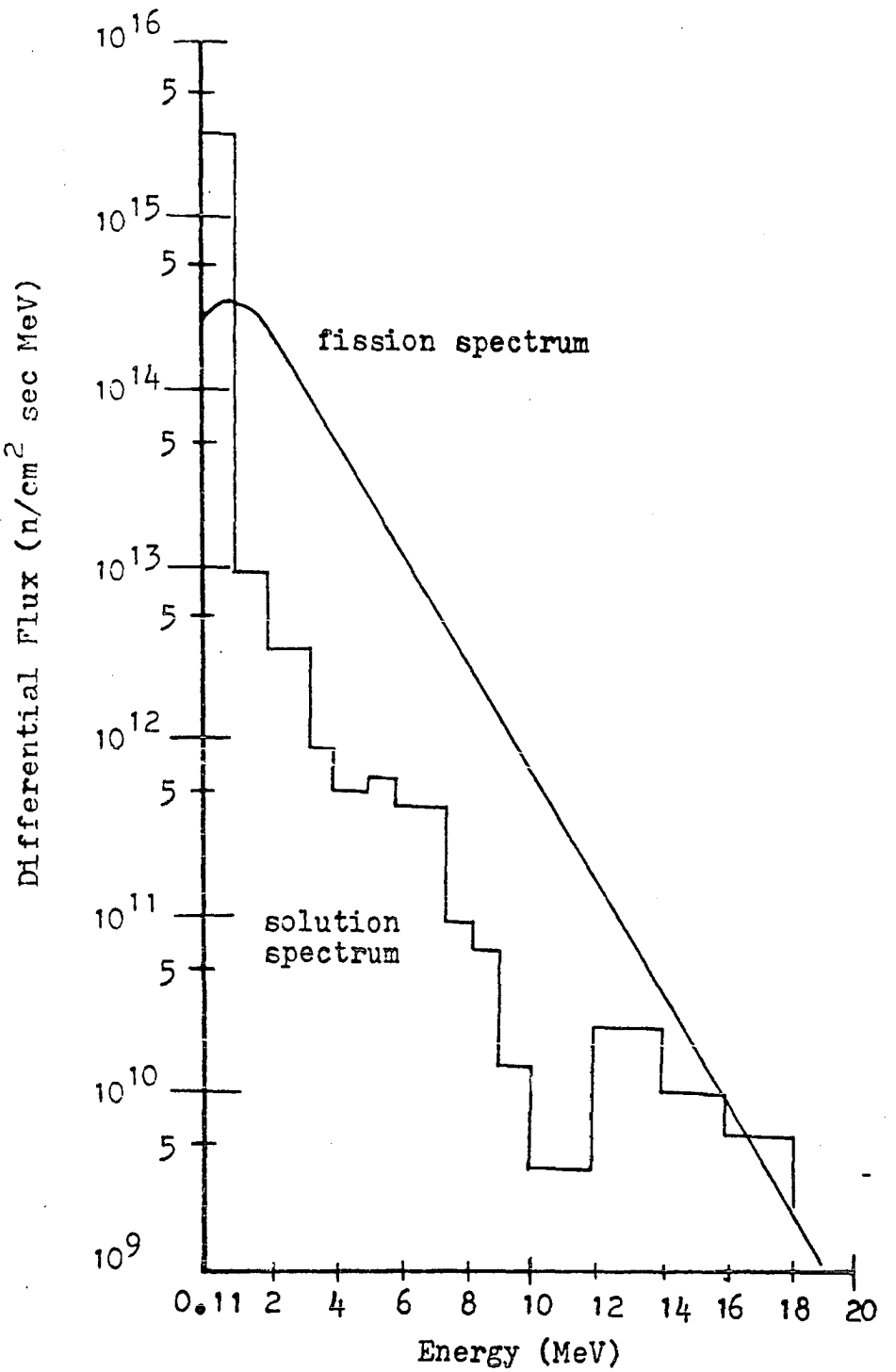
Differential Flux (n/cm² sec MeV)
10¹⁶
5
10¹⁵
5
10¹⁴
5
10¹³
5
10¹²
5
10¹¹
5
10¹⁰
5
10⁹
fission spectrum
solution spectrum
0.11 2 4 6 8 10 12 14 16 18 20
Energy (MeV)

Figure 12. High energy portion of the V-1 input spectrum

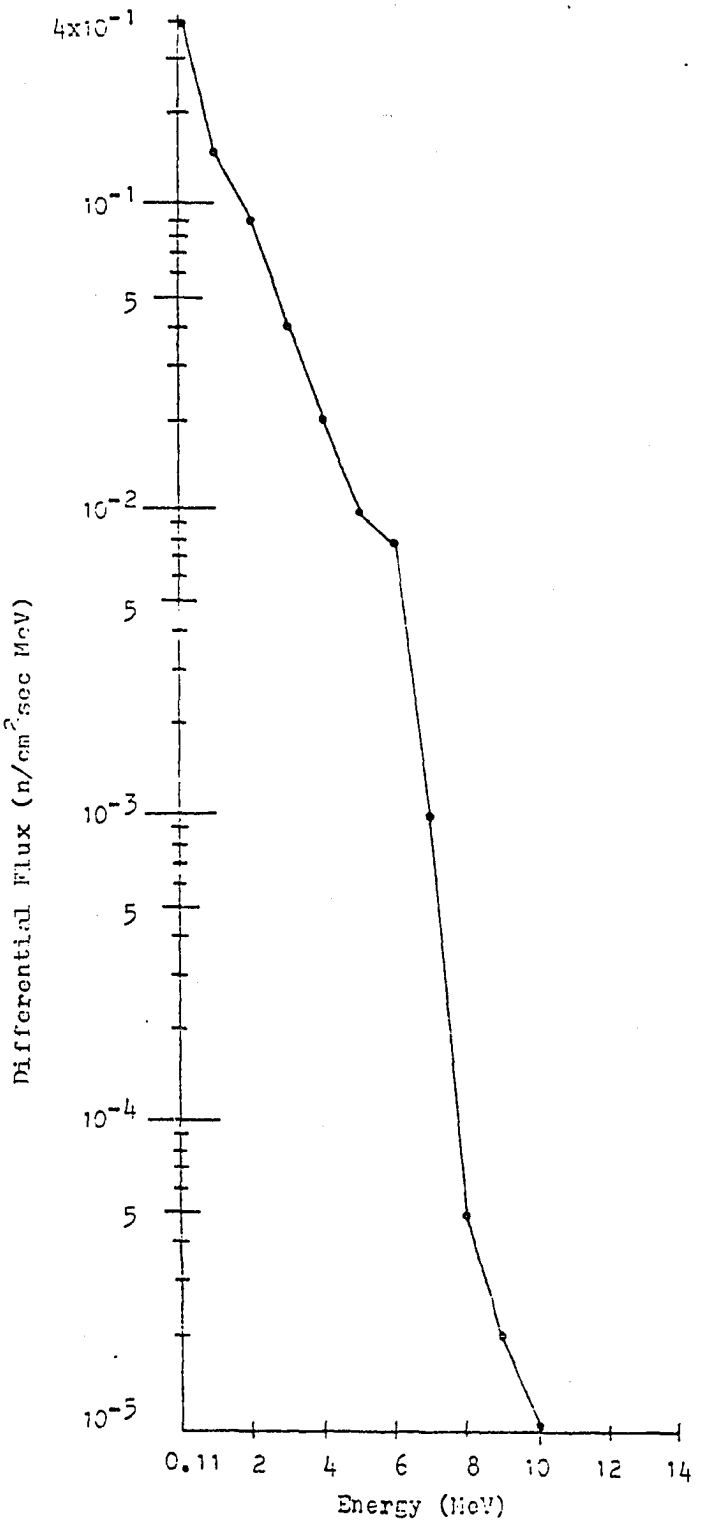
4x10⁻¹
10⁻¹
5
10⁻²
5
10⁻³
5
10⁻⁴
5
10⁻⁵
Differential Flux (n/cm²sec MeV)
0.11
2
4
6
8
10
12
14
Energy (MeV)

VII. SUMMARY AND CONCLUSIONS

The state of the art of multiple foil unfolding techniques has been reviewed. Of the procedures which have been explored and are available for consideration, Ringle (26) found that the Cross Section Expansion method provided the best agreement between actual (test) spectra and deduced profiles in the 2-30 MeV region selected for analysis. Of the three computer codes recommended for use, Dierckx (36,37) identified the SAND-II code as being somewhat superior to SPECTRA and CRYSTALL BALL. Consequently, the SAND-II code was selected for use in exploring the neutron energy distribution in the two ALRR irradiation facilities R-3 and V-1.

Activation detectors providing seventeen reactions were employed covering an energy range from 0.5 eV to 20 MeV. Because of the interest in exploring the higher energy region, twelve of the reactions had threshold energies in the MeV region.

The unfolding code iterates the flux distribution from a selected input spectrum until the calculated foil activations agree, within a predetermined limit of 5% total deviation from the experimentally determined values. The final solution is heavily dependent on the input spectrum due to the fact that the seventeen pieces of input activation data are much less than the 100 energy group flux amplitudes which must be specified to establish the spectrum. The number of iterations required to

complete the analysis is also dependent on the input spectra. For example, if by chance the selected input spectrum is correct the calculated and input activations will agree and no modification of the amplitude in any energy group will be required.

The selection of an appropriate input spectrum is facilitated by the existence within the code of a collection of potentially useful spectra. A choice of input spectrum was made for each of the two cases by testing all possibilities and selecting the one which required the smallest number of iterations to achieve the given level of agreement between measured and calculated activations. The input spectra for the R-3 and V-1 cases are shown in Figures 1 and 2 respectively. It will be noted that the input spectrum chosen by this method for the V-1 is somewhat "harder" than is the case for R-3.

The code measures the inconsistency between the evolving best fit spectrum and the individual contributions from the detectors. When a contribution deviates from the best fit value in excess of a predetermined amount, the contribution is dropped and the fitting procedure is carried out using the remaining data. Figures 3 and 4 show the spectrum obtained with and without a contribution from the $^{48}Ti(n,p)^{48}Sc$ reaction. The curves are seen to be identical which is not surprising since a number of other detectors are sensitive over part or

all of the same energy range. The consistency which results when the $^{48}Ti(n,p)^{48}Sc$ contribution is dropped, is improved to the extent that the deviation is reduced from 3.87 to 3.36% (Appendix B). It will be observed that the final solution for the R-3 spectrum (Figure 4) shows a significant decrease in the number of neutrons in the energy range between 0.5 MeV and 20 MeV as compared to the input spectrum (Figure 1). Figure 7a provides a direct comparison between the input and unfolded spectra for the R-3 facility.

As might be expected, the $^{48}Ti(n,p)^{48}Sc$ contribution was also rejected during the analysis of the data obtained in the V-1 facility. As before, the spectra obtained with and without the ^{48}Ti reaction (Figures 5 and 6) are identical. In this case the standard deviation after nine iterations is reduced from 11.3% to 4.9% (Appendix C). Although there is some evidence of structure in the spectrum for higher energies, the most striking observation is that the initially high neutron density for energies greater than 0.2 MeV (Figure 2) is adjusted downward in the energy range between 0.2 MeV and 20 MeV (Figures 6 and 8a).

A comparison of the spectra for the two facilities (R-3 and V-1) as shown in Figures 4, 6, 7, 7a, 8, and 8a reveals that much of the difference between the two distributions can be explained by the difference in the two input spectra. The higher relative neutron density in the energy range between

10^{-3} MeV and 0.5 MeV for V-1 as compared to R-3, as shown in Figures 4 and 6 or Figures 7 and 8, corresponds to the higher neutron density characteristics of the input spectrum for V-1 as shown in Figure 2. It will be noted that in the energy range between 10^{-3} and 0.5 MeV the modifications of the input spectra for the two cases must come from contributions from (n,γ) reactions with the ^{58}Fe, ^{59}Co, ^{63}Cu and ^{197}Au. Since all the detector foils were shielded by cadmium, they were responsive only to neutron energies greater than about 5×10^{-7} MeV. In the energy range of interest, 1×10^{-3} to 5×10^{-1} MeV, the gold cross section decreases monotonically from 5 barns to 0.2 barns with the bulk of its activation originating from the 3×10^{4} barn resonance at 4.8×10^{-6} MeV. Thus it is not to be expected that the integral gold activation data can provide a significant correction in this relatively narrow energy region of interest. The situation for cobalt is similar in that resonance contributions are significant (7000 barns and 260 barns) at 1.35×10^{-4} MeV and between 4.3×10^{-3} and 5×10^{-3} MeV. In this case roughly two energy groups around 4.5×10^{-3} MeV would be affected and examination of Figure 6 seems to support this conclusion. Although iron and copper have resonances they are not as pronounced as those just described. They do however fall within the region of interest; the iron resonances are found between 8×10^{-3} and 5×10^{-1} MeV while those for copper are found between 2×10^{-4}

and 5×10^{-2} MeV. For both of these detectors the cross section is roughly constant with energy which implies that their effect will be roughly proportional to the width of the energy range of interest or 0.5/20 = 0.025. Thus the corrections would once again be small. The overall conclusion is that with the detectors used no significant modification of the input spectrum is to be expected in the energy region between 1×10^{-3} and 5×10^{-1} MeV.

The difference between the spectra in the two facilities was explored with the aid of the differential flux curves (Figures 1-8a) and the values of both the normalized and the absolute integral fluxes tabulated in Appendices B and C corresponding to R-3 and V-1 respectively. The tabulated data gives the integral fluxes above selected or specified energy values. The absolute values provide information reflecting spacial and configuration dependent factors. For example since V-1 is in the center of the core and R-3 is in the moderator/reflector outside the core it would be expected that the magnitude of the flux in V-1 would exceed that found in R-3. In addition it would be expected that the energy dependent flux (the spectrum) would be "harder" in V-1 than in R-3 due to the flux-trap nature of the coaxial fuel element in the V-1 position and the proximity of moderator to the R-3 position. On the other hand the fact that the moderator and coolant are heavy water would tend to smooth out rapid or local variations in the

spectrum. The integral normalized fluxes should be better indicators of the energy dependence of the fluxes on the two facilities. For convenience selected data has been abstracted from the Appendices and is presented in table 7.

The interesting figures are the ratios of the integral fluxes in V-1 to those in R-3 for the various indicated lower energies. The ratio of absolute integral fluxes is 0.90 for neutrons with energies greater than 2 MeV and is 4.36 for neutrons with energies greater than 0.11 MeV (the energy range of greatest importance when considering neutron damage). From an experimental point of view the V-1 facility is clearly the better place in which to carry out fast neutron effect studies. This conclusion is not as easily drawn from examination of the differential flux curves (Figures 4 and 6) although V-1/R-3 differential flux ratios do provide supporting information.

Examination of the relative integral flux ratios reveals that for neutron energies above 2 MeV, above 1 MeV and above 0.5 MeV, the relative neutron density is greater in R-3 than in V-1. Only for energy ranges with lower limits below 0.11 MeV does V-1 offer a harder spectrum. The total flux in V-1 is seen to be about 2.5 times larger than the corresponding flux in R-3.

To establish confidence in the results of the SAND-II analysis, a Monte Carlo error study was carried out using the uncertainties in detector cross sections and experimentally determined activations as input. The results of the analyses

Table 7. Integral flux data taken from Appendices B and C

Energy MeV		2	0.5	0.11	1.275×10^{-3}	1.350×10^{-5}	1.275×10^{-6}
R-3	Absolute	5.869×10^{12}	3.860×10^{13}	1.547×10^{14}	2.793×10^{14}	3.990×10^{14}	4.574×10^{14}
	Relative	1.049×10^{-2}	6.896×10^{-2}	2.764×10^{-1}	4.989×10^{-1}	7.128×10^{-1}	8.172×10^{-1}
V-1	Absolute	5.308×10^{12}	7.262×10^{13}	6.745×10^{14}	1.138×10^{15}	1.263×10^{15}	1.348×10^{15}
	Relative	3.753×10^{-3}	5.135×10^{-2}	4.769×10^{-1}	8.048×10^{-1}	8.927×10^{-1}	9.531×10^{-1}
$\frac{(V-1)}{(R-3)}$	Abs.	0.904	1.881	4.360	4.074	3.165	2.947
$\frac{(V-1)}{(R-3)}$	Rel.	0.358	0.745	1.725	1.613	1.252	1.166

are shown in Figures 7 and 8. Comparison between Figures 7 and 7a, and 8 and 8a shows the uncertainty zones of the unfolded spectra.

The computed values of the high, low, mean and true flux values and the percent variations from the mean for the fluxes in R-3 and V-1 are presented in Appendix D. It will be noted that the percent uncertainties are higher by a factor of 2 for V-1 fluxes as compared to R-3 fluxes in the energy range below 1 x 10^{-6} MeV. For energies between 1 x 10^{-6} and 3 x 10^{-1} MeV and V-1 flux uncertainties are higher by approximately 25% and for energies greater than about 8 x 10^{-1} MeV (Table 8). In the main, these peculiarities correlate well with the differences between the mean and true flux values. For energies below about 1 x 10^{-6}MeV the mean value of the flux in R-3 is greater than the true value while for the flux in V-1 the reverse is true. For energies in the interval between 1 x 10^{-6} and 3 x 10^{-1} MeV, the mean values of the flux are smaller than the true values of the flux for both facilities. For energies between 1 and 6 MeV there is some oscillation but in the main whatever is the case for one facility the reverse is true for the other. Finally, for energies above 6 MeV the mean flux is greater than the true flux for both facilities.

There is a significant departure in the patterns for energies in the range 1 x 10^{-1} to 1 MeV and for energies greater than 10 MeV. For these energy regions, the variations are significantly larger than they are for adjacent energies.

Table 8. Differential flux data taken from Appendices B and C

Energy MeV		2	0.5	0.11	1.275×10^{-3}	1.350×10^{-5}	1.275×10^{-6}
V-1	Absolute	3.399×10^{12}	2.597×10^{14}	3.044×10^{15}	1.358×10^{16}	1.054×10^{18}	1.200×10^{19}
	Relative	2.403×10^{-3}	1.837×10^{-1}	2.152×10^{0}	9.599×10^{0}	7.456×10^{2}	8.485×10^{3}
R-3	Absolute	3.307×10^{12}	1.685×10^{14}	3.517×10^{14}	1.691×10^{16}	1.624×10^{18}	1.581×10^{19}
	Relative	5.908×10^{-3}	3.011×10^{-1}	6.283×10^{-1}	3.021×10^{1}	2.901×10^{3}	2.825×10^{4}
$\frac{(V-1)}{(R-3)}$	Abs.	1.028	1.541	8.655	0.803	0.649	0.759
$\frac{(V-1)}{(R-3)}$	Rel.	0.407	0.610	3.425	0.318	0.257	0.300

As noted before, the detectors with energy sensitivities in the ranges 1×10^{-2} and 5×10^{-1} MeV were sensitive over a broad energy range and no detectors were used with energy sensitivities greater than 20 MeV, or less than 5×10^{-7} MeV; consequently it is not too surprising that the SAND-II iteration procedure was unable to accomplish necessary corrections and reduce the variations in these regions.

The four wide range (n,γ) detectors are the only detectors used with sensitivities between energies of 4×10^{-4} and 5×10^{-1} MeV. This fact, provides an explanation for the remaining principal features of the Monte Carlo error analysis viz. the large variations between 1×10^{-1} and 1 MeV.

For those energies where suitable detectors were not available or, if available, were not used, any agreement between a smooth curve based on an iterated input spectrum and the true spectrum would be accidental. Moreover, the variation between highest and lowest values could be large.

As would be expected the change of the flux variation with energy reflects the changing uncertainty in the cross sections, as reported in Table 6.

The final unfolded spectra for R-3 and V-1 were compared with fission spectra as shown in Figures 9 and 11. It was observed that contrary to reason and expectations the unfolded spectra for energies greater than about 10 MeV had high energy components greater than would an appropriately normalized

fission spectrum. Although these observations can be explained in terms of cross section uncertainties or lack of sensitivity of available detectors in this high energy region another possibility is that the original input spectra are involved. Inspection of Figure 7a shows how the low energy portion of the input spectrum was drastically reduced which implies that for a constant neutron population, the high energy portion is relatively augmented. Had suitable detectors been available the iteration procedure would have provided appropriate corrections. The significance for this work is that the indicated high energy neutron flux is in error. However, the importance of the effect is academic. From the point of view of radiation damage effects, the magnitude of the integrated flux for energies above 0.11 MeV and the (V-1)/(R-3) ratios are essentially unchanged from the tabulated values if contributions for energies above 10 MeV are ignored.

The results clearly indicates: (a) the importance of the input spectrum in determining the shape of the final spectrum in energy regions not adequately explored by detection reactions; (b) the value of having a number of detectors sensitive in the same energy range as revealed by the stability of the spectrum to rejection of the ^{48}Ti contributions; (c) the relative ineffectiveness of a detector, like ^{63}Cu, sensitive over a wide energy range as demonstrated by the lack of change in the spectrum for the V-1 facility in the energy range 4×10^{-4} to

2×10^{-2} MeV; (d) the ability of SAND-II to rapidly modify an incorrect input spectrum in accordance with information obtained from a number of detectors as shown by the results from both sets of data in the energy range from 0.5 to 20 MeV.

VIII. SUGGESTIONS FOR FUTURE WORK

The input spectra in this work were "best guess-empirical" distributions. Their selection, among the distributions tested, was based primarily on the fact that they yielded the minimum number of iterations required to reach a final solution. Hence, future use of the unfolding codes could be improved by using more suitable input spectra established by sophisticated calculations.

A related area of interest is a study of the sensitivity of the unfolding code results to the choice of input spectrum. One possible approach would be as follows:

1 - select a number of different spectra $\varphi(E)$, actual or purely mathematical, to serve as the unknown spectrum to be determined by the unfolding procedure;

2 - calculate the reaction rates of several foils, using these spectra;

3 - choose a number of input spectra $\varphi_1^0(E)$ for each $\varphi(E)$;

4 - quantify the variation of the solution spectra $\tilde{\varphi}(E)$ as a function of the variation in $\varphi_1^0(E)$. This may be accomplished by studying the following expressions:

$$\Delta\varphi_1(E) = \tilde{\varphi}(E) - \varphi_1^0(E) = \sum_{i,j} k_{ij} \left[A_{spi} - \int_0^\infty \sigma_i(E)\ \varphi_1^0(E)\, dE \right]$$

$$\Delta\varphi_2 = \tilde{\varphi}(E) - \varphi_2^0(E) = \sum_{i,j} k_{ij} \left[A_{spi} - \int_0^\infty \sigma_i(E)\, \varphi_2^0(E) dE \right]$$

$$\vdots$$

$$\Delta\varphi_1 = \tilde{\varphi}(E) - \varphi_1^0(E) = \sum_{i,j} k_{ij} \left[A_{spi} - \int_0^\infty \sigma_i(E)\, \varphi_1^0(E) dE \right]$$

which lead to

$$(\delta_1^2) = (\Delta\varphi_1)^2 / \tilde{\varphi}(E)$$

where i = 1, ..., N denotes the specific reaction used, j = 1, ..., M indicates the energy interval, and A_{spi} is the reaction rate calculated with $\varphi(E)$ for reaction i.

This sensitivity study could be complemented by further investigating the "importance" of the response functions in energy regions which are not sufficiently covered by the detectors.

IX. ACKNOWLEDGMENTS

The author wishes to express his gratitude to Dr. D. M. Roberts for his assistance and patience during the course of this work.

Many thanks to Dr. Larry Greenwood of Argonne National Laboratory who provided detector foils and computer time for the completion of this work. Mr. Willem Zijp of RCN was helpful in providing literature and discussion.

Appreciation is also expressed to the Ames Laboratory Research Reactor personnel for assisting with the author's experimental work. This study could not have been completed without the help of Dr. A. F. Voigt director of the Ames Laboratory Reactor Division and his staff Mr. D. Hull, Mr. B. Link, Mr. K. Malaby, and the ALRR Health Physics staff Mr. J. Jones, Mr. P. Milis, and Mr. M. Voss.

The financial support of the ISU Graduate College is gratefully acknowledged.

The author is also grateful to the members of his committee Drs. R. A. Hendrickson, A. Valfells, A. F. Voigt, and M. S. Wechsler for their support.

The author wishes to thank Pericu for her moral support.

X. LITERATURE CITED

1. Crouthamel, C. E. 1971. Applied gamma-ray spectrometry. 2nd ed. Pergamon Press, New York. 620 pp.

2. Cohen, B. L. 1951. Nucleonics 8(2): 1-29.

3. Hurst, G. S. 1956. Techniques of measuring neutron spectra... . Rev. Sci. Inst. 27:150-153.

4. Reinhardt, P. W. and F. J. Davis. 1958. Improvements in the threshold detector method in fast neutron dosimetry. Health Phys. 1:165-169

5. Hurst, G. S., and R. H. Ritchie. 1959. Dosimetric aspects of neutron and gamma-ray exposures. ORNL-2748. (Oak Ridge National Laboratory, Oak Ridge, Tennessee). 56 pp.

6. Wechsler, M. S., and J. B. Trice. 1963. Tentative procedures for measuring neutron flux by radioactivation techniques. ORNL-63-46R2. (Oak Ridge National Laboratory, Oak Ridge, Tennessee). 28 pp.

7. Stiller, G. 1964. Determination of fast neutron spectra with threshold detectors (in German). ABS-THH-1016. (Hanover Institute of Technology, Radiation Protection Division). 17 pp.

8. Grundl, J. A., and A. Usner. 1960. Spectral comparisons with high energy activation detectors. Nuc. Sci. Eng. 8:595-598.

9. Levine, S. H., J. H. Olafson, and B. Faulkenberry. 1964. Neutron spectrum measurements for the Northrop reactor. NSL-64-187. (Northrop Space Labs.). 59 pp.

10. Zijp, W. L. 1965. Review of activation method for the determination of intermediate neutron spectra. RCN-40. (Reactor Centrum Nederland). 104 pp.

11. Zijp, W. L. 1965. Review of activation method for the determination of fast neutron spectra. RCN-37. (Reactor Centrum Nederland). 85 pp.

12. McElroy, W. N., S. Berg, and G. Gigas. 1967. Neutron-flux spectral determination by foil activation. Nuc. Sci. Eng. 27:533-541.

13. McElroy, W. N., S. Berg, and J. Tuttle. 1969. Measurement of neutron flux spectra by a multiple foil activation iterative method and comparison with reactor physics calculations and spectrometer measurement. Nuc. Sci. Eng. 36:15-27.

14. McElroy, W. N., S. Berg, and T. Crockett. 1967. A computer-automated iterative method for neutron flux spectra determination by foil activation. AFWL-TR-67-41. (Air Force Weapons Laboratory). Four volumes.

15. Grundl, J. A. 1968. A study of fission neutron spectra with high-energy activation detectors, part II: Fission spectra. Nuc. Sci. Eng. 31:191-206.

16. Dodds, H. L. 1969. Experimental determination of the differential fast neutron flux in the High Flux Isotope Reactor using threshold detectors. ORNL-TM-2565. (Oak Ridge National Laboratory, Oak Ridge, Tennessee). 139 pp.

17. Di Cola, G., and A. Rota. 1965. Calculation of differential fast neutron spectra from threshold foil activation data by least squares series expansion methods. Nuc. Sci. Eng. 23:344-353.

18. McElroy, W. N., and L. S. Kellog. 1975. Fuels and materials for fast-reactor dosimetry data development and testing. Nuc. Tech. 25(2):180-223.

19. Greenwood, R. C., et al. 1975. Nonfission reaction rate measurements. Nuc. Tech. 25(2):274-293.

20. Hughes, D. J. 1953. Pile neutron research. Addison-Wesley Publishing Co., Inc., Reading, Massachusetts.

21. Hurst, G. S., and J. A. Harter. 1956. Techniques of measuring neutron spectra with threshold detectors. Rev. Sci. Instr. 27:148-153.

22. Delattre, P. 1961. Methods of fast neutron spectrum measurement with threshold detectors (in French). CEA-1979. (Atomic Energy Commission, France). 23 pp.

23. Uthe, P. M. 1957. Attainment of neutron flux spectra foil activation. WADC-TR-57-3. (Wright Air Development Center). 17 pp.

24. Trice, J. B. 1957. Preliminary report of an analytical method for measuring neutron spectra. APEX-408. (General Electric). 26 pp.

25. Hartmann, S. R. 1957. A method for determining neutron flux spectra from activation measurements. WADC-TR-57-375. (Wright Air Development Center). 23 pp.

26. Ringle, J. C. 1963. A technique for measuring neutron spectra in the range 2.5 to 30 MeV using threshold detectors. UCRL-10732. (University of California Radiation Laboratory). 221 pp.

27. Bresesti, M., Del Turco A. M., and Ostidich, A. M. 1963. Fast neutron measurements by threshold detectors in Ispra I and Avogadro R5-1. IAEA. Vol. 1. (International Atomic Energy Agency).

28. Lanning, W. D., and Brown, K. W. 1961. Calculated and measured neutron energy spectral distributions using the threshold detector technique. WAPD-T-1380. (Westinghouse Electric Corp.). 18 pp.

29. Trubey, D. K., compiler. 1976. Radiation Shielding Information Center. A review of radiation energy spectra unfolding. ORNL-RSIC-40. (Oak Ridge National Laboratory, Oak Ridge, Tennessee). 255 pp.

30. Narum, R. E. 1972. INSPECT-interactive computer code for unfolding neutron spectra from activation measurement. ANCR-1035. (Aerojet Nuclear Company). 66 pp.

31. Morgan, W. C. 1964. FOILS: A program for computing neutron exposures from foil activation data. HW-81367. (Hanford Atomic Products Operation). 20 pp.

32. Greer, C. L., and Walker, J. V. 1967. A procedure for the computation of neutron flux from foil activation data - SPECTRA code. SC-R-67-1066. (Sandia Laboratory). 9 pp.

33. Greer, C. L., Halbleib, J. A., and Walker, J. V. 1967. A technique for unfolding neutron spectra from activation measurement. SC-RR-67-746. (Sandia Laboratory). 33 pp.

34. Kam, F. B. K., and Stallman, F. W. 1974. CRYSTALL BALL-A computer program for determining neutron spectra from activation measurements. ORNL-TM-4601. (Oak Ridge National Laboratory, Oak Ridge, Tennessee). 30 pp.

35. Stallman, F. W. 1970. Numerical solution of integral equations. Numerische Mathematik 15:297-305.

36. Dierckx, R. 1973. Critical comparison of spectrum unfolding codes. INDC-NDS-56-U. (International Atomic Energy Agency). 34 pp.

37. Dierckx, R., and Sangiust, V. 1975. Intercomparison of neutron spectra evaluation methods using activation detectors. Paper presented at the first ASTM-Euratom Symposium on Reactor Dosimetry, Petten, Holland, September 22-26, 1975.

38. Fischer, A. 1975. International intercomparison of neutron spectra evaluating methods using activation detectors. JUL-1196. (International Atomic Energy Agency). 23 pp.

39. Zijp, W. L. 1976. Intercomparison of unfolding procedures (programs and libraries). Progress Report R. M. G. Note 76/09.

40. Dudey, N. D., Heinrich, R. R., and Popek, R. J. 1971. Activation-rate measurements in the ZPR-3 mockup critical experiments. ANL-7781. (Argonne National Laboratory). 73 pp.

41. Templin, L. J., compiler. 1963. Reactor physics constants. ANL-5800. (Argonne National Laboratory). p. 669.

42. Gill, R. L., and Stensland, W. A. 1973. Unpublished program instruction manual. Radiochemistry Group I, Ames Laboratory, Ames, Iowa.

43. Oster, C. A., McElroy, W. N., and Marr, J. M. 1973. A Monte Carlo program for SAND-II error analysis. HEDL-TME 73-20. (Hanford Engineering Development Laboratory). p. 14.

44. Simons, R. L., and McElroy, W. N. 1970. Evaluated reference cross section library. BNWL-1312. (Battelle-Northwest Laboratories).

45. Serpan, C. Z. Jr. 1974. Nuclear reactor neutron energy spectra. ASTM-DS-52. (American Society for Testing and Materials). pp. 158-161.

46. Boot, S. J. 1972. The use of threshold detectors to evaluate neutron leakage spectra for dosimetry calculation. AERE-R-7294.

47. Oster, C. A., Simons, R. L., Odette, G. R., McElroy, W. N., and Lippincott, E. P. 1976. Solution Weighting for the SAND-II Monte Carlo code. Paper presented at the Radiation Shielding Information Center Seminar-Workshop, Radiation Energy Spectra Unfolding, Oak Ridge National Laboratory, April 12-13, 1976.

48. Bohl, H. 1959. P1MG - A one-dimensional multigroup P1 code for the IBM-704. WAPD-TM-135. (Westinghouse Atomic Power Laboratory).

49. Duane, B. H. 1959. Neutron and photon transport plane-cylinder-sphere (GE-ANDP) program S variational optimum formulation. XDC-9-118. (General Electric Co.).

50. Shure, K. 1964. P-3 multigroup calculations of neutron attenuation. Nuc. Sci. Eng. 19:310-318.

XI. APPENDIX A

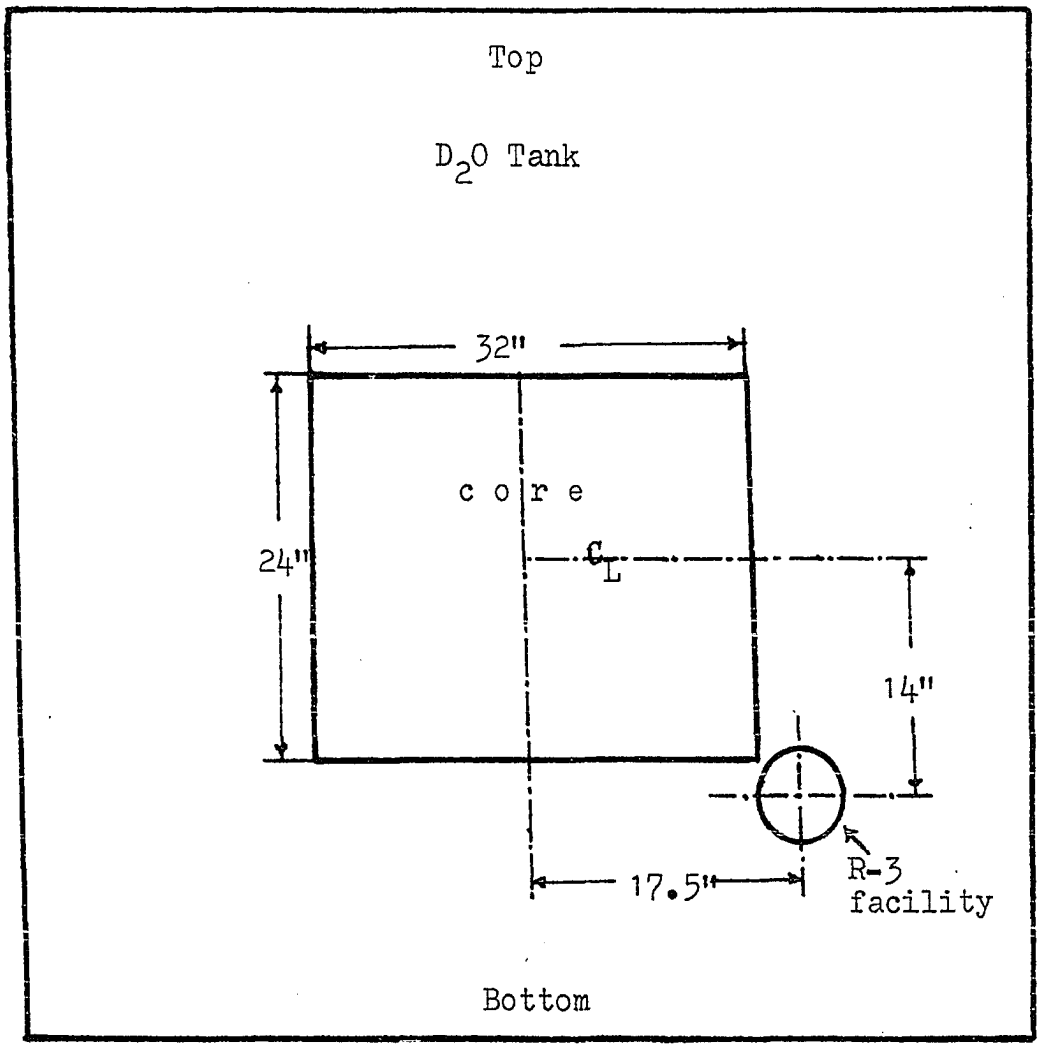

Figure 13. R-3 facility

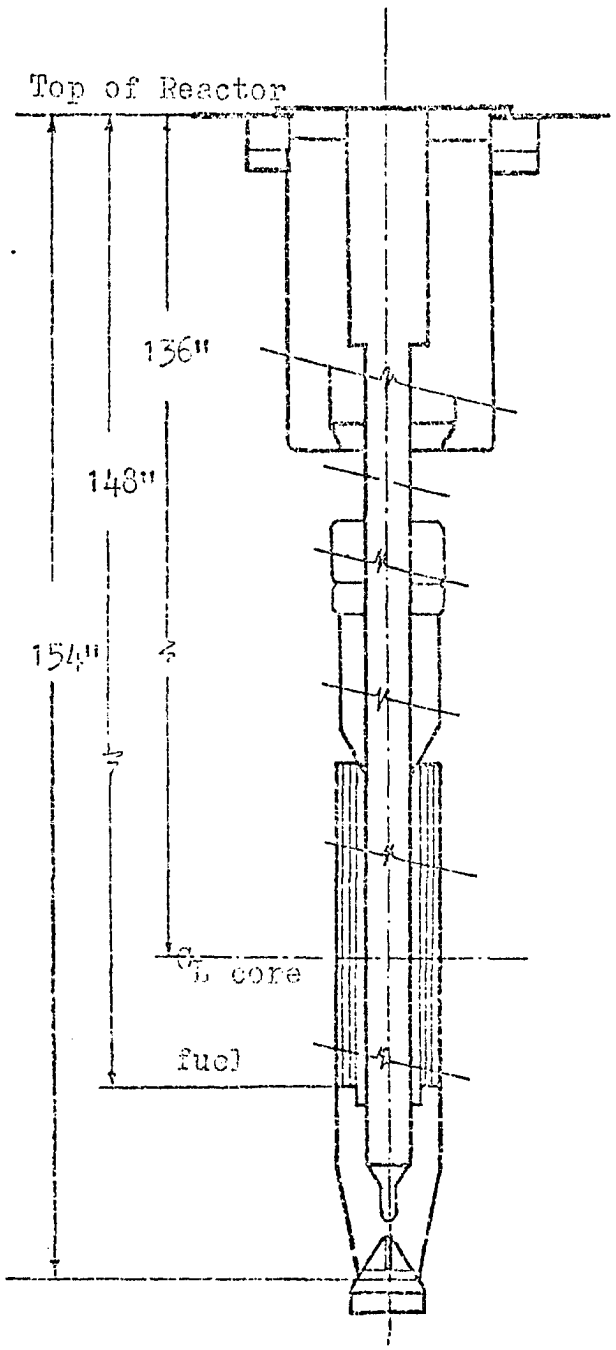

Figure 14. V-1 facility

XII. APPENDIX B

```
T
ITERATION
17 FOILS
AL27A     1.580E-14   CADMIUM    ISTP   20.
AU197G    3.605E-08   CADMIUM    ISTP   20.
CD59G     1.826E-09   CADMIUM    ISTP   20.
CU63G     1.288E-10   CADMIUM    ISTP   20.
FE58G     4.165E-11   CADMIUM    ISTP   20.
FE54G     1.137E-12   CADMIUM    ISTP   20.
NI58P     1.373E-12   CADMIUM    ISTP   20.
ZR90P     4.185E-14   CADMIUM    ISTP   20.
TI46P     1.362E-13   CADMIUM    ISTP   20.
TI47P     2.967E-13   CADMIUM    ISTP   20.
TI48P     7.635E-15   CADMIUM    ISTP   20.
FE56P     1.846E-14   CADMIUM    ISTP   20.
MG24P     2.989E-14   CADMIUM    ISTP   20.
TH232F    1.082E-12   CADMIUM    ISTP   20.
U238F     4.496E-12   CADMIUM    ISTP   20.
IN115N    3.014E-12   CADMIUM    ISTP   20.
CU63A     6.734E-15   CADMIUM    ISTP   20.
SPECTRUM TABULAR
18 POINTS
ENER  1.-10  1.-9  2.5-8  1.1-7  1.1-6  1.1-5  1.1-4  1.1-3  1.1-2  1.1-1
ENER  1.1  2.1  3.1  4.1  5.1  6.1  10.1  20.
FLUX  1.2+4  1.2+5  1.2+6  5.1+5  4.5+4  5.1+3  5.1+2  4.5+1  4.5  .71  .62
FLUX  .33  .21  .1  .05  .01  .001  0.0
LIMIT 30
DEVIATION 5
DISCARD 2
LOW END THERMAL
HIGH END FISSION
NORM  1.0-10
PLOT, NO CARDS
SMOOTH 5
```

INTERIM RESULTS AFTER 0 ITERATIONS

FOIL REACTION		NOMINAL 5.00 PERCENT ACTIVITY LIMITS (MEV) LOWER	UPPER	RATIO MEASURED TO CALCULATED ACTIVITIES	DEVIATION OF MEASURED FROM CALCULATED ACTIVITY (PERCENT)
AL27(N,A)NA24	CD	6.700E 00	1.600E 01	0.1364	-86.36
AU197(N,G)AU198	CD	4.250E-06	4.500E-05	3.7255	272.55
CO59(N,G)CO60	CD	8.400E-07	1.700E-04	3.7624	276.24
CU63(N,G)CU64	CD	8.400E-07	3.600E-01	3.8679	286.79
FE58(N,G)FE59	CD	8.400E-07	9.200E-03	4.1307	313.07
FE54(N,P)54MN	CD	2.300E 00	7.400E 00	0.0944	-90.56
IN115(N,N)IN115M	CD	1.000E 00	5.000E 00	0.0968	-90.32
NI58(N,P)CO58	CD	2.000E 00	7.400E 00	0.0851	-91.49
ZR90(N,2N)ZR89	CD	1.300E 01	1.900E 01	0.1697	-83.03
TI46(N,P)SC46	CD	3.700E 00	1.300E 01	0.1049	-89.51
TI47(N,P)SC47	CD	1.800E 00	7.400E 00	0.0841	-91.59
TI48(N,P)SC48	CD	6.000E 00	1.700E 01	0.1541	-84.59
TH232(N,F)FSPR	CD	1.400E 00	6.700E 00	0.0909	-90.91
U238(N,F)FSPR	CD	1.400E 00	6.000E 00	0.0867	-91.33
CU63(N,A)CO60	CD	6.000E 00	1.600E 01	0.1407	-85.93
FE56(N,P)MN56	CD	5.500E 00	1.600E 01	0.1333	-86.67
MG24(N,P)NA24	CD	6.700E 00	1.600E 01	0.1367	-86.33

STANDARD DEVIATION OF MEASURED ACTIVITIES (PERCENT)					164.40

AVERAGE TOTAL FLUX (ABOVE 1.00E-10 MEV) 2.974E 14

INTERIM RESULTS AFTER 1 ITERATIONS

FOIL REACTION		NOMINAL 5.00 PERCENT ACTIVITY LIMITS (MEV) LOWER	UPPER	RATIO MEASURED TO CALCULATED ACTIVITIES	DEVIATION OF MEASURED FROM CALCULATED ACTIVITY (PERCENT)
AL27(N,A)NA24	CD	6.700E 00	1.700E 01	1.0061	0.61
AU197(N,G)AU198	CD	4.250E-06	4.500E-05	0.9971	-0.29
CO59(N,G)CO60	CD	8.400E-07	1.700E-04	1.0027	0.27
CU63(N,G)CU64	CD	5.500E-07	1.900E-02	1.0502	5.02
FE58(N,G)FE59	CD	8.400E-07	3.600E-04	1.0660	6.60
FE54(N,P)54MN	CD	2.300E 00	8.200E 00	0.9723	-2.77
IN115(N,N)IN115M	CD	6.600E-01	5.000E 00	0.9308	-6.92
NI58(N,P)CO58	CD	2.000E 00	8.200E 00	0.8817	-11.83
ZR90(N,2N)ZR89	CD	1.300E 01	1.900E 01	1.1458	14.58
TI46(N,P)SC46	CD	3.700E 00	1.400E 01	0.9606	-3.94
TI47(N,P)SC47	CD	1.800E 00	8.200E 00	0.8772	-12.28
TI48(N,P)SC48	CD	6.000E 00	1.700E 01	1.1355	13.55
TH232(N,F)FSPR	CD	1.400E 00	7.400E 00	0.9543	-4.57
U238(N,F)FSPR	CD	1.400E 00	6.700E 00	0.9075	-9.25
CU63(N,A)CO60	CD	6.000E 00	1.600E 01	1.0604	6.04
FE56(N,P)MN56	CD	5.500E 00	1.600E 01	1.0327	3.27
MG24(N,P)NA24	CD	6.700E 00	1.600E 01	1.0193	1.93

STANDARD DEVIATION OF MEASURED ACTIVITIES (PERCENT) 7.84

AVERAGE TOTAL FLUX (ABOVE 1.00E-10 MEV) 5.455E 14

SOLUTION SPECTRUM OBTAINED AFTER 2 ITERATIONS

ENERGY (MEV)	ABSOLUTE VALUES DIFFERENTIAL FLUX	ABSOLUTE VALUES INTEGRAL FLUX	NORMALIZED TO 1.00E-10 MEV DIFFERENTIAL FLUX	NORMALIZED TO 1.00E-10 MEV INTEGRAL FLUX	AVERAGE ENERGY (MEV)
1.000E-10	2.032E 19	5.596E 14	3.631E 04	1.000E 00	1.477E-01
1.000E-09	1.951E 20	5.596E 14	3.504E 05	1.000E 00	1.477E-01
1.000E-08	4.393E 20	5.579E 14	7.850E 05	9.968E-01	1.482E-01
2.300E-08	4.644E 20	5.522E 14	8.298E 05	9.866E-01	1.497E-01
5.000E-08	3.509E 20	5.396E 14	6.271E 05	9.642E-01	1.532E-01
7.600E-08	2.730E 20	5.305E 14	4.878E 05	9.479E-01	1.558E-01
1.150E-07	1.949E 20	5.198E 14	3.483E 05	9.289E-01	1.590E-01
1.700E-07	1.290E 20	5.091E 14	2.287E 05	9.097E-01	1.624E-01
2.550E-07	8.376E 19	4.932E 14	1.497E 05	8.903E-01	1.659E-01
3.300E-07	5.588E 19	4.878E 14	9.985E 04	8.716E-01	1.695E-01
5.500E-07	3.670E 19	4.783E 14	6.557E 04	8.546E-01	1.729E-01
3.400E-07	2.372E 19	4.676E 14	4.239E 04	8.356E-01	1.768E-01
1.275E-06	1.581E 19	4.573E 14	2.825E 04	8.171E-01	1.808E-01
1.700E-06	1.079E 19	4.474E 14	1.839E 04	7.995E-01	1.848E-01
2.800E-06	7.003E 18	4.382E 14	1.251E 04	7.829E-01	1.887E-01
4.250E-06	4.760E 18	4.280E 14	8.506E 03	7.648E-01	1.932E-01
6.300E-06	3.297E 18	4.133E 14	5.890E 03	7.474E-01	1.977E-01
9.200E-06	2.279E 18	4.087E 14	4.072E 03	7.303E-01	2.023E-01
1.350E-05	1.624E 18	3.989E 14	2.901E 03	7.128E-01	2.073E-01
2.100E-05	1.078E 18	3.857E 14	1.926E 03	6.910E-01	2.138E-01
3.000E-05	7.256E 17	3.770E 14	1.298E 03	6.737E-01	2.193E-01
4.500E-05	4.592E 17	3.661E 14	8.205E 02	6.542E-01	2.258E-01
6.900E-05	3.078E 17	3.551E 14	5.499E 02	6.345E-01	2.328E-01
1.000E-04	2.190E 17	3.456E 14	3.912E 02	6.175E-01	2.392E-01
1.350E-04	1.729E 17	3.379E 14	3.090E 02	6.038E-01	2.447E-01
1.700E-04	1.375E 17	3.318E 14	2.456E 02	5.929E-01	2.491E-01
2.200E-04	1.114E 17	3.250E 14	1.991E 02	5.807E-01	2.544E-01
2.800E-04	8.773E 16	3.193E 14	1.568E 02	5.687E-01	2.597E-01
3.500E-04	6.656E 16	3.113E 14	1.193E 02	5.562E-01	2.656E-01
4.500E-04	5.153E 16	3.053E 14	9.208E 01	5.454E-01	2.708E-01
5.700E-04	3.771E 16	2.988E 14	6.737E 01	5.339E-01	2.766E-01
7.500E-04	2.876E 16	2.918E 14	5.139E 01	5.215E-01	2.832E-01
9.600E-04	2.196E 16	2.861E 14	3.924E 01	5.112E-01	2.889E-01
1.275E-03	1.691E 16	2.792E 14	3.022E 01	4.988E-01	2.960E-01
1.600E-03	1.351E 16	2.737E 14	2.415E 01	4.890E-01	3.019E-01
2.000E-03	1.039E 16	2.683E 14	1.856E 01	4.794E-01	3.080E-01
2.700E-03	7.985E 15	2.610E 14	1.427E 01	4.664E-01	3.165E-01

	ABSOLUTE VALUES		NORMALIZED TO 1.00E-10 MEV		
ENERGY (MEV)	DIFFERENTIAL FLUX	INTEGRAL FLUX	DIFFERENTIAL FLUX	INTEGRAL FLUX	AVERAGE ENERGY (MEV)
3.400E-03	6.234E 15	2.594E 14	1.114E 01	4.564E-01	3.234E-01
4.500E-03	4.936E 15	2.486E 14	8.819E 00	4.441E-01	3.322E-01
5.500E-03	3.925E 15	2.436E 14	7.014E 00	4.353E-01	3.388E-01
7.200E-03	3.037E 15	2.369E 14	5.426E 00	4.234E-01	3.482E-01
9.200E-03	2.380E 15	2.309E 14	4.253E 00	4.125E-01	3.571E-01
1.200E-02	1.904E 15	2.242E 14	3.403E 00	4.006E-01	3.674E-01
1.500E-02	1.587E 15	2.185E 14	2.835E 00	3.904E-01	3.767E-01
1.900E-02	1.264E 15	2.121E 14	2.259E 00	3.791E-01	3.874E-01
2.550E-02	1.032E 15	2.039E 14	1.844E 00	3.644E-01	4.021E-01
3.200E-02	8.652E 14	1.972E 14	1.546E 00	3.524E-01	4.148E-01
4.000E-02	7.100E 14	1.903E 14	1.269E 00	3.400E-01	4.286E-01
5.250E-02	5.841E 14	1.814E 14	1.044E 00	3.242E-01	4.473E-01
6.600E-02	4.742E 14	1.735E 14	8.473E-01	3.101E-01	4.649E-01
8.800E-02	3.867E 14	1.631E 14	6.909E-01	2.914E-01	4.898E-01
1.100E-01	3.517E 14	1.546E 14	6.284E-01	2.762E-01	5.113E-01
1.350E-01	3.471E 14	1.458E 14	6.203E-01	2.605E-01	5.347E-01
1.600E-01	3.430E 14	1.371E 14	6.129E-01	2.450E-01	5.592E-01
1.900E-01	3.392E 14	1.268E 14	6.061E-01	2.266E-01	5.904E-01
2.200E-01	3.358E 14	1.167E 14	6.001E-01	2.085E-01	6.240E-01
2.550E-01	3.311E 14	1.049E 14	5.916E-01	1.875E-01	6.673E-01
2.900E-01	3.151E 14	9.332E 13	5.631E-01	1.668E-01	7.163E-01
3.200E-01	2.906E 14	8.387E 13	5.193E-01	1.499E-01	7.627E-01
3.600E-01	2.671E 14	7.224E 13	4.773E-01	1.291E-01	8.307E-01
4.000E-01	2.456E 14	6.156E 13	4.388E-01	1.100E-01	9.089E-01
4.500E-01	2.149E 14	4.928E 13	3.841E-01	8.805E-02	1.029E 00
5.000E-01	1.683E 14	3.853E 13	3.007E-01	6.885E-02	1.184E 00
5.500E-01	1.183E 14	3.012E 13	2.114E-01	5.382E-02	1.368E 00
6.000E-01	7.942E 13	2.420E 13	1.419E-01	4.325E-02	1.562E 00
6.600E-01	5.263E 13	1.944E 13	9.404E-02	3.473E-02	1.791E 00
7.200E-01	3.212E 13	1.628E 13	5.740E-02	2.909E-02	2.004E 00
7.800E-01	2.142E 13	1.435E 13	3.828E-02	2.564E-02	2.173E 00
8.400E-01	1.342E 13	1.307E 13	2.399E-02	2.335E-02	2.307E 00
9.200E-01	9.608E 12	1.199E 13	1.717E-02	2.143E-02	2.435E 00
1.000E 00	7.505E 12	1.122E 13	1.341E-02	2.005E-02	2.536E 00
1.200E 00	6.119E 12	9.723E 12	1.093E-02	1.737E-02	2.757E 00
1.400E 00	5.090E 12	8.499E 12	9.095E-03	1.519E-02	2.967E 00
1.600E 00	4.311E 12	7.481E 12	7.702E-03	1.337E-02	3.167E 00

	ABSOLUTE VALUES		NORMALIZED TO 1.00E-10 MEV		
ENERGY (MEV)	DIFFERENTIAL FLUX	INTEGRAL FLUX	DIFFERENTIAL FLUX	INTEGRAL FLUX	AVERAGE ENERGY (MEV)
3.400E-03	6.234E 15	2.554E 14	1.114E 01	4.564E-01	3.234E-01
4.500E-03	4.936E 15	2.486E 14	8.819E 00	4.441E-01	3.322E-01
5.500E-03	3.925E 15	2.436E 14	7.014E 00	4.353E-01	3.388E-01
7.200E-03	3.037E 15	2.369E 14	5.426E 00	4.234E-01	3.482E-01
9.200E-03	2.380E 15	2.309E 14	4.253E 00	4.125E-01	3.571E-01
1.200E-02	1.904E 15	2.247E 14	3.403E 00	4.006E-01	3.674E-01
1.500E-02	1.587E 15	2.185E 14	2.835E 00	3.904E-01	3.767E-01
1.900E-02	1.264E 15	2.121E 14	2.259E 00	3.791E-01	3.874E-01
2.550E-02	1.032E 15	2.039E 14	1.844E 00	3.644E-01	4.021E-01
3.200E-02	8.652E 14	1.972E 14	1.546E 00	3.524E-01	4.148E-01
4.000E-02	7.100E 14	1.903E 14	1.269E 00	3.400E-01	4.286E-01
5.250E-02	5.841E 14	1.814E 14	1.044E 00	3.242E-01	4.473E-01
6.600E-02	4.742E 14	1.735E 14	8.473E-01	3.101E-01	4.649E-01
8.800E-02	3.867E 14	1.631E 14	6.909E-01	2.914E-01	4.898E-01
1.100E-01	3.517E 14	1.546E 14	6.284E-01	2.762E-01	5.113E-01
1.350E-01	3.471E 14	1.458E 14	6.203E-01	2.605E-01	5.347E-01
1.600E-01	3.430E 14	1.371E 14	6.129E-01	2.450E-01	5.592E-01
1.900E-01	3.392E 14	1.268E 14	6.061E-01	2.266E-01	5.904E-01
2.200E-01	3.358E 14	1.167E 14	6.001E-01	2.085E-01	6.240E-01
2.550E-01	3.311E 14	1.049E 14	5.916E-01	1.875E-01	6.673E-01
2.900E-01	3.151E 14	9.332E 13	5.631E-01	1.668E-01	7.163E-01
3.200E-01	2.906E 14	8.387E 13	5.193E-01	1.499E-01	7.627E-01
3.600E-01	2.671E 14	7.224E 13	4.773E-01	1.291E-01	8.307E-01
4.000E-01	2.456E 14	6.156E 13	4.388E-01	1.100E-01	9.089E-01
4.500E-01	2.149E 14	4.928E 13	3.841E-01	8.805E-02	1.029E 00
5.000E-01	1.683E 14	3.853E 13	3.007E-01	6.885E-02	1.184E 00
5.500E-01	1.183E 14	3.012E 13	2.114E-01	5.382E-02	1.368E 00
6.000E-01	7.942E 13	2.420E 13	1.419E-01	4.325E-02	1.562E 00
6.600E-01	5.263E 13	1.944E 13	9.404E-02	3.473E-02	1.791E 00
7.200E-01	3.212E 13	1.628E 13	5.740E-02	2.909E-02	2.004E 00
7.800E-01	2.142E 13	1.435E 13	3.828E-02	2.564E-02	2.173E 00
8.400E-01	1.342E 13	1.307E 13	2.399E-02	2.335E-02	2.307E 00
9.200E-01	9.608E 12	1.199E 13	1.717E-02	2.143E-02	2.435E 00
1.000E 00	7.505E 12	1.122E 13	1.341E-02	2.005E-02	2.536E 00
1.200E 00	6.119E 12	9.723E 12	1.093E-02	1.737E-02	2.757E 00
1.400E 00	5.090E 12	8.499E 12	9.095E-03	1.519E-02	2.967E 00
1.600E 00	4.311E 12	7.481E 12	7.702E-03	1.337E-02	3.167E 00

ENERGY (MEV)	ABSOLUTE VALUES DIFFERENTIAL FLUX	ABSOLUTE VALUES INTEGRAL FLUX	NORMALIZED TO 1.00E-10 MEV DIFFERENTIAL FLUX	NORMALIZED TO 1.00E-10 MEV INTEGRAL FLUX	AVERAGE ENERGY (MEV)
1.800E 00	3.786E 12	6.619E 12	6.764E-03	1.183E-02	3.358E 00
2.000E 00	3.295E 12	5.861E 12	5.888E-03	1.047E-02	3.546E 00
2.300E 00	2.852E 12	4.873E 12	5.042E-03	8.707E-03	3.829E 00
2.600E 00	2.462E 12	4.026E 12	4.399E-03	7.195E-03	4.119E 00
2.900E 00	2.048E 12	3.288E 12	3.659E-03	5.875E-03	4.427E 00
3.300E 00	1.566E 12	2.489E 12	2.799E-03	4.411E-03	4.867E 00
3.700E 00	1.186E 12	1.842E 12	2.119E-03	3.292E-03	5.332E 00
4.100E 00	9.116E 11	1.368E 12	1.629E-03	2.444E-03	5.828E 00
4.500E 00	6.888E 11	1.003E 12	1.231E-03	1.793E-03	6.383E 00
5.000E 00	4.394E 11	6.590E 11	7.852E-04	1.178E-03	7.237E 00
5.500E 00	2.244E 11	4.393E 11	4.010E-04	7.849E-04	8.230E 00
6.000E 00	1.242E 11	3.271E 11	2.219E-04	5.844E-04	9.081E 00
6.700E 00	7.955E 10	2.402E 11	1.421E-04	4.291E-04	1.007E 01
7.400E 00	5.235E 10	1.845E 11	9.355E-05	3.296E-04	1.098E 01
8.200E 00	3.439E 10	1.426E 11	6.144E-05	2.548E-04	1.192E 01
9.000E 00	2.228E 10	1.151E 11	3.981E-05	2.056E-04	1.271E 01
1.000E 01	1.655E 10	9.279E 10	2.958E-05	1.658E-04	1.348E 01
1.100E 01	1.494E 10	7.624E 10	2.669E-05	1.362E-04	1.413E 01
1.200E 01	1.359E 10	6.130E 10	2.428E-05	1.095E-04	1.477E 01
1.300E 01	1.212E 10	4.771E 10	2.165E-05	8.526E-05	1.541E 01
1.400E 01	1.055E 10	3.560E 10	1.885E-05	6.360E-05	1.606E 01
1.500E 01	8.857E 09	2.504E 10	1.583E-05	4.475E-05	1.672E 01
1.600E 01	7.016E 09	1.619E 10	1.254E-05	2.892E-05	1.739E 01
1.700E 01	5.057E 09	9.170E 09	9.037E-06	1.639E-05	1.807E 01
1.800E 01	3.029E 09	4.113E 09	5.412E-06	7.350E-06	1.876E 01
1.900E 01	1.084E 09	1.084E 09	1.937E-06	1.937E-06	1.950E 01
2.000E 01	0.0	0.0	0.0	0.0	0.0

CALCULATION WILL NOW BEGIN FOR A NEW SOLUTION WITHTHE FOLLOWING DISCARDED FOILS OMITTED --
T146(N,P)SC46 CD

INTERIM RESULTS AFTER 0 ITERATIONS

FOIL REACTION		NOMINAL 5.00 PERCENT ACTIVITY LIMITS (MEV) LOWER	UPPER	RATIO MEASURED TO CALCULATED ACTIVITIES	DEVIATION OF MEASURED FROM CALCULATED ACTIVITY (PERCENT)
AL27(N,A)NA24	CD	6.700E 00	1.600E 01	0.1295	-87.05
AU197(N,G)AU198	CD	4.250E-06	4.500E-05	3.5384	253.84
CO59(N,G)CO60	CD	8.400E-07	1.700E-04	3.5735	257.35
CU63(N,G)CU64	CD	8.400E-07	3.600E-01	3.6736	267.36
FE58(N,G)FE59	CD	8.400E-07	9.200E-03	3.9233	292.33
FE54(N,P)54MN	CD	2.300E 00	7.400E 00	0.0897	-91.03
IN115(N,N)IN115M	CD	1.000E 00	5.000E 00	0.0920	-90.80
NI58(N,P)CO58	CD	2.000E 00	7.400E 00	0.0808	-91.92
ZR90(N,2N)ZR89	CD	1.300E 01	1.900E 01	0.1612	-83.88
TI46(N,P)SC46	CD	3.700E 00	1.300E 01	0.0996	-90.04
TI47(N,P)SC47	CD	1.800E 00	7.400E 00	0.0799	-92.01
TH232(N,F)FSPR	CD	1.400E 00	6.700E 00	0.0863	-91.37
U238(N,F)FSPR	CD	1.400E 00	6.000E 00	0.0823	-91.77
CU63(N,A)CO60	CD	6.000E 00	1.600E 01	0.1337	-86.63
FE56(N,P)MN56	CD	5.500E 00	1.600E 01	0.1266	-87.34
MG24(N,P)NA24	CD	6.700E 00	1.600E 01	0.1299	-87.01

STANDARD DEVIATION OF MEASURED ACTIVITIES (PERCENT) 159.84

AVERAGE TOTAL FLUX (ABOVE 1.00E-10 MEV) 3.132E 14

INTERIM RESULTS AFTER 1 ITERATIONS

FOIL REACTION		NOMINAL 5.00 PERCENT ACTIVITY LIMITS (MEV) LOWER	UPPER	RATIO MEASURED TO CALCULATED ACTIVITIES	DEVIATION OF MEASURED FROM CALCULATED ACTIVITY (PERCENT)
AL27(N,A)NA24	CD	6.700E 00	1.700E 01	1.0259	2.59
AU197(N,G)AU198	CD	4.250E-06	4.500E-05	0.9977	-0.23
CO59(N,G)CO60	CD	8.400E-07	1.700E-04	1.0033	0.33
CU63(N,G)CU64	CD	5.500E-07	1.900E-02	1.0508	5.08
FE58(N,G)FE59	CD	8.400E-07	3.600E-04	1.0666	6.66
FE54(N,P)54MN	CD	2.300E 00	8.200E 00	0.9798	-2.02
IN115(N,N)IN115M	CD	6.600E-01	5.000E 00	0.9329	-6.71
NI58(N,P)CO58	CD	2.000E 00	8.200E 00	0.8876	-11.24
ZR90(N,2N)ZR89	CD	1.300E 01	1.900E 01	1.1531	15.31
TI46(N,P)SC46	CD	3.700E 00	1.400E 01	0.9754	-2.46
TI47(N,P)SC47	CD	1.800E 00	8.200E 00	0.8821	-11.79
TH232(N,F)FSPR	CD	1.400E 00	7.400E 00	0.9579	-4.21
U238(N,F)FSPR	CD	1.400E 00	6.700E 00	0.9104	-8.96
CU63(N,A)CO60	CD	6.000E 00	1.600E 01	1.0830	8.30
FE56(N,P)MN56	CD	5.500E 00	1.600E 01	1.0537	5.37
MG24(N,P)NA24	CD	6.700E 00	1.600E 01	1.0401	4.01

SOLUTION HAS BEEN ACHIEVED.
STANDARD DEVIATION OF MEASURED-TO-CALCULATED ACTIVITY RATIOS IS LESS THAN 5.00 PERCENT.

SOLUTION RESULTS OBTAINED AFTER 2 ITERATIONS

FOIL REACTION		SATURATED MEASURED ACTIVITY (DPS/NUCLEUS)	SATURATED CALCULATED ACTIVITY (DPS/NUCLEUS)	NOMINAL 5.00 PERCENT ACTIVITY LIMITS (MEV) LOWER	NOMINAL 5.00 PERCENT ACTIVITY LIMITS (MEV) UPPER	RATIO MEASURED TO CALCULATED ACTIVITIES	DEVIATION OF MEASURED FROM CALCULATED ACTIVITY (PERCENT)
AL27(N,A)NA24	CD	1.580E-14	1.612E-14	6.700E 00	1.700E 01	0.9799	-2.01
AU197(N,G)AU198	CD	3.605E-08	3.652E-08	4.250E-06	4.500E-05	0.9870	-1.30
CU59(N,G)CU60	CD	1.826E-09	1.843E-09	8.400E-07	1.700E-04	0.9908	-0.92
CU63(N,G)CU64	CD	1.288E-10	1.277E-10	5.500E-07	1.900E-02	1.0084	0.84
FE58(N,G)FE59	CD	4.165E-11	4.102E-11	8.400E-07	3.600E-04	1.0154	1.54
FE54(N,P)54MN	CD	1.137E-12	1.100E-12	2.300E 00	9.000E 00	1.0338	3.38
IN115(N,N)IN115M	CD	3.014E-12	3.011E-12	6.600E-01	5.500E 00	1.0008	0.08
NI58(N,P)CO58	CD	1.373E-12	1.461E-12	2.000E 00	8.200E 00	0.9397	-6.03
ZR90(N,2N)ZR89	CD	4.185E-14	3.945E-14	1.300E 01	1.900E 01	1.0607	6.07
TI46(N,P)SC46	CD	1.362E-13	1.374E-13	3.700E 00	1.400E 01	0.9915	-0.85
TI47(N,P)SC47	CD	2.967E-13	3.169E-13	1.800E 00	8.200E 00	0.9363	-6.37
TH232(N,F)FSPR	CD	1.082E-12	1.059E-12	1.400E 00	8.200E 00	1.0218	2.18
U238(N,F)FSPR	CD	4.496E-12	4.617E-12	1.400E 00	6.700E 00	0.9737	-2.63
CU63(N,A)CO60	CD	6.734E-15	6.461E-15	6.000E 00	1.600E 01	1.0423	4.23
FE56(N,P)MN56	CD	1.846E-14	1.808E-14	5.500E 00	1.600E 01	1.0208	2.08
MG24(N,P)NA24	CD	2.989E-14	2.998E-14	6.700E 00	1.700E 01	0.9971	-0.29

STANDARD DEVIATION OF MEASURED ACTIVITIES (PERCENT) 3.36

SOLUTION SPECTRUM OBTAINED AFTER 2 ITERATIONS

ENERGY (MEV)	ABSOLUTE VALUES DIFFERENTIAL FLUX	ABSOLUTE VALUES INTEGRAL FLUX	NORMALIZED TO 1.00E-10 MEV DIFFERENTIAL FLUX	NORMALIZED TO 1.00E-10 MEV INTEGRAL FLUX	AVERAGE ENERGY (MEV)
1.000E-10	2.032E 19	5.597E 14	3.631E 04	1.000E 00	1.478E-01
1.000E-09	1.961E 20	5.597E 14	3.503E 05	1.000E 00	1.478E-01
1.000E-08	4.393E 20	5.579E 14	7.848E 05	9.968E-01	1.483E-01
2.300E-08	4.644E 20	5.522E 14	8.296E 05	9.866E-01	1.498E-01
5.000E-08	3.509E 20	5.397E 14	6.269E 05	9.642E-01	1.533E-01
7.600E-08	2.729E 20	5.306E 14	4.876E 05	9.479E-01	1.559E-01
1.150E-07	1.949E 20	5.199E 14	3.482E 05	9.289E-01	1.591E-01
1.700E-07	1.280E 20	5.092E 14	2.287E 05	9.097E-01	1.624E-01
2.550E-07	8.375E 19	4.983E 14	1.496E 05	8.903E-01	1.660E-01
3.800E-07	5.588E 19	4.879E 14	9.983E 04	8.716E-01	1.696E-01
5.500E-07	3.669E 19	4.784E 14	6.555E 04	8.546E-01	1.729E-01
8.400E-07	2.372E 19	4.677E 14	4.238E 04	8.356E-01	1.769E-01
1.275E-06	1.581E 19	4.574E 14	2.825E 04	8.172E-01	1.808E-01
1.900E-06	1.029E 19	4.475E 14	1.839E 04	7.995E-01	1.848E-01
2.800E-06	7.002E 18	4.383E 14	1.251E 04	7.830E-01	1.887E-01
4.250E-06	4.760E 18	4.281E 14	8.504E 03	7.648E-01	1.932E-01
6.300E-06	3.296E 18	4.183E 14	5.889E 03	7.474E-01	1.977E-01
9.200E-06	2.279E 18	4.088E 14	4.071E 03	7.303E-01	2.024E-01
1.350E-05	1.624E 18	3.990E 14	2.901E 03	7.128E-01	2.073E-01
2.100E-05	1.078E 18	3.868E 14	1.925E 03	6.911E-01	2.138E-01
3.000E-05	7.265E 17	3.771E 14	1.298E 03	6.737E-01	2.193E-01
4.500E-05	4.591E 17	3.662E 14	8.203E 02	6.543E-01	2.259E-01
6.900E-05	3.077E 17	3.552E 14	5.498E 02	6.346E-01	2.329E-01
1.000E-04	2.189E 17	3.457E 14	3.911E 02	6.175E-01	2.393E-01
1.350E-04	1.729E 17	3.380E 14	3.089E 02	6.039E-01	2.447E-01
1.700E-04	1.375E 17	3.319E 14	2.456E 02	5.930E-01	2.492E-01
2.200E-04	1.114E 17	3.251E 14	1.990E 02	5.808E-01	2.544E-01
2.800E-04	8.773E 16	3.184E 14	1.567E 02	5.688E-01	2.598E-01
3.600E-04	6.675E 16	3.114E 14	1.193E 02	5.563E-01	2.656E-01
4.500E-04	5.153E 16	3.054E 14	9.206E 01	5.456E-01	2.709E-01
5.750E-04	3.770E 16	2.989E 14	6.736E 01	5.340E-01	2.767E-01
7.600E-04	2.876E 16	2.919E 14	5.138E 01	5.216E-01	2.833E-01
9.600E-04	2.196E 16	2.862E 14	3.923E 01	5.113E-01	2.889E-01
1.275E-03	1.691E 16	2.793E 14	3.021E 01	4.989E-01	2.961E-01
1.600E-03	1.351E 16	2.738E 14	2.414E 01	4.891E-01	3.020E-01
2.000E-03	1.039E 16	2.684E 14	1.856E 01	4.795E-01	3.080E-01
2.700E-03	7.984E 15	2.611E 14	1.426E 01	4.665E-01	3.165E-01

	ABSOLUTE VALUES		NORMALIZED TO 1.00E-10 MEV		
ENERGY (MEV)	DIFFERENTIAL FLUX	INTEGRAL FLUX	DIFFERENTIAL FLUX	INTEGRAL FLUX	AVERAGE ENERGY (MEV)
3.400E-03	6.233E 15	2.555E 14	1.114E 01	4.565E-01	3.234E-01
4.500E-03	4.935E 15	2.487E 14	8.817E 00	4.442E-01	3.322E-01
5.500E-03	3.925E 15	2.437E 14	7.012E 00	4.354E-01	3.388E-01
7.200E-03	3.036E 15	2.370E 14	5.425E 00	4.235E-01	3.482E-01
9.200E-03	2.366E 15	2.310E 14	4.252E 00	4.127E-01	3.571E-01
1.200E-02	1.904E 15	2.243E 14	3.402E 00	4.008E-01	3.674E-01
1.500E-02	1.587E 15	2.186E 14	2.835E 00	3.906E-01	3.767E-01
1.900E-02	1.264E 15	2.123E 14	2.259E 00	3.792E-01	3.874E-01
2.550E-02	1.032E 15	2.040E 14	1.843E 00	3.645E-01	4.021E-01
3.200E-02	8.651E 14	1.973E 14	1.546E 00	3.525E-01	4.148E-01
4.000E-02	7.100E 14	1.904E 14	1.268E 00	3.402E-01	4.286E-01
5.250E-02	5.840E 14	1.815E 14	1.043E 00	3.243E-01	4.473E-01
6.600E-02	4.742E 14	1.736E 14	8.471E-01	3.102E-01	4.649E-01
8.800E-02	3.866E 14	1.632E 14	6.908E-01	2.916E-01	4.897E-01
1.100E-01	3.517E 14	1.547E 14	6.283E-01	2.764E-01	5.112E-01
1.350E-01	3.471E 14	1.459E 14	6.202E-01	2.607E-01	5.346E-01
1.600E-01	3.430E 14	1.372E 14	6.128E-01	2.452E-01	5.591E-01
1.900E-01	3.392E 14	1.270E 14	6.061E-01	2.268E-01	5.902E-01
2.200E-01	3.358E 14	1.168E 14	6.000E-01	2.086E-01	6.238E-01
2.550E-01	3.311E 14	1.050E 14	5.915E-01	1.876E-01	6.670E-01
2.900E-01	3.152E 14	9.343E 13	5.632E-01	1.669E-01	7.160E-01
3.200E-01	2.908E 14	8.398E 13	5.196E-01	1.500E-01	7.622E-01
3.600E-01	2.673E 14	7.234E 13	4.776E-01	1.292E-01	8.301E-01
4.000E-01	2.458E 14	6.165E 13	4.392E-01	1.101E-01	9.082E-01
4.500E-01	2.152E 14	4.936E 13	3.845E-01	8.818E-02	1.029E 00
5.000E-01	1.685E 14	3.860E 13	3.011E-01	6.896E-02	1.183E 00
5.500E-01	1.185E 14	3.017E 13	2.117E-01	5.391E-02	1.367E 00
6.000E-01	7.955E 13	2.425E 13	1.421E-01	4.332E-02	1.560E 00
6.600E-01	5.272E 13	1.947E 13	9.419E-02	3.479E-02	1.788E 00
7.200E-01	3.218E 13	1.631E 13	5.749E-02	2.914E-02	2.001E 00
7.800E-01	2.146E 13	1.438E 13	3.834E-02	2.569E-02	2.169E 00
8.400E-01	1.345E 13	1.309E 13	2.403E-02	2.339E-02	2.302E 00
9.200E-01	9.631E 12	1.202E 13	1.721E-02	2.147E-02	2.430E 00
1.000E 00	7.524E 12	1.125E 13	1.344E-02	2.009E-02	2.530E 00
1.200E 00	6.136E 12	9.742E 12	1.096E-02	1.741E-02	2.751E 00
1.400E 00	5.105E 12	8.515E 12	9.120E-03	1.521E-02	2.961E 00
1.600E 00	4.324E 12	7.494E 12	7.725E-03	1.339E-02	3.160E 00

	ABSOLUTE VALUES		NORMALIZED TO 1.00E-10 MEV		
ENERGY (MEV)	DIFFERENTIAL FLUX	INTEGRAL FLUX	DIFFERENTIAL FLUX	INTEGRAL FLUX	AVERAGE ENERGY (MEV)
1.800E 00	3.798E 12	6.629E 12	6.786E-03	1.184E-02	3.350E 00
2.000E 00	3.307E 12	5.869E 12	5.908E-03	1.049E-02	3.538E 00
2.300E 00	2.833E 12	4.877E 12	5.061E-03	8.714E-03	3.820E 00
2.600E 00	2.472E 12	4.028E 12	4.416E-03	7.196E-03	4.109E 00
2.900E 00	2.057E 12	3.286E 12	3.674E-03	5.871E-03	4.415E 00
3.300E 00	1.573E 12	2.463E 12	2.811E-03	4.401E-03	4.855E 00
3.700E 00	1.191E 12	1.834E 12	2.128E-03	3.276E-03	5.320E 00
4.100E 00	9.141E 11	1.357E 12	1.633E-03	2.425E-03	5.818E 00
4.500E 00	6.875E 11	9.919E 11	1.228E-03	1.772E-03	6.378E 00
5.000E 00	4.346E 11	6.481E 11	7.764E-04	1.158E-03	7.241E 00
5.500E 00	2.202E 11	4.308E 11	3.935E-04	7.697E-04	8.245E 00
6.000E 00	1.213E 11	3.207E 11	2.167E-04	5.730E-04	9.102E 00
6.700E 00	7.774E 10	2.358E 11	1.389E-04	4.213E-04	1.009E 01
7.400E 00	5.124E 10	1.814E 11	9.155E-05	3.241E-04	1.101E 01
8.200E 00	3.367E 10	1.404E 11	6.016E-05	2.508E-04	1.194E 01
9.000E 00	2.180E 10	1.135E 11	3.894E-05	2.027E-04	1.273E 01
1.000E 01	1.618E 10	9.167E 10	2.890E-05	1.638E-04	1.350E 01
1.100E 01	1.462E 10	7.549E 10	2.611E-05	1.349E-04	1.415E 01
1.200E 01	1.334E 10	6.087E 10	2.384E-05	1.088E-04	1.478E 01
1.300E 01	1.196E 10	4.753E 10	2.137E-05	8.491E-05	1.542E 01
1.400E 01	1.047E 10	3.557E 10	1.871E-05	6.354E-05	1.607E 01
1.500E 01	8.839E 09	2.509E 10	1.579E-05	4.483E-05	1.672E 01
1.600E 01	7.028E 09	1.625E 10	1.256E-05	2.904E-05	1.739E 01
1.700E 01	5.079E 09	9.225E 09	9.074E-06	1.648E-05	1.807E 01
1.800E 01	3.051E 09	4.146E 09	5.452E-06	7.408E-06	1.876E 01
1.900E 01	1.095E 09	1.095E 09	1.956E-06	1.956E-06	1.950E 01
2.000E 01	0.0	0.0	0.0	0.0	0.0

XIII. APPENDIX C

```
T
ITERATION
17 FOILS
AL27A    2.109E-14    CADMIUM    ISTP 20.0
AU197G   5.712E-08    CADMIUM    ISTP 20.0
CO59G    2.701E-09    CADMIUM    ISTP 20.0
CU63G    1.405E-10    CADMIUM    ISTP 20.0
FE58G    5.193E-11    CADMIUM    ISTP 20.0
FE54P    1.096E-12    CADMIUM    ISTP 20.0
NI58P    1.596E-12    CADMIUM    ISTP 20.0
ZR90Z    3.707E-14    CADMIUM    ISTP 20.0
TI46P    1.939E-13    CADMIUM    ISTP 20.0
TI47P    3.368E-13    CADMIUM    ISTP 20.0
TI48P    1.289E-14    CADMIUM    ISTP 20.0
FE56P    2.800E-14    CADMIUM    ISTP 20.0
MG24P    4.109E-14    CADMIUM    ISTP 20.0
TH232F   1.191E-12    CADMIUM    ISTP 20.0
U238F    3.000E-12    CADMIUM    ISTP 20.0
IN115N   3.168E-12    CADMIUM    ISTP 20.0
CU63A    9.239E-15    CADMIUM    ISTP 20.0
SPECTRUM TABULAR
22 POINTS
ENER  1.-10  1.-9  1.-8  1.-7  1.-6  1.-5  1.-4  1.-3  1.-2  1.-1  1.  2.  3.
ENER  4.  5.  6.  7.  8.  9.  10.  15.  20.
FLUX  1.+3  1.+4  30000.  1.+4  1.+3  1.+2  10.  3.5  1.  .4  .15  .09  .04
FLUX  .02  .01  .008  .001  .0005  .0002  1.-5  1.-6  0.
LIMIT 30
DEVIATION 5
DISCARD 2
LOW END THERMAL
HIGH END FISSION
NORM  1.0-10
PLOT, NO CARDS
SMOOTH 5
```

INTERIM RESULTS AFTER 0 ITERATIONS

FOIL REACTION		NOMINAL 5.00 PERCENT ACTIVITY LIMITS (MEV) LOWER	UPPER	RATIO MEASURED TO CALCULATED ACTIVITIES	DEVIATION OF MEASURED FROM CALCULATED ACTIVITY (PERCENT)
AL27(N,A)NA24	CD	6.000E 00	1.000E 01	0.0530	-94.70
AU197(N,G)AU198	CD	4.250E-06	5.500E-03	6.1415	514.15
CO59(N,G)CO60	CD	8.400E-07	1.200E-02	5.5127	451.27
CU63(N,G)CU64	CD	2.800E-06	1.600E 00	1.1408	14.08
FE58(N,G)FE59	CD	1.275E-06	1.600E 00	2.4811	148.11
FE54(N,P)54MN	CD	2.300E 00	6.700E 00	0.0090	-99.10
IN115(N,N)IN115M	CD	1.000E 00	5.500E 00	0.0097	-99.03
NI58(N,P)CO58	CD	2.000E 00	6.700E 00	0.0097	-99.03
ZR90(N,2N)ZR89	CD	1.300E 01	1.900E 01	1.4276	42.76
TI46(N,P)SC46	CD	3.700E 00	7.400E 00	0.0144	-98.56
TI47(N,P)SC47	CD	1.800E 00	6.700E 00	0.0094	-99.06
TI48(N,P)SC48	CD	5.500E 00	9.000E 00	0.0666	-93.34
TH232(N,F)FSPR	CD	1.400E 00	6.000E 00	0.0094	-99.06
U238(N,F)FSPR	CD	1.400E 00	6.000E 00	0.0093	-99.07
CU63(N,A)CO60	CD	6.000E 00	9.000E 00	0.0365	-96.35
FE56(N,P)MN56	CD	5.000E 00	9.000E 00	0.0278	-97.22
MG24(N,P)NA24	CD	6.000E 00	9.000E 00	0.0416	-95.84

STANDARD DEVIATION OF MEASURED ACTIVITIES (PERCENT) 194.64

AVERAGE TOTAL FLUX (ABOVE 1.00E-10 MEV) 2.896E 15

INTERIM RESULTS AFTER 1 ITERATIONS

FOIL REACTION		NOMINAL 5.00 PERCENT ACTIVITY LIMITS (MEV) LOWER	UPPER	RATIO MEASURED TO CALCULATED ACTIVITIES	DEVIATION OF MEASURED FROM CALCULATED ACTIVITY (PERCENT)
AL27(N,A)NA24	CD	6.000E 00	1.600E 01	1.2537	25.37
AU197(N,G)AU198	CD	4.250E-06	4.500E-05	1.3880	38.80
CO59(N,G)CO60	CD	1.275E-06	1.700E-04	1.3275	32.75
CU63(N,G)CU64	CD	1.275E-06	4.000E-01	0.8050	-19.50
FE58(N,G)FE59	CD	8.400E-07	2.550E-01	1.2181	21.81
FE54(N,P)54MN	CD	2.600E 00	7.400E 00	0.6497	-35.03
IN115(N,N)IN115M	CD	5.000E-01	5.500E 00	0.4327	-56.73
NI58(N,P)CO58	CD	1.800E 00	7.400E 00	0.7284	-27.16
ZR90(N,2N)ZR89	CD	1.300E 01	1.900E 01	1.3909	39.09
TI46(N,P)SC46	CD	4.100E 00	1.000E 01	0.7384	-26.16
TI47(N,P)SC47	CD	1.800E 00	7.400E 00	0.7506	-24.94
TI48(N,P)SC48	CD	5.500E 00	1.700E 01	1.6517	65.17
TH232(N,F)FSPR	CD	1.400E 00	7.400E 00	0.7982	-20.18
U238(N,F)FSPR	CD	7.800E-01	6.700E 00	0.7436	-25.64
CU63(N,A)CO60	CD	6.000E 00	1.500E 01	1.0749	7.49
FE56(N,P)MN56	CD	5.500E 00	1.500E 01	0.9414	-5.86
MG24(N,P)NA24	CD	6.000E 00	1.500E 01	1.1073	10.73

STANDARD DEVIATION OF MEASURED ACTIVITIES (PERCENT) 33.18

AVERAGE TOTAL FLUX (ABOVE 1.00E-10 MEV) 2.064E 15

INTERIM RESULTS AFTER 2 ITERATIONS

FOIL REACTION		NOMINAL 5.00 PERCENT ACTIVITY LIMITS (MEV) LOWER	NOMINAL 5.00 PERCENT ACTIVITY LIMITS (MEV) UPPER	RATIO MEASURED TO CALCULATED ACTIVITIES	DEVIATION OF MEASURED FROM CALCULATED ACTIVITY (PERCENT)
AL27(N,A)NA24	CD	6.000E 00	1.600E 01	1.1442	14.42
AU197(N,G)AU198	CD	4.250E-05	4.500E-05	1.0685	6.85
CO59(N,G)CO60	CD	1.900E-06	1.700E-04	1.0272	2.72
CU63(N,G)CU64	CD	8.400E-07	3.200E-01	0.8559	-14.41
FE58(N,G)FE59	CD	1.275E-06	1.350E-01	1.0626	6.26
FE54(N,P)54MN	CD	2.600E 00	8.200E 00	0.7936	-20.64
IN115(N,N)IN115M	CD	5.000E-01	6.000E 00	0.6980	-30.20
NI58(N,P)CO58	CD	2.000E 00	8.200E 00	0.9087	-9.13
ZR90(N,2N)ZR89	CD	1.300E 01	1.900E 01	1.0696	6.96
TI46(N,P)SC46	CD	4.100E 00	1.300E 01	0.8183	-18.17
TI47(N,P)SC47	CD	1.800E 00	8.200E 00	0.9544	-4.56
TI48(N,P)SC48	CD	6.000E 00	1.700E 01	1.5242	52.42
TH232(N,F)FSPR	CD	1.400E 00	8.200E 00	1.0537	5.37
U238(N,F)FSPR	CD	8.400E-01	7.400E 00	1.0170	1.70
CU63(N,A)CO60	CD	6.000E 00	1.500E 01	1.0311	3.11
FE56(N,P)MN56	CD	5.500E 00	1.500E 01	0.9378	-6.22
MG24(N,P)NA24	CD	6.000E 00	1.600E 01	1.0354	3.54

STANDARD DEVIATION OF MEASURED ACTIVITIES (PERCENT) 17.98

AVERAGE TOTAL FLUX (ABOVE 1.00E-10 MEV) 1.764E 15

INTERIM RESULTS AFTER 9 ITERATIONS

FOIL REACTION		NOMINAL 5.00 PERCENT ACTIVITY LIMITS (MEV) LOWER	UPPER	RATIO MEASURED TO CALCULATED ACTIVITIES	DEVIATION OF MEASURED FROM CALCULATED ACTIVITY (PERCENT)
AL27(N,A)NA24	CD	6.000E 00	1.600E 01	1.0116	1.16
AU197(N,G)AU198	CD	4.250E-06	6.300E-06	0.9953	-0.47
CO59(N,G)CO60	CD	1.900E-06	1.700E-04	0.9947	-0.53
CU63(N,G)CU64	CD	8.400E-07	2.550E-01	0.9940	-0.60
FE58(N,G)FE59	CD	1.275E-06	6.600E-02	0.9967	-0.33
FE54(N,P)54MN	CD	2.600E 00	8.200E 00	0.8955	-10.45
IN115(N,N)IN115M	CD	5.500E-01	6.000E 00	0.9236	-7.64
NI58(N,P)CO58	CD	2.000E 00	8.200E 00	1.0157	1.57
ZR90(N,2N)ZR89	CD	1.300E 01	1.900E 01	0.9126	-8.74
TI46(N,P)SC46	CD	4.100E 00	1.300E 01	0.8941	-10.59
TI47(N,P)SC47	CD	1.800E 00	8.200E 00	1.0349	3.49
TI48(N,P)SC48	CD	6.000E 00	1.700E 01	1.3812	38.12
TH232(N,F)FSPR	CD	1.400E 00	8.200E 00	1.0730	7.30
U238(N,F)FSPR	CD	1.200E 00	7.400E 00	1.0614	6.14
CU63(N,A)CO60	CD	6.000E 00	1.500E 01	0.9594	-4.06
FE56(N,P)MN56	CD	5.500E 00	1.500E 01	0.9165	-8.35
MG24(N,P)NA24	CD	6.000E 00	1.600E 01	0.9397	-6.03

STANDARD DEVIATION OF MEASURED ACTIVITIES (PERCENT) 11.29

AVERAGE TOTAL FLUX (ABOVE 1.00E-10 MEV) 1.427E 15

INTERIM RESULTS AFTER 15 ITERATIONS

FOIL REACTION		NOMINAL 5.00 PERCENT ACTIVITY LIMITS (MEV) LOWER	UPPER	RATIO MEASURED TO CALCULATED ACTIVITIES	DEVIATION OF MEASURED FROM CALCULATED ACTIVITY (PERCENT)
AL27(N,A)NA24	CD	6.000E 00	1.600E 01	0.9907	-0.93
AU197(N,G)AU198	CD	4.250E-06	6.300E-06	0.9956	-0.44
CO59(N,G)CO60	CD	1.900E-06	1.700E-04	0.9957	-0.43
CU63(N,G)CU64	CD	8.400E-07	2.550E-01	0.9966	-0.34
FE58(N,G)FE59	CD	1.275E-06	6.600E-02	0.9959	-0.41
FE54(N,P)54MN	CD	2.300E 00	8.200E 00	0.9229	-7.71
IN115(N,N)IN115M	CD	5.500E-01	6.000E 00	0.9469	-5.31
NI58(N,P)CO58	CD	1.800E 00	8.200E 00	1.0360	3.60
ZR90(N,2N)ZR89	CD	1.300E 01	1.900E 01	0.9242	-7.58
TI46(N,P)SC46	CD	4.100E 00	1.300E 01	0.9299	-7.01
TI47(N,P)SC47	CD	1.600E 00	8.200E 00	1.0351	3.51
TI48(N,P)SC48	CD	6.000E 00	1.700E 01	1.3673	36.73
TH232(N,F)FSPR	CD	1.400E 00	8.200E 00	1.0344	3.44
U238(N,F)FSPR	CD	1.200E 00	7.400E 00	1.0239	2.39
CO63(N,A)CO60	CD	6.000E 00	1.500E 01	0.9525	-4.75
FE56(N,P)MN56	CD	5.500E 00	1.500E 01	0.9243	-7.57
MG24(N,P)NA24	CD	6.000E 00	1.600E 01	0.9280	-7.20

STANDARD DEVIATION OF MEASURED ACTIVITIES (PERCENT)					10.37
AVERAGE TOTAL FLUX (ABOVE 1.00E-10 MEV)					1.399E 15

STANDARD DEVIATION OF MEASURED-TO-CALCULATED ACTIVITY RATIOS HAS BECOME STABLE (TO WITHIN LESS THAN ONE PERCENT CHANGE PER ITERATION) AT A HIGHER VALUE THAN THE SPECIFIED 5.00 PERCENT.

RESULTS OBTAINED AFTER 16 ITERATIONS

FOIL REACTION		SATURATED MEASURED ACTIVITY (DPS/NUCLEUS)	SATURATED CALCULATED ACTIVITY (DPS/NUCLEUS)	NOMINAL 5.00 PERCENT ACTIVITY LIMITS (MEV) LOWER	NOMINAL 5.00 PERCENT ACTIVITY LIMITS (MEV) UPPER	RATIO MEASURED TO CALCULATED ACTIVITIES	DEVIATION OF MEASURED FROM CALCULATED ACTIVITY (PERCENT)
AL27(N,A)NA24	CD	2.109E-14	2.135E-14	6.700E 00	1.600E 01	0.9881	-1.19
AU197(N,G)AU198	CD	5.712E-08	5.737E-08	4.250E-06	6.300E-06	0.9957	-0.43
CO59(N,G)CO60	CD	2.701E-09	2.712E-09	1.900E-06	1.700E-04	0.9958	-0.42
CU63(N,G)CU64	CD	1.405E-10	1.410E-10	8.400E-07	2.550E-01	0.9966	-0.34
FE58(N,G)FE59	CD	5.193E-11	5.214E-11	1.275E-06	6.600E-02	0.9960	-0.40
FE54(N,P)54MN	CD	1.096E-12	1.184E-12	2.300E 00	8.200E 00	0.9260	-7.40
IN115(N,N)I115M	CD	3.168E-12	3.335E-12	5.500E-01	6.000E 00	0.9498	-5.02
NI58(N,P)CO58	CD	1.596E-12	1.537E-12	1.800E 00	8.200E 00	1.0382	3.82
ZR90(N,2N)ZR89	CD	3.707E-14	4.004E-14	1.300E 01	1.900E 01	0.9258	-7.42
TI46(N,P)SC46	CD	1.939E-13	2.076E-13	4.100E 00	1.300E 01	0.9342	-6.58
TI47(N,P)SC47	CD	3.368E-13	3.254E-13	1.600E 00	8.200E 00	1.0349	3.49
TI48(N,P)SC48	CD	1.269E-14	9.441E-15	6.000E 00	1.700E 01	1.3653	36.53
TH232(N,F)FSPR	CD	1.151E-12	1.117E-12	1.400E 00	8.200E 00	1.0303	3.03
U238(N,F)FSPR	CD	5.000E-12	4.903E-12	1.400E 00	7.400E 00	1.0198	1.98
CU63(N,A)CO60	CD	9.239E-15	9.708E-15	6.000E 00	1.500E 01	0.9517	-4.83
FE56(N,P)MN56	CD	2.800E-14	3.027E-14	5.500E 00	1.500E 01	0.9252	-7.48
MG24(N,P)NA24	CD	4.109E-14	4.434E-14	6.000E 00	1.600E 01	0.9266	-7.34

STANDARD DEVIATION OF MEASURED ACTIVITIES (PERCENT) 10.27

THE FOLLOWING FOIL MEASUREMENT SHOULD BE DISCARDED BECAUSE OF EXCESSIVE DEVIATION --
(AFTER TABULATION OF THE SOLUTION SPECTRUM, A NEW SOLUTION WILL BE CALCULATED OMITTING THIS FOIL)

DISCARDED FOIL		NUMBER OF STANDARD DEVIATIONS
TI48(N,P)SC48	CD	3.557

SOLUTION SPECTRUM OBTAINED AFTER 16 ITERATIONS

ENERGY (MEV)	ABSOLUTE VALUES DIFFERENTIAL FLUX	ABSOLUTE VALUES INTEGRAL FLUX	NORMALIZED TO 1.00E-10 MEV DIFFERENTIAL FLUX	NORMALIZED TO 1.00E-10 MEV INTEGRAL FLUX	AVERAGE ENERGY (MEV)
1.000E-10	3.639E 19	1.396E 15	2.606E 04	1.000E 00	1.579E-01
1.000E-09	3.512E 20	1.396E 15	2.515E 05	1.000E 00	1.579E-01
1.000E-08	3.881E 20	1.393E 15	2.779E 05	9.977E-01	1.582E-01
2.300E-08	2.651E 20	1.388E 15	1.898E 05	9.941E-01	1.588E-01
5.000E-08	2.019E 20	1.381E 15	1.446E 05	9.890E-01	1.596E-01
7.600E-08	1.594E 20	1.376E 15	1.142E 05	9.852E-01	1.602E-01
1.150E-07	1.153E 20	1.370E 15	8.259E 04	9.808E-01	1.610E-01
1.700E-07	7.775E 19	1.363E 15	5.568E 04	9.762E-01	1.617E-01
2.550E-07	5.230E 19	1.357E 15	3.745E 04	9.715E-01	1.625E-01
3.800E-07	3.589E 19	1.350E 15	2.570E 04	9.668E-01	1.633E-01
5.500E-07	2.435E 19	1.344E 15	1.744E 04	9.624E-01	1.640E-01
8.400E-07	1.634E 19	1.337E 15	1.170E 04	9.574E-01	1.649E-01
1.275E-06	1.205E 19	1.330E 15	8.630E 03	9.523E-01	1.658E-01
1.900E-06	1.627E 19	1.322E 15	1.168E 04	9.469E-01	1.667E-01
2.800E-06	1.117E 19	1.308E 15	7.997E 03	9.364E-01	1.686E-01
4.250E-06	7.618E 18	1.291E 15	5.455E 03	9.248E-01	1.707E-01
6.300E-06	5.343E 18	1.276E 15	3.827E 03	9.136E-01	1.728E-01
9.200E-06	3.765E 18	1.260E 15	2.696E 03	9.025E-01	1.749E-01
1.350E-05	1.059E 18	1.244E 15	7.583E 02	8.909E-01	1.772E-01
2.100E-05	8.668E 17	1.236E 15	6.208E 02	8.852E-01	1.783E-01
3.000E-05	6.810E 17	1.228E 15	4.877E 02	8.796E-01	1.795E-01
4.500E-05	6.480E 17	1.218E 15	4.640E 02	8.723E-01	1.810E-01
6.900E-05	4.429E 17	1.203E 15	3.172E 02	8.612E-01	1.833E-01
1.000E-04	3.473E 17	1.189E 15	2.487E 02	8.513E-01	1.854E-01
1.350E-04	2.660E 17	1.177E 15	1.905E 02	8.426E-01	1.873E-01
1.700E-04	2.078E 17	1.167E 15	1.488E 02	8.360E-01	1.888E-01
2.200E-04	1.440E 17	1.157E 15	1.031E 02	8.285E-01	1.905E-01
2.800E-04	1.012E 17	1.148E 15	7.245E 01	8.223E-01	1.920E-01
3.600E-04	5.813E 16	1.140E 15	4.163E 01	8.166E-01	1.933E-01
4.500E-04	4.270E 16	1.135E 15	3.058E 01	8.128E-01	1.942E-01
5.750E-04	1.757E 16	1.130E 15	1.258E 01	8.090E-01	1.951E-01
7.600E-04	1.499E 16	1.126E 15	1.074E 01	8.067E-01	1.957E-01
9.600E-04	1.321E 16	1.123E 15	9.459E 00	8.045E-01	1.962E-01
1.275E-03	1.362E 16	1.119E 15	9.754E 00	8.015E-01	1.969E-01
1.600E-03	1.191E 16	1.115E 15	8.527E 00	7.984E-01	1.977E-01
2.000E-03	1.071E 16	1.110E 15	7.671E 00	7.949E-01	1.985E-01
2.700E-03	8.867E 15	1.103E 15	6.350E 00	7.896E-01	1.999E-01

	ABSOLUTE VALUES		NORMALIZED TO 1.00E-10 MEV		
ENERGY (MEV)	DIFFERENTIAL FLUX	INTEGRAL FLUX	DIFFERENTIAL FLUX	INTEGRAL FLUX	AVERAGE ENERGY (MEV)
3.400E-03	9.809E 15	1.096E 15	7.025E 00	7.851E-01	2.010E-01
4.500E-03	1.044E 16	1.086E 15	7.478E 00	7.774E-01	2.029E-01
5.500E-03	1.005E 16	1.075E 15	7.195E 00	7.699E-01	2.049E-01
7.200E-03	7.939E 15	1.058E 15	5.685E 00	7.577E-01	2.081E-01
9.200E-03	7.241E 15	1.042E 15	5.185E 00	7.463E-01	2.111E-01
1.200E-02	5.634E 15	1.022E 15	4.035E 00	7.318E-01	2.151E-01
1.500E-02	5.434E 15	1.005E 15	3.892E 00	7.197E-01	2.185E-01
1.900E-02	4.016E 15	9.832E 14	2.876E 00	7.041E-01	2.229E-01
2.350E-02	4.074E 15	9.571E 14	2.918E 00	6.854E-01	2.284E-01
3.200E-02	4.063E 15	9.306E 14	2.909E 00	6.665E-01	2.341E-01
4.000E-02	3.829E 15	8.981E 14	2.742E 00	6.432E-01	2.413E-01
5.250E-02	3.754E 15	8.503E 14	2.689E 00	6.089E-01	2.522E-01
6.600E-02	3.500E 15	7.996E 14	2.507E 00	5.726E-01	2.645E-01
8.800E-02	3.282E 15	7.226E 14	2.350E 00	5.175E-01	2.845E-01
1.100E-01	3.096E 15	6.504E 14	2.217E 00	4.658E-01	3.051E-01
1.350E-01	2.917E 15	5.730E 14	2.089E 00	4.103E-01	3.297E-01
1.600E-01	2.662E 15	5.001E 14	1.906E 00	3.581E-01	3.563E-01
1.900E-01	2.403E 15	4.202E 14	1.721E 00	3.009E-01	3.907E-01
2.200E-01	2.165E 15	3.481E 14	1.565E 00	2.493E-01	4.292E-01
2.550E-01	1.948E 15	2.716E 14	1.395E 00	1.945E-01	4.831E-01
2.900E-01	1.439E 15	2.035E 14	1.031E 00	1.457E-01	5.537E-01
3.200E-01	9.187E 14	1.603E 14	6.579E-01	1.148E-01	6.207E-01
3.600E-01	6.183E 14	1.236E 14	4.428E-01	8.848E-02	7.042E-01
4.000E-01	4.640E 14	9.892E 13	3.323E-01	7.077E-02	7.854E-01
4.500E-01	3.489E 14	7.562E 13	2.499E-01	5.416E-02	8.959E-01
5.000E-01	2.648E 14	5.818E 13	1.896E-01	4.166E-02	1.022E 00
5.500E-01	1.944E 14	4.494E 13	1.392E-01	3.218E-02	1.169E 00
6.000E-01	1.428E 14	3.521E 13	1.023E-01	2.522E-02	1.332E 00
6.600E-01	1.010E 14	2.665E 13	7.236E-02	1.908E-02	1.550E 00
7.200E-01	6.141E 13	2.058E 13	4.398E-02	1.474E-02	1.814E 00
7.800E-01	3.550E 13	1.691E 13	2.542E-02	1.211E-02	2.046E 00
8.400E-01	1.720E 13	1.478E 13	1.232E-02	1.058E-02	2.224E 00
9.200E-01	1.117E 13	1.340E 13	7.996E-03	9.596E-03	2.362E 00
1.000E 00	9.799E 12	1.251E 13	7.017E-03	8.956E-03	2.462E 00
1.200E 00	8.342E 12	1.055E 13	5.974E-03	7.552E-03	2.715E 00
1.400E 00	7.047E 12	8.877E 12	5.047E-03	6.358E-03	2.981E 00
1.600E 00	5.823E 12	7.463E 12	4.170E-03	5.348E-03	3.260E 00

	ABSOLUTE VALUES		NORMALIZED TO 1.00E-10 MEV		
ENERGY (MEV)	DIFFERENTIAL FLUX	INTEGRAL FLUX	DIFFERENTIAL FLUX	INTEGRAL FLUX	AVERAGE ENERGY (MEV)
1.800E 00	4.966E 12	6.303E 12	3.556E-03	4.514E-03	3.549E 00
2.000E 00	3.744E 12	5.310E 12	2.682E-03	3.803E-03	3.857E 00
2.300E 00	2.581E 12	4.187E 12	1.849E-03	2.998E-03	4.315E 00
2.600E 00	1.845E 12	3.413E 12	1.322E-03	2.444E-03	4.738E 00
2.900E 00	1.280E 12	2.859E 12	9.168E-04	2.047E-03	5.123E 00
3.300E 00	8.871E 11	2.347E 12	6.353E-04	1.681E-03	5.565E 00
3.700E 00	6.293E 11	1.992E 12	4.507E-04	1.427E-03	5.933E 00
4.100E 00	4.562E 11	1.740E 12	3.281E-04	1.246E-03	6.227E 00
4.500E 00	4.184E 11	1.557E 12	2.996E-04	1.115E-03	6.453E 00
5.000E 00	5.773E 11	1.348E 12	4.134E-04	9.652E-04	6.718E 00
5.500E 00	7.110E 11	1.059E 12	5.092E-04	7.585E-04	7.118E 00
6.000E 00	4.707E 11	7.837E 11	3.371E-04	5.039E-04	7.809E 00
6.700E 00	1.807E 11	3.742E 11	1.294E-04	2.680E-04	9.093E 00
7.400E 00	1.109E 11	2.477E 11	7.943E-05	1.774E-04	1.014E 01
8.200E 00	7.397E 10	1.590E 11	5.298E-05	1.139E-04	1.144E 01
9.000E 00	1.814E 10	9.981E 10	1.299E-05	7.148E-05	1.312E 01
1.000E 01	3.412E 09	8.167E 10	2.443E-06	5.849E-05	1.393E 01
1.100E 01	7.950E 09	7.826E 10	5.693E-06	5.605E-05	1.408E 01
1.200E 01	1.957E 10	7.031E 10	1.401E-05	5.035E-05	1.437E 01
1.300E 01	1.643E 10	5.074E 10	1.177E-05	3.634E-05	1.509E 01
1.400E 01	1.211E 10	3.431E 10	8.673E-06	2.457E-05	1.585E 01
1.500E 01	8.684E 09	2.220E 10	6.219E-06	1.590E-05	1.659E 01
1.600E 01	6.362E 09	1.352E 10	4.556E-06	9.681E-06	1.730E 01
1.700E 01	4.250E 09	7.157E 09	3.044E-06	5.125E-06	1.800E 01
1.800E 01	2.217E 09	2.906E 09	1.587E-06	2.081E-06	1.874E 01
1.900E 01	6.897E 08	6.897E 08	4.939E-07	4.939E-07	1.950E 01
2.000E 01	0.0	0.0	0.0	0.0	0.0

CALCULATION WILL NOW BEGIN FOR A NEW SOLUTION WITHTHE FOLLOWING DISCARDED FOILS OMITTED
TIME(N,P)SCAB CO

INTERIM RESULTS AFTER 0 ITERATIONS

FOIL REACTION		NOMINAL 5.00 PERCENT ACTIVITY LIMITS (MEV) LOWER	UPPER	RATIO MEASURED TO CALCULATED ACTIVITIES	DEVIATION OF MEASURED FROM CALCULATED ACTIVITY (PERCENT)
AL27(N,A)NA24	CD	6.000E 00	1.000E 01	0.0501	-94.99
AU197(N,G)AU198	CD	4.250E-06	5.500E-03	5.8029	480.29
CO59(N,G)CO60	CD	8.400E-07	1.200E-02	5.2088	420.88
CU63(N,G)CU64	CD	2.800E-06	1.600E 00	1.0779	7.79
FE58(N,G)FE59	CD	1.275E-06	1.600E 00	2.3443	134.43
FE54(N,P)54MN	CD	2.300E 00	6.700E 00	0.0085	-99.15
IN115(N,N)IN115M	CD	1.000E 00	5.500E 00	0.0091	-99.09
NI58(N,P)CO58	CD	2.000E 00	6.700E 00	0.0092	-99.08
ZR90(N,2N)ZR89	CD	1.300E 01	1.900E 01	1.3489	34.89
TI46(N,P)SC46	CD	3.700E 00	7.400E 00	0.0136	-98.64
TI47(N,P)SC47	CD	1.800E 00	6.700E 00	0.0089	-99.11
TH232(N,F)FSPR	CD	1.400E 00	6.000E 00	0.0089	-99.11
U238(N,F)FSPR	CD	1.400E 00	6.000E 00	0.0087	-99.13
CU63(N,A)CO60	CD	6.000E 00	9.000E 00	0.0345	-96.55
FE56(N,P)MN56	CD	5.000E 00	9.000E 00	0.0262	-97.38
MG24(N,P)NA24	CD	6.000E 00	9.000E 00	0.0393	-96.07

STANDARD DEVIATION OF MEASURED ACTIVITIES (PERCENT) 188.48

AVERAGE TOTAL FLUX (ABOVE 1.00E-10 MEV) 3.065E 15

INTERIM RESULTS AFTER 1 ITERATIONS

FOIL REACTION		NOMINAL 5.00 PERCENT ACTIVITY LIMITS (MEV) LOWER	NOMINAL 5.00 PERCENT ACTIVITY LIMITS (MEV) UPPER	RATIO MEASURED TO CALCULATED ACTIVITIES	DEVIATION OF MEASURED FROM CALCULATED ACTIVITY (PERCENT)
AL27(N,A)NA24	CD	6.000E 00	1.600E 01	1.3308	33.08
AU197(N,G)AU198	CD	4.250E-06	4.500E-05	1.3946	39.46
CO59(N,G)CO60	CD	1.275E-06	1.700E-04	1.3338	33.38
CU63(N,G)CU64	CD	1.275E-06	4.000E-01	0.8089	-19.11
FE58(N,G)FE59	CD	8.400E-07	2.550E-01	1.2239	22.39
FE54(N,P)54MN	CD	2.300E 00	7.400E 00	0.7062	-29.38
IN115(N,N)IN115M	CD	5.000E-01	5.500E 00	0.4402	-55.98
NI58(N,P)CO58	CD	1.800E 00	7.400E 00	0.7842	-21.58
ZR90(N,2N)ZR89	CD	1.300E 01	1.900E 01	1.3428	34.28
TI46(N,P)SC46	CD	4.100E 00	1.200E 01	0.8276	-17.24
TI47(N,P)SC47	CD	1.600E 00	7.400E 00	0.7974	-20.26
TH232(N,F)FSPR	CD	1.400E 00	7.400E 00	0.8294	-17.06
U238(N,F)FSPR	CD	7.200E-01	6.700E 00	0.7674	-23.26
CU63(N,A)CO60	CD	6.000E 00	1.500E 01	1.1746	17.46
FE56(N,P)MN56	CD	5.500E 00	1.500E 01	1.0411	4.11
MG24(N,P)NA24	CD	6.000E 00	1.600E 01	1.1973	19.73

STANDARD DEVIATION OF MEASURED ACTIVITIES (PERCENT) 28.89

AVERAGE TOTAL FLUX (ABOVE 1.00E-10 MEV) 2.054E 15

INTERIM RESULTS AFTER 2 ITERATIONS

FOIL REACTION		NOMINAL 5.00 PERCENT ACTIVITY LIMITS (MEV) LOWER	UPPER	RATIO MEASURED TO CALCULATED ACTIVITIES	DEVIATION OF MEASURED FROM CALCULATED ACTIVITY (PERCENT)
AL27(N,A)NA24	CD	6.000E 00	1.600E 01	1.2091	20.91
AU197(N,G)AU198	CD	4.250E-06	4.500E-05	1.0730	7.30
CO59(N,G)CO60	CD	1.900E-06	1.700E-04	1.0314	3.14
CU63(N,G)CU64	CD	8.400E-07	3.200E-01	0.8591	-14.09
FE58(N,G)FE59	CD	1.275E-06	1.350E-01	1.0668	6.68
FE54(N,P)54MN	CD	2.600E 00	8.200E 00	0.8390	-16.10
IN115(N,N)IN115M	CD	5.000E-01	6.000E 00	0.6930	-30.70
NI58(N,P)CO58	CD	2.000E 00	8.200E 00	0.9512	-4.88
ZR90(N,2N)ZR89	CD	1.300E 01	1.900E 01	1.0703	7.03
TI46(N,P)SC46	CD	4.100E 00	1.300E 01	0.8971	-10.29
TI47(N,P)SC47	CD	1.800E 00	8.200E 00	0.9843	-1.57
TH232(N,F)FSPR	CD	1.400E 00	7.400E 00	1.0610	6.10
U238(N,F)FSPR	CD	8.400E-01	7.400E 00	1.0174	1.74
CU63(N,A)CO60	CD	6.000E 00	1.500E 01	1.1144	11.44
FE56(N,P)MN56	CD	5.500E 00	1.5 E 01	1.0220	2.20
MG24(N,P)NA24	CD	6.000E 00	1.6 E 01	1.1109	11.09

STANDARD DEVIATION OF MEASURED ACTIVITIES (PERCENT) 12.72

AVERAGE TOTAL FLUX (ABOVE 1.00E-10 MEV) 1.761E 15

INTERIM RESULTS AFTER 7 ITERATIONS

FOIL REACTION		NOMINAL 5.00 PERCENT ACTIVITY LIMITS (MEV) LOWER	UPPER	RATIO MEASURED TO CALCULATED ACTIVITIES	DEVIATION OF MEASURED FROM CALCULATED ACTIVITY (PERCENT)
AL27(N,A)NA24	CD	6.000E 00	1.600E 01	1.0835	8.35
AU197(N,G)AU198	CD	4.250E-06	6.300E-06	1.0003	0.03
CO59(N,G)CO60	CD	1.900E-06	1.700E-04	0.9980	-0.20
CU63(N,G)CU64	CD	8.400E-07	2.550E-01	0.9935	-0.65
FE58(N,G)FE59	CD	1.275E-06	6.600E-02	1.0039	0.39
FE54(N,P)54MN	CD	2.600E 00	8.200E 00	0.8950	-10.50
IN115(N,N)IN115M	CD	5.000E-01	6.000E 00	0.9121	-8.79
NI58(N,P)CO58	CD	2.000E 00	8.200E 00	1.0144	1.44
ZR90(N,2N)ZR89	CD	1.300E 01	1.900E 01	0.9677	-3.23
TI46(N,P)SC46	CD	4.100E 00	1.300E 01	0.9245	-7.55
TI47(N,P)SC47	CD	1.800E 00	8.200E 00	1.0361	3.61
TH232(N,F)FSPR	CD	1.400E 00	8.200E 00	1.0878	8.78
U238(N,F)FSPR	CD	1.200E 00	7.400E 00	1.0729	7.29
CU63(N,A)CO60	CD	6.000E 00	1.500E 01	1.0271	2.71
FE56(N,P)MN56	CD	5.500E 00	1.500E 01	0.9752	-2.48
MG24(N,P)NA24	CD	6.000E 00	1.600E 01	1.0079	0.79

STANDARD DEVIATION OF MEASURED ACTIVITIES (PERCENT) 5.69

AVERAGE TOTAL FLUX (ABOVE 1.00E-10 MEV) 1.433E 15

SOLUTION HAS BEEN ACHIEVED.
STANDARD DEVIATION OF MEASURED-TO-CALCULATED ACTIVITY RATIOS IS LESS THAN 5.00 PERCENT.

SOLUTION RESULTS OBTAINED AFTER 9 ITERATIONS

FOIL REACTION		SATURATED MEASURED ACTIVITY (DPS/NUCLEUS)	SATURATED CALCULATED ACTIVITY (DPS/NUCLEUS)	NOMINAL 5.00 PERCENT ACTIVITY LIMITS (MEV) LOWER	UPPER	RATIO MEASURED TO CALCULATED ACTIVITIES	DEVIATION OF MEASURED FROM CALCULATED ACTIVITY (PERCENT)
AL27(N,A)NA24	CD	2.109E-14	1.962E-14	6.000E 00	1.600E 01	1.0749	7.49
AU197(N,G)AU198	CD	5.712E-08	5.716E-08	4.250E-06	6.300E-06	0.9993	-0.07
CO59(N,G)CO60	CD	2.701E-09	2.704E-09	1.900E-06	1.700E-04	0.9987	-0.13
CU63(N,G)CU64	CD	1.405E-10	1.407E-10	8.400E-07	2.550E-01	0.9982	-0.18
FE58(N,G)FE59	CD	5.193E-11	5.189E-11	1.275E-06	6.600E-02	1.0007	0.07
FE54(N,P)54MN	CD	1.096E-12	1.212E-12	2.300E 00	8.200E 00	0.9043	-9.57
IN115(N,N)IN115M	CD	3.166E-12	3.415E-12	5.500E-01	6.000E 00	0.9276	-7.24
NI58(N,P)CO58	CD	1.596E-12	1.563E-12	2.000E 00	8.200E 00	1.0210	2.10
ZR90(N,2N)ZR89	CD	3.707E-14	3.805E-14	1.300E 01	1.900E 01	0.9743	-2.57
TI46(N,P)SC46	CD	1.939E-13	2.069E-13	4.100E 00	1.300E 01	0.9370	-6.30
TI47(N,P)SC47	CD	3.368E-13	3.254E-13	1.800E 00	8.200E 00	1.0351	3.51
TH232(N,F)FSPR	CD	1.151E-12	1.075E-12	1.400E 00	8.200E 00	1.0705	7.05
U238(N,F)FSPR	CD	5.000E-12	4.730E-12	1.200E 00	7.400E 00	1.0572	5.72
CU63(N,A)CO60	CD	9.239E-15	9.035E-15	6.000E 00	1.500E 01	1.0226	2.26
FE56(N,P)MN56	CD	2.800E-14	2.865E-14	5.500E 00	1.500E 01	0.9773	-2.27
MG24(N,P)NA24	CD	4.109E-14	4.104E-14	6.000E 00	1.600E 01	1.0013	0.13

STANDARD DEVIATION OF MEASURED ACTIVITIES (PERCENT) 4.87

SOLUTION SPECTRUM OBTAINED AFTER 9 ITERATIONS

ENERGY (MEV)	ABSOLUTE VALUES DIFFERENTIAL FLUX	ABSOLUTE VALUES INTEGRAL FLUX	NORMALIZED TO 1.00E-10 MEV DIFFERENTIAL FLUX	NORMALIZED TO 1.00E-10 MEV INTEGRAL FLUX	AVERAGE ENERGY (MEV)
1.000E-10	3.623E 19	1.414E 15	2.562E 04	1.000E 00	1.659E-01
1.000E-09	3.497E 20	1.414E 15	2.472E 05	1.000E 00	1.659E-01
1.000E-08	3.864E 20	1.411E 15	2.732E 05	9.978E-01	1.662E-01
2.300E-08	2.639E 20	1.406E 15	1.866E 05	9.942E-01	1.668E-01
5.000E-08	2.010E 20	1.399E 15	1.421E 05	9.892E-01	1.677E-01
7.600E-08	1.587E 20	1.394E 15	1.122E 05	9.855E-01	1.683E-01
1.150E-07	1.148E 20	1.388E 15	8.119E 04	9.811E-01	1.691E-01
1.700E-07	7.741E 19	1.381E 15	5.474E 04	9.766E-01	1.698E-01
2.550E-07	5.207E 19	1.375E 15	3.682E 04	9.720E-01	1.707E-01
3.800E-07	3.574E 19	1.368E 15	2.527E 04	9.674E-01	1.715E-01
5.500E-07	2.424E 19	1.362E 15	1.714E 04	9.631E-01	1.722E-01
8.400E-07	1.627E 19	1.355E 15	1.151E 04	9.581E-01	1.731E-01
1.275E-06	1.200E 19	1.348E 15	8.485E 03	9.531E-01	1.740E-01
1.900E-06	1.676E 19	1.340E 15	1.149E 04	9.478E-01	1.750E-01
2.800E-06	1.113E 19	1.326E 15	7.868E 03	9.374E-01	1.769E-01
4.250E-06	7.590E 18	1.310E 15	5.367E 03	9.260E-01	1.791E-01
6.300E-06	5.324E 18	1.294E 15	3.765E 03	9.150E-01	1.813E-01
9.200E-06	3.752E 18	1.279E 15	2.653E 03	9.041E-01	1.835E-01
1.350E-05	1.054E 18	1.263E 15	7.456E 02	8.927E-01	1.858E-01
2.100E-05	8.634E 17	1.255E 15	6.105E 02	8.871E-01	1.870E-01
3.000E-05	6.796E 17	1.247E 15	4.798E 02	8.816E-01	1.881E-01
4.500E-05	6.462E 17	1.237E 15	4.569E 02	8.744E-01	1.897E-01
6.900E-05	4.417E 17	1.221E 15	3.123E 02	8.635E-01	1.921E-01
1.000E-04	3.464E 17	1.207E 15	2.449E 02	8.538E-01	1.943E-01
1.350E-04	2.650E 17	1.195E 15	1.874E 02	8.452E-01	1.962E-01
1.700E-04	2.069E 17	1.186E 15	1.463E 02	8.386E-01	1.978E-01
2.200E-04	1.431E 17	1.176E 15	1.012E 02	8.313E-01	1.995E-01
2.800E-04	1.005E 17	1.167E 15	7.105E 01	8.253E-01	2.010E-01
3.600E-04	5.777E 16	1.159E 15	4.085E 01	8.196E-01	2.024E-01
4.500E-04	4.245E 16	1.154E 15	3.002E 01	8.159E-01	2.033E-01
5.750E-04	1.751E 16	1.149E 15	1.238E 01	8.122E-01	2.042E-01
7.600E-04	1.494E 16	1.145E 15	1.057E 01	8.099E-01	2.048E-01
9.600E-04	1.317E 16	1.142E 15	9.309E 00	8.077E-01	2.053E-01
1.275E-03	1.358E 16	1.138E 15	9.599E 00	8.048E-01	2.061E-01
1.600E-03	1.197E 16	1.134E 15	8.391E 00	8.017E-01	2.069E-01
2.000E-03	1.068E 16	1.129E 15	7.549E 00	7.983E-01	2.077E-01
2.700E-03	8.839E 15	1.122E 15	6.250E 00	7.931E-01	2.091E-01

	ABSOLUTE VALUES		NORMALIZED TO 1.00E-10 MEV		
ENERGY (MEV)	DIFFERENTIAL FLUX	INTEGRAL FLUX	DIFFERENTIAL FLUX	INTEGRAL FLUX	AVERAGE ENERGY (MEV)
3.400E-03	9.772E 15	1.115E 15	6.909E 00	7.887E-01	2.102E-01
4.500E-03	1.040E 16	1.105E 15	7.353E 00	7.811E-01	2.123E-01
5.500E-03	9.996E 15	1.094E 15	7.068E 00	7.737E-01	2.142E-01
7.200E-03	7.894E 15	1.077E 15	5.582E 00	7.617E-01	2.175E-01
9.200E-03	7.193E 15	1.061E 15	5.086E 00	7.505E-01	2.206E-01
1.200E-02	5.589E 15	1.041E 15	3.952E 00	7.363E-01	2.247E-01
1.500E-02	5.380E 15	1.025E 15	3.804E 00	7.245E-01	2.281E-01
1.900E-02	3.970E 15	1.003E 15	2.807E 00	7.092E-01	2.327E-01
2.550E-02	4.026E 15	9.772E 14	2.847E 00	6.910E-01	2.382E-01
3.200E-02	4.014E 15	9.511E 14	2.838E 00	6.725E-01	2.440E-01
4.000E-02	3.783E 15	9.190E 14	2.675E 00	6.498E-01	2.513E-01
5.250E-02	3.708E 15	8.717E 14	2.622E 00	6.163E-01	2.624E-01
6.800E-02	3.454E 15	8.216E 14	2.442E 00	5.810E-01	2.747E-01
8.800E-02	3.233E 15	7.456E 14	2.286E 00	5.272E-01	2.949E-01
1.100E-01	3.044E 15	6.745E 14	2.152E 00	4.769E-01	3.156E-01
1.350E-01	2.862E 15	5.984E 14	2.024E 00	4.231E-01	3.401E-01
1.600E-01	2.607E 15	5.269E 14	1.843E 00	3.726E-01	3.663E-01
1.900E-01	2.350E 15	4.487E 14	1.661E 00	3.173E-01	3.996E-01
2.200E-01	2.134E 15	3.782E 14	1.509E 00	2.674E-01	4.359E-01
2.550E-01	1.909E 15	3.035E 14	1.350E 00	2.146E-01	4.847E-01
2.900E-01	1.469E 15	2.367E 14	1.038E 00	1.674E-01	5.445E-01
3.200E-01	1.006E 15	1.926E 14	7.113E-01	1.362E-01	5.993E-01
3.600E-01	7.248E 14	1.524E 14	5.125E-01	1.078E-01	6.678E-01
4.000E-01	5.700E 14	1.234E 14	4.030E-01	8.726E-02	7.354E-01
4.500E-01	4.458E 14	9.491E 13	3.152E-01	6.711E-02	8.286E-01
5.000E-01	3.465E 14	7.262E 13	2.450E-01	5.135E-02	9.372E-01
5.500E-01	2.597E 14	5.530E 13	1.837E-01	3.910E-02	1.066E 00
6.000E-01	1.929E 14	4.231E 13	1.364E-01	2.992E-02	1.217E 00
6.600E-01	1.373E 14	3.073E 13	9.711E-02	2.173E-02	1.438E 00
7.200E-01	8.336E 13	2.249E 13	5.894E-02	1.591E-02	1.712E 00
7.800E-01	4.799E 13	1.749E 13	3.393E-02	1.237E-02	1.987E 00
8.400E-01	2.209E 13	1.461E 13	1.562E-02	1.033E-02	2.220E 00
9.200E-01	1.261E 13	1.285E 13	8.918E-03	9.083E-03	2.404E 00
1.000E 00	9.423E 12	1.184E 13	6.663E-03	8.370E-03	2.527E 00
1.200E 00	7.529E 12	9.952E 12	5.323E-03	7.037E-03	2.797E 00
1.400E 00	6.226E 12	8.447E 12	4.402E-03	5.972E-03	3.064E 00
1.600E 00	5.092E 12	7.201E 12	3.600E-03	5.092E-03	3.334E 00

ENERGY (MEV)	ABSOLUTE VALUES DIFFERENTIAL FLUX	ABSOLUTE VALUES INTEGRAL FLUX	NORMALIZED TO 1.00E-10 MEV DIFFERENTIAL FLUX	NORMALIZED TO 1.00E-10 MEV INTEGRAL FLUX	AVERAGE ENERGY (MEV)
1.800E 00	4.375E 12	6.183E 12	3.094E-03	4.372E-03	3.603E 00
2.000E 00	3.399E 12	5.308E 12	2.403E-03	3.753E-03	3.884E 00
2.300E 00	2.435E 12	4.289E 12	1.722E-03	3.032E-03	4.297E 00
2.600E 00	1.818E 12	3.556E 12	1.285E-03	2.516E-03	4.676E 00
2.900E 00	1.330E 12	3.013E 12	9.404E-04	2.130E-03	5.024E 00
3.300E 00	9.684E 11	2.481E 12	6.847E-04	1.754E-03	5.437E 00
3.700E 00	7.282E 11	2.093E 12	5.149E-04	1.480E-03	5.795E 00
4.100E 00	5.591E 11	1.802E 12	3.953E-04	1.274E-03	6.102E 00
4.500E 00	4.858E 11	1.578E 12	3.435E-04	1.116E-03	6.357E 00
5.000E 00	6.081E 11	1.336E 12	4.300E-04	9.443E-04	6.649E 00
5.500E 00	7.210E 11	1.031E 12	5.098E-04	7.293E-04	7.062E 00
6.000E 00	4.615E 11	6.710E 11	3.263E-04	4.744E-04	7.766E 00
6.700E 00	1.723E 11	3.480E 11	1.218E-04	2.460E-04	9.081E 00
7.400E 00	1.035E 11	2.274E 11	7.317E-05	1.608E-04	1.016E 01
8.200E 00	6.761E 10	1.446E 11	4.780E-05	1.022E-04	1.151E 01
9.000E 00	1.605E 10	9.051E 10	1.135E-05	6.400E-05	1.325E 01
1.000E 01	2.889E 09	7.446E 10	2.043E-06	5.265E-05	1.405E 01
1.100E 01	7.165E 09	7.157E 10	5.066E-06	5.061E-05	1.420E 01
1.200E 01	1.721E 10	6.440E 10	1.217E-05	4.554E-05	1.450E 01
1.300E 01	1.432E 10	4.720E 10	1.013E-05	3.337E-05	1.523E 01
1.400E 01	1.066E 10	3.288E 10	7.537E-06	2.325E-05	1.598E 01
1.500E 01	8.061E 09	2.222E 10	5.699E-06	1.571E-05	1.669E 01
1.600E 01	6.279E 09	1.416E 10	4.439E-06	1.001E-05	1.736E 01
1.700E 01	4.440E 09	7.878E 09	3.140E-06	5.571E-06	1.805E 01
1.800E 01	2.565E 09	3.438E 09	1.814E-06	2.431E-06	1.875E 01
1.900E 01	8.727E 08	8.727E 08	6.171E-07	6.171E-07	1.950E 01
2.000E 01	0.0	0.0	0.0	0.0	0.0

XIV. APPENDIX D

Results of Monte Carlo error analysis for R-3

ANALYSIS OF INTEGRAL FLUENCE

ENERGY	TRUE	MINUS	MEAN	PLUS	
1.0000E-10	4.9847E+14	4.5095E+14	5.0307E+14	5.4549E+14	9.38
1.0000E-09	4.9847E+14	4.5095E+14	5.0307E+14	5.4549E+14	9.38
1.0000E-08	4.9847E+14	4.5095E+14	5.0307E+14	5.4549E+14	9.38
2.3000E-08	4.9847E+14	4.5095E+14	5.0307E+14	5.4549E+14	9.38
5.0000E-08	4.9847E+14	4.5095E+14	5.0307E+14	5.4549E+14	9.38
7.6000E-08	4.9847E+14	4.5095E+14	5.0307E+14	5.4549E+14	9.38
1.1500E-07	4.9847E+14	4.5095E+14	5.0307E+14	5.4549E+14	9.38
1.7000E-07	4.9843E+14	4.5086E+14	5.0298E+14	5.4540E+14	9.38
2.5500E-07	4.9822E+14	4.5046E+14	5.0259E+14	5.4503E+14	9.39
3.8000E-07	4.9761E+14	4.4931E+14	5.0145E+14	5.4398E+14	9.42
5.5000E-07	4.9619E+14	4.4679E+14	4.9902E+14	5.4173E+14	9.50
8.4000E-07	4.9220E+14	4.3954E+14	4.9256E+14	5.3598E+14	9.77
1.2750E-06	4.8409E+14	4.2202E+14	4.8050E+14	5.2447E+14	10.57
1.9000E-06	4.7361E+14	4.0315E+14	4.6691E+14	5.1317E+14	11.68
2.8000E-06	4.6365E+14	3.8920E+14	4.5699E+14	5.0234E+14	12.13
4.2500E-06	4.5279E+14	3.7814E+14	4.4644E+14	4.9189E+14	12.48
6.3000E-06	4.4234E+14	3.7082E+14	4.3656E+14	4.8327E+14	12.77
9.2000E-06	4.3169E+14	3.5515E+14	4.2574E+14	4.7195E+14	13.44
1.3500E-05	4.2061E+14	3.4076E+14	4.1430E+14	4.6174E+14	14.31
2.1000E-05	4.0758E+14	3.2265E+14	4.0058E+14	4.5000E+14	15.58
3.0000E-05	3.9741E+14	3.1131E+14	3.9067E+14	4.4074E+14	16.24
4.5000E-05	3.8600E+14	2.9996E+14	3.7972E+14	4.2999E+14	16.78
6.9000E-05	3.7427E+14	2.8950E+14	3.6839E+14	4.1823E+14	17.13
1.0000E-04	3.6423E+14	2.8035E+14	3.5863E+14	4.0851E+14	17.50
1.3500E-04	3.5623E+14	2.7331E+14	3.5118E+14	4.0059E+14	17.76
1.7000E-04	3.4996E+14	2.6774E+14	3.4501E+14	3.9395E+14	17.93
2.2000E-04	3.4268E+14	2.6114E+14	3.3740E+14	3.8540E+14	18.05
2.8000E-04	3.3573E+14	2.5471E+14	3.2947E+14	3.7630E+14	18.09
3.6000E-04	3.2856E+14	2.4836E+14	3.2195E+14	3.6804E+14	18.22
4.5000E-04	3.2233E+14	2.4302E+14	3.1592E+14	3.6154E+14	18.39
5.7500E-04	3.1572E+14	2.3769E+14	3.0962E+14	3.5455E+14	18.50
7.6000E-04	3.0843E+14	2.3207E+14	3.0229E+14	3.4616E+14	18.53
9.6000E-04	3.0256E+14	2.2713E+14	2.9552E+14	3.3847E+14	18.46
1.2750E-03	2.9543E+14	2.2114E+14	2.8769E+14	3.2969E+14	18.49
1.6000E-03	2.8970E+14	2.1658E+14	2.8193E+14	3.2319E+14	18.52
2.0000E-03	2.8403E+14	2.1217E+14	2.7644E+14	3.1684E+14	18.56
2.7000E-03	2.7696E+14	2.0345E+14	2.6907E+14	3.0740E+14	18.62
3.4000E-03	2.7050E+14	1.9898E+14	2.6347E+14	3.0109E+14	18.67
4.5000E-03	2.6324E+14	1.9359E+14	2.5660E+14	2.9334E+14	18.73
5.5000E-03	2.5802E+14	1.8981E+14	2.5175E+14	2.8785E+14	18.77
7.2000E-03	2.5089E+14	1.8466E+14	2.4492E+14	2.8015E+14	18.78
9.2000E-03	2.4444E+14	1.8003E+14	2.3888E+14	2.7337E+14	18.83
1.2000E-02	2.3733E+14	1.7489E+14	2.3225E+14	2.6601E+14	18.91
1.5000E-02	2.3133E+14	1.6766E+14	2.2665E+14	2.5908E+14	19.03
1.9000E-02	2.2463E+14	1.6266E+14	2.2045E+14	2.5248E+14	19.23
2.5500E-02	2.1579E+14	1.5602E+14	2.1220E+14	2.4378E+14	19.53
3.2000E-02	2.0863E+14	1.5315E+14	2.0547E+14	2.3756E+14	19.81

4.0000E-02	2.0126E+14	1.4747E+14	1.9838E+14	2.3012E+14	20.09
5.2500E-02	1.9172E+14	1.4014E+14	1.8920E+14	2.2051E+14	20.49
6.6000E-02	1.8332E+14	1.3562E+14	1.8102E+14	2.1284E+14	20.91
8.8000E-02	1.7217E+14	1.2842E+14	1.7009E+14	2.0244E+14	21.57
1.1000E-01	1.6312E+14	1.2099E+14	1.6119E+14	1.9330E+14	22.24
1.3500E-01	1.5382E+14	1.1326E+14	1.5203E+14	1.8402E+14	23.08
1.6000E-01	1.4464E+14	1.0552E+14	1.4303E+14	1.7502E+14	24.12
1.9000E-01	1.3376E+14	9.6200E+13	1.3241E+14	1.6457E+14	25.66
2.2000E-01	1.2298E+14	8.8072E+13	1.2197E+14	1.5543E+14	27.60
2.5500E-01	1.1054E+14	7.6877E+13	1.0999E+14	1.4392E+14	30.51
2.9000E-01	9.8271E+13	6.6623E+13	9.8253E+13	1.3380E+14	34.15
3.2000E-01	8.8258E+13	5.9238E+13	8.8888E+13	1.2540E+14	37.10
3.6000E-01	7.5959E+13	5.0954E+13	7.7558E+13	1.1355E+14	40.00
4.0000E-01	6.4931E+13	4.3646E+13	6.7347E+13	9.9764E+13	41.30
4.5000E-01	5.2518E+13	3.6030E+13	5.5703E+13	8.2742E+13	41.57
5.0000E-01	4.1673E+13	2.9214E+13	4.5340E+13	6.6116E+13	40.68
5.5000E-01	3.3024E+13	2.4360E+13	3.6751E+13	5.2871E+13	38.79
6.0000E-01	2.6604E+13	2.0802E+13	3.0123E+13	4.2442E+13	35.93
6.6000E-01	2.1754E+13	1.8129E+13	2.4314E+13	3.3775E+13	31.53
7.2000E-01	1.8371E+13	1.5636E+13	2.0082E+13	2.6321E+13	26.38
7.8000E-01	1.6019E+13	1.3979E+13	1.7101E+13	2.1317E+13	21.26
8.4000E-01	1.4426E+13	1.2653E+13	1.5025E+13	1.8061E+13	17.06
9.2000E-01	1.2956E+13	1.1672E+13	1.3101E+13	1.5036E+13	12.60
1.0000E+00	1.1883E+13	1.0592E+13	1.1781E+13	1.2846E+13	9.51
1.2000E+00	9.9196E+12	9.0470E+12	9.5423E+12	1.0201E+13	6.90
1.4000E+00	8.4949E+12	7.8080E+12	8.1671E+12	8.6869E+12	5.27
1.6000E+00	7.4059E+12	6.7916E+12	7.1441E+12	7.6455E+12	5.93
1.8000E+00	6.5167E+12	5.9556E+12	6.3478E+12	6.8533E+12	6.78
2.0000E+00	5.7367E+12	5.3353E+12	5.6696E+12	6.1705E+12	7.22
2.3000E+00	4.7012E+12	4.4667E+12	4.7786E+12	5.1929E+12	7.33
2.6000E+00	3.9543E+12	3.7707E+12	4.0000E+12	4.3491E+12	7.08
2.9000E+00	3.2676E+12	3.1009E+12	3.2999E+12	3.5665E+12	6.99
3.3000E+00	2.4414E+12	2.3240E+12	2.5093E+12	2.7508E+12	8.14
3.7000E+00	1.8306E+12	1.7133E+12	1.8885E+12	2.0942E+12	10.06
4.1000E+00	1.3687E+12	1.2739E+12	1.4160E+12	1.5992E+12	11.39
4.5000E+00	1.0122E+12	9.3975E+11	1.0456E+12	1.1723E+12	11.10
5.0000E+00	6.7014E+11	6.3769E+11	6.9242E+11	7.6992E+11	9.36
5.5000E+00	4.4242E+11	4.2668E+11	4.5523E+11	4.9134E+11	7.10
6.0000E+00	3.2512E+11	3.1722E+11	3.3285E+11	3.5535E+11	5.62
6.7000E+00	2.3751E+11	2.3373E+11	2.4244E+11	2.5735E+11	4.69
7.4000E+00	1.8272E+11	1.7998E+11	1.8723E+11	1.9699E+11	4.59
8.2000E+00	1.4185E+11	1.4018E+11	1.4582E+11	1.5475E+11	4.97
9.0000E+00	1.1417E+11	1.1320E+11	1.1822E+11	1.2674E+11	5.62
1.0000E+01	9.1952E+10	9.0661E+10	9.5362E+10	1.0301E+11	6.35
1.1000E+01	7.5738E+10	7.4199E+10	7.8565E+10	8.5400E+10	6.95
1.2000E+01	6.1089E+10	5.9359E+10	6.3621E+10	6.9421E+10	7.76
1.3000E+01	4.7694E+10	4.5585E+10	4.9670E+10	5.4598E+10	9.02
1.4000E+01	3.5652E+10	3.3424E+10	3.7436E+10	4.1509E+10	10.80
1.5000E+01	2.5126E+10	2.3124E+10	2.6512E+10	3.0022E+10	13.01
1.6000E+01	1.6259E+10	1.4843E+10	1.7282E+10	2.0269E+10	15.57
1.7000E+01	9.7699E+09	8.2965E+09	9.8931E+09	1.1902E+10	18.05
1.8000E+01	4.1535E+09	3.6922E+09	4.4629E+09	5.5310E+09	20.20
1.9000E+01	1.0431E+09	9.2650E+08	1.1264E+09	1.4289E+09	21.54

Results of Monte Carlo analysis for V-1

ANALYSIS OF INTEGRAL FLUENCE

ENERGY	TRUE	MINUS	MEAN	PLUS	
1.0000E-10	1.0852E+15	8.6813E+14	1.0154E+15	1.2318E+15	17.78
1.0000E-09	1.0852E+15	8.6813E+14	1.0154E+15	1.2318E+15	17.78
1.0000E-08	1.0852E+15	8.6813E+14	1.0154E+15	1.2318E+15	17.78
2.3000E-08	1.0852E+15	8.6813E+14	1.0154E+15	1.2318E+15	17.78
5.0000E-08	1.0852E+15	8.6813E+14	1.0154E+15	1.2318E+15	17.78
7.6000E-08	1.0852E+15	8.6813E+14	1.0154E+15	1.2318E+15	17.78
1.1500E-07	1.0852E+15	8.6812E+14	1.0154E+15	1.2319E+15	17.78
1.7000E-07	1.0852E+15	8.6802E+14	1.0153E+15	1.2317E+15	17.78
2.5500E-07	1.0850E+15	8.6765E+14	1.0150E+15	1.2315E+15	17.79
3.8000E-07	1.0876E+15	8.6665E+14	1.0142E+15	1.2306E+15	17.81
5.5000E-07	1.0865E+15	8.6456E+14	1.0124E+15	1.2289E+15	17.86
8.4000E-07	1.0834E+15	8.5437E+14	1.0076E+15	1.2162E+15	17.98
1.2700E-06	1.0775E+15	8.4453E+14	9.9925E+14	1.2079E+15	18.20
1.9000E-06	1.0692E+15	8.3262E+14	9.8893E+14	1.1976E+15	18.46
2.6000E-06	1.0559E+15	8.1749E+14	9.7454E+14	1.1835E+15	18.79
4.2500E-06	1.0392E+15	7.9395E+14	9.5666E+14	1.1662E+15	19.20
6.3000E-06	1.0243E+15	7.8302E+14	9.4100E+14	1.1509E+15	19.56
9.2000E-06	1.0151E+15	7.7312E+14	9.3155E+14	1.1413E+15	19.77
1.3500E-05	1.0071E+15	7.6438E+14	9.2333E+14	1.1329E+15	19.96
2.1000E-05	9.9872E+14	7.5502E+14	9.1464E+14	1.1240E+15	20.17
3.0000E-05	9.9004E+14	7.4629E+14	9.0610E+14	1.1153E+15	20.36
4.5000E-05	9.7804E+14	7.3440E+14	8.9428E+14	1.1035E+15	20.64
6.9000E-05	9.6155E+14	7.1765E+14	8.7760E+14	1.0874E+15	21.07
1.0000E-04	9.4746E+14	7.0328E+14	8.6374E+14	1.0741E+15	21.47
1.3500E-04	9.3494E+14	6.9543E+14	8.5142E+14	1.0702E+15	21.82
1.7000E-04	9.2500E+14	6.8607E+14	8.4186E+14	1.0601E+15	22.03
2.2000E-04	9.1388E+14	6.7628E+14	8.3122E+14	1.0473E+15	22.13
2.8000E-04	9.0301E+14	6.6213E+14	8.2049E+14	1.0255E+15	22.13
3.6000E-04	8.9523E+14	6.5565E+14	8.1311E+14	1.0161E+15	22.16
4.5000E-04	8.9107E+14	6.5227E+14	8.0933E+14	1.0116E+15	22.19
5.7500E-04	8.8699E+14	6.4903E+14	8.0566E+14	1.0076E+15	22.24
7.6000E-04	8.8013E+14	6.4334E+14	7.9902E+14	1.0006E+15	22.35
9.6000E-04	8.7032E+14	6.3096E+14	7.8567E+14	9.8821E+14	22.74
1.2750E-03	8.5968E+14	6.1762E+14	7.7184E+14	9.7556E+14	23.20
1.6000E-03	8.5350E+14	6.1180E+14	7.6539E+14	9.6927E+14	23.36
2.0000E-03	8.4838E+14	6.0745E+14	7.6041E+14	9.6423E+14	23.48
2.7000E-03	8.4000E+14	6.0069E+14	7.5200E+14	9.5630E+14	23.65
3.4000E-03	8.3270E+14	5.9467E+14	7.4572E+14	9.4933E+14	23.81
4.5000E-03	8.2195E+14	5.9084E+14	7.3607E+14	9.4679E+14	23.99
5.5000E-03	8.1546E+14	5.8620E+14	7.3052E+14	9.4069E+14	24.08
7.2000E-03	8.0338E+14	5.7767E+14	7.2017E+14	9.2643E+14	24.17
9.2000E-03	7.9416E+14	5.7132E+14	7.1234E+14	9.1910E+14	24.23
1.2000E-02	7.8275E+14	5.6342E+14	7.0258E+14	9.0728E+14	24.29
1.5000E-02	7.7379E+14	5.5703E+14	6.9480E+14	8.9816E+14	24.37
1.9000E-02	7.6287E+14	5.4908E+14	6.8522E+14	8.8701E+14	24.49
2.5500E-02	7.4504E+14	5.3610E+14	6.6947E+14	8.6805E+14	24.62
3.2000E-02	7.2794E+14	5.2361E+14	6.5431E+14	8.4952E+14	24.73

5.2500E-02	6.7153E+14	4.8272E+14	6.0348E+14	7.8309E+14	24.71
6.0000E-02	5.3547E+14	4.5277E+14	5.7046E+14	7.3299E+14	24.61
8.6000E-02	5.7785E+14	4.1000E+14	5.1685E+14	6.6234E+14	24.45
1.1000E-01	5.2195E+14	3.6409E+14	4.6400E+14	5.8856E+14	24.37
1.3500E-01	4.6218E+14	3.1742E+14	4.0698E+14	5.1586E+14	24.49
1.6000E-01	4.0770E+14	2.7130E+14	3.5497E+14	4.4742E+14	24.92
1.9000E-01	3.4927E+14	2.2531E+14	2.9949E+14	3.7992E+14	25.90
2.2000E-01	2.9720E+14	1.8700E+14	2.5045E+14	3.2442E+14	27.52
2.5500E-01	2.4240E+14	1.4924E+14	1.9917E+14	2.7377E+14	30.63
2.9000E-01	1.9342E+14	1.1172E+14	1.5394E+14	2.2597E+14	35.77
3.2000E-01	1.5997E+14	8.5957E+13	1.2467E+14	1.8841E+14	40.30
3.6000E-01	1.2717E+14	6.4793E+13	9.7789E+13	1.5369E+14	44.61
4.0000E-01	1.0406E+14	5.1256E+13	7.9906E+13	1.2589E+14	46.51
4.5000E-01	8.1557E+13	4.0174E+13	6.2955E+13	9.9849E+13	47.23
5.0000E-01	6.3402E+13	3.1884E+13	4.9527E+13	7.8106E+13	46.50
5.5000E-01	4.9004E+13	2.5752E+13	3.9111E+13	6.0624E+13	44.41
6.0000E-01	3.8355E+13	2.1540E+13	3.1618E+13	4.7694E+13	41.18
6.6000E-01	2.9273E+13	1.8400E+13	2.5374E+13	3.7290E+13	34.54
7.2000E-01	2.2907E+13	1.6084E+13	2.1006E+13	2.9500E+13	.36
7.8000E-01	1.8709E+13	1.4540E+13	1.8012E+13	2.4076E+13	26.01
8.4000E-01	1.6078E+13	1.3495E+13	1.6002E+13	2.0383E+13	21.14
9.2000E-01	1.3917E+13	1.2444E+13	1.4156E+13	1.6900E+13	15.67
1.0000E+00	1.2529E+13	1.1721E+13	1.2856E+13	1.4894E+13	11.89
1.2000E+00	1.0149E+13	9.7912E+12	1.0538E+13	1.1289E+13	7.11
1.4000E+00	8.4725E+12	8.2891E+12	8.8677E+12	9.4367E+12	6.47
1.6000E+00	7.1703E+12	6.9498E+12	7.5149E+12	8.1325E+12	7.85
1.8000E+00	6.1196E+12	5.7883E+12	6.3930E+12	6.9571E+12	9.15
2.0000E+00	5.2489E+12	4.8683E+12	5.4439E+12	5.9228E+12	9.67
2.3000E+00	4.2449E+12	3.8670E+12	4.3458E+12	4.7073E+12	9.58
2.6000E+00	3.5283E+12	3.2237E+12	3.5658E+12	3.8646E+12	9.01
2.9000E+00	2.9922E+12	2.7264E+12	2.9937E+12	3.2169E+12	8.14
3.3000E+00	2.4548E+12	2.2558E+12	2.4259E+12	2.5907E+12	6.90
3.7000E+00	2.0611E+12	1.8947E+12	2.0119E+12	2.1406E+12	6.10
4.1000E+00	1.7625E+12	1.5993E+12	1.7001E+12	1.8034E+12	6.01
4.5000E+00	1.5315E+12	1.3912E+12	1.4631E+12	1.5697E+12	6.38
5.0000E+00	1.2958E+12	1.1525E+12	1.2307E+12	1.3287E+12	7.10
5.5000E+00	1.0536E+12	9.2505E+11	1.0012E+12	1.0821E+12	7.83
6.0000E+00	7.4036E+11	6.5074E+11	7.1430E+11	7.6753E+11	8.16
6.7000E+00	3.6322E+11	3.3763E+11	3.6606E+11	3.8939E+11	7.06
7.4000E+00	2.2972E+11	2.2095E+11	2.3864E+11	2.5274E+11	6.65
8.2000E+00	1.4273E+11	1.3950E+11	1.5103E+11	1.6338E+11	7.87
9.0000E+00	8.9256E+10	8.8493E+10	9.5151E+10	1.0554E+11	8.78
1.0000E+01	6.3895E+10	6.1017E+10	6.7579E+10	7.6557E+10	11.52
1.1000E+01	6.0033E+10	5.6799E+10	6.3326E+10	7.2237E+10	12.21
1.2000E+01	5.4479E+10	5.1111E+10	5.7243E+10	6.6190E+10	13.07
1.3000E+01	4.4669E+10	4.1349E+10	4.6615E+10	5.4810E+10	14.15
1.4000E+01	3.4461E+10	3.1283E+10	3.5663E+10	4.2512E+10	15.42
1.5000E+01	2.5012E+10	2.2240E+10	2.5701E+10	3.1039E+10	16.77
1.6000E+01	1.6848E+10	1.4720E+10	1.7194E+10	2.1250E+10	18.31
1.7000E+01	9.7844E+09	8.3160E+09	9.9258E+09	1.2358E+10	19.95
1.8000E+01	4.4369E+09	3.6930E+09	4.4836E+09	5.6652E+09	21.55
1.9000E+01	1.1196E+09	9.1937E+08	1.1296E+09	1.4417E+09	22.65